# APPLICATIONS OF PULSED FIELD GRADIENT TECHNIQUES AND SLICE SELECTIVE METHODS IN NMR SPECTROSCOPY

by

Kaitlyn Doolittle

A thesis submitted to the Faculty of the University of Delaware in partial fulfillment of the requirements for the degree of Master of Science in Chemistry and Biochemistry

Fall 2022

© 2022 Kaitlyn Doolittle
All Rights Reserved

**APPLICATIONS OF PULSED FIELD GRADIENT TECHNIQUES AND SLICE SELECTIVE METHODS IN NMR SPECTROSCOPY**

by

Kaitlyn Doolittle

Approved: _____

Murray V. Johnston, Ph.D.
Professor in charge of thesis on behalf of the Advisory Committee

Approved: _____

Joel Rosenthal, Ph.D.
Chair of the Department of Chemistry and Biochemistry

Approved: _____

John Pelesko, Ph.D.
Dean of the College of Arts and Sciences

Approved: _____

Louis F. Rossi, Ph.D.
Vice Provost for Graduate and Professional Education and
Dean of the Graduate College

## ACKNOWLEDGMENTS

First and foremost, I need to give a special thanks to my co-advisor, Steve Bai. Without your support, dedication, and patience, I would not have made it to this point. Not only did you agree to advise me as a part-time student, but you were also willing to stick with me when I had to relocate across the country for work, and through the obstacles that followed. It has been such a pleasure to have had this opportunity to work with you, and I am so grateful for all that I have learned from you on this journey over the past several years.

To Murray Johnston, thank you for your willingness to be my official advisor, and for your support to Steve and me along the way.

To the Chemistry and Biochemistry department, thank you for accepting me as a part-time student, and for working with me when I had to finish my degree as a remote student. Thank you to Susan Cheadle and Mary Martin for all of your assistance as I worked to finish this degree.

There are several colleagues that I would like to thank from my time at DuPont and Genentech whose support was key to this endeavor. Thank you to Mark Kennedy, my former manager, for starting me down this road; I will always think of you when I reflect on this accomplishment. To my current manager, Ken Skidmore, thank you for continuing to support me at Genentech as I worked to finish what I set out to do. Thank you to Gennady Khirich for many thought-provoking discussions about NMR that were a source of inspiration during this work and thank you for cheering me on over the past several years. Also, to Joe McAuliffe, thank you for the instrument time

in your lab, when I came out to California with no access to any other NMR equipment.

Thank you to Kevin Penfield of Croda International Plc for providing the Natsurf 265 material and the surface tension data from your lab.

To my husband, Glenn: thank you for your unwavering support as I worked towards this goal. Thank you for being by my side throughout this journey and for sitting with me on the latest nights, helping me remain calm when my laptop stopped working, or some other technical issue presented itself at the worst possible time. Your help, love, and reassurance over the past several years were vital to me achieving this goal.

To my parents, thank you for always believing in me and for always being an inspiration in my life. Without your support and encouragement, I wouldn't be where I am today.

To my newborn daughter, Jocelyn: whether you will ever realize it or not, you were a huge part of this journey for me. You were already with me as we worked on publishing our research, and as I composed this thesis. You've been an inspiration, not just in terms of motivation to get this done, but also from the standpoint of wanting to accomplish something that you could look at and be inspired by some day. I love you so much.

Finally, thank you to the rest of my family and to my friends for your love and support along this journey.

## TABLE OF CONTENTS

LIST OF TABLES ..... vii
LIST OF FIGURES ..... viii
ABSTRACT ..... xiii

Chapter

1 INTRODUCTION ..... 1

REFERENCES ..... 4

2 APPLICATIONS OF PULSED FIELD GRADIENTS ..... 5

2.1 Background of Pulsed Field Gradients ..... 5
2.2 NMR Diffusion Measurements of Surfactants ..... 10

2.2.1 Experimental Methods ..... 13
2.2.2 Results and Discussion ..... 15
2.2.3 Conclusions ..... 29

2.3 One-Dimensional Imaging of Biphasic Samples Using Pulsed Field Gradients ..... 29

2.3.1 Experimental Methods ..... 31
2.3.2 Results and Discussion ..... 32
2.3.3 Conclusions ..... 37

REFERENCES ..... 38

3 APPLICATION OF RADIO FREQUENCY SHAPED PULSES TO SLICE SELECTIVE NMR SPECTROSCOPY ..... 39

3.1 Background of Shaped Radio Frequency Pulses ..... 39
3.2 The Combination of Shaped Pulses with Pulsed Field Gradients for Slice Selection NMR ..... 43
3.3 The Design of One-Shot Double-Slice Experiments ..... 50
3.4 Application to Model Biphasic Samples ..... 54

3.4.1 Experimental Methods ..... 55
3.4.2 Results and Discussion ..... 57
3.4.3 Conclusions ..... 64

REFERENCES ..... 65

4 THE APPLICATION OF ONE-SHOT DOUBLE-SLICE NMR EXPERIMENTS TO COMPLEX BIPHASIC SAMPLES ..... 68

4.1 Background on Recent Applications of Slice Selection NMR to Real-life Biphasic Samples ..... 68
4.2 Biphasic Tea Extracts ..... 68

4.2.1 Experimental Methods ..... 72
4.2.2 Results and Discussion ..... 73
4.2.3 Conclusions ..... 75

4.3 Biphasic Coffee Extracts ..... 75

4.3.1 Experimental Methods ..... 77
4.3.2 Results and Discussion ..... 78
4.3.3 Conclusions ..... 79

REFERENCES ..... 80

5 CONCLUSIONS AND FUTURE WORK ..... 82

Appendix

A PERMISSIONS ..... 85
B PULSE SEQUENCE: 1D GRADIENT IMAGING ..... 86
C PULSE SEQUENCE: 1D ONE-SHOT DOUBLE-SLICE ..... 89
D PULSE SEQUENCE: 2D OSDS-TOCSY ..... 92
E PUBLISHED WORK ..... 97

## LIST OF TABLES


Table 1. DOSY experimental parameters used for each concentration of Natsurf 265 in $D_2O$. ..... 15

Table 2. Calculated Natsurf 265 concentrations (in $D_2O$) and corresponding self-diffusion coefficients for the ethylene oxide group signal (3.57 ppm) ..... 16

Table 3. Bandwidths, Effective offsets, Effective bandwidths of the ReBurp[a] Pulse ..... 61

Table 4. $^1H$ Chemical shift assignments for BGT. ..... 70

Table 5. $^1H$ Chemical shift assignments for CHT. ..... 71

Table 6. $^1H$ Chemical shift assignments for HBC. ..... 76

## LIST OF FIGURES


Figure 1. a) An NMR sample tube surrounded by an NMR coil in an external magnetic field, $B_0$, along the z-axis. b) The NMR sample tube subjected to an applied magnetic field gradient, $G_z$, centered at $z_0$..... 6

Figure 2. Schematic of the pulse sequence for the DBPPSTE version of DOSY experiments. ..... 9

Figure 3. The components of the Natsurf 265 surfactant. The $CH_2$ signals that produce signals at 3.57 ppm are highlighted in blue here. ..... 11

Figure 4. Surface tension measurements vs. concentration of Natsurf 265 in water at 298 K. ..... 12

Figure 5. DOSY NMR spectrum of Natsurf 265 at a concentration of 20 % w/w. 17

Figure 6. Self-diffusion coefficients for the long chain ethylene oxide signal at 3.57 ppm over a range of concentration of Natsurf 265 in $D_2O$. ..... 18

Figure 7. Surfactant region in the DOSY spectra of four Natsurf 265 solutions in $D_2O$ at concentrations of a) 0.01, b) 0.1, c) 0.2, d) 1, e) 5, and f) 20 % w/w. ..... 19

Figure 8. A comparison of surface tension values and self-diffusion coefficients across various concentrations of Natsurf 265. ..... 21

Figure 9. Plots of the measured self-diffusion coefficients for Natsurf 265 as a function of the inverse of the total concentration a) on a logarithmic scale, showing all concentration data collected, and b) on a linear scale, zoomed in to show the region for concentrations above the CMC (with low $1/C_T$ values). The linear segments above and below the CMC are fit to equations to determine their intersection. ..... 23

Figure 10. Plot of the measured surface tension for Natsurf 265 as a function of the total concentration on a logarithmic scale, showing all concentration data collected. The linear segment above and the logarithmic segment below the CMC are fit to equations to determine their intersection. ..... 24

Figure 11. The experimental diffusion coefficients of Natsurf 265 above the CMC fit a power function with a -1/2 exponent (within experimental error). ..... 26

Figure 12. Schematic of Natsurf 265 in solution at concentrations a) below the CMC, b) at the CMC, c) just above the CMC where additional surfactant molecules start to form micelles, and d) further above the CMC, at which point the micelle mass increases, but the volume and the radius, r, stay constant. ..... 28

Figure 13. Schematic of the pulse sequence for the 1D gradient-echo experiment used for 1D NMR imaging in this work. ..... 31

Figure 14. 1D NMR image of a homogeneous sample of 1% Natsurf in $D_2O$. ..... 33

Figure 15. 1D NMR images of biphasic samples a) GNE M1 and b) GNE M2. ..... 34

Figure 16. a) GNE M1 NMR tube inside sample gauge, confirming that the interface is much higher than the center of the receiving coil, and that the majority of the aqueous phase is not within the receiving coil; b) GNE M1 NMR tube marked with the proper biphasic interface for reference during preparation of GNE M2 ..... 36

Figure 17. Fourier transforms of rectangular pulses with a) high power and short duration, b) slightly lower power and slightly longer duration, and c) much lower power and much longer duration. ..... 40

Figure 18. The Fourier transform of a Gaussian pulse will also generate a Gaussian excitation profile; the narrower the pulse width, the broader the resultant excitation profile will be, as indicated by the color coding in the figure. In addition, the Gaussian shaped pulses do not generate the sinc wiggles that square pulses do. ..... 41

Figure 19. The Fourier transform of a sinc pulse will generate a square shape excitation profile. This results in an excitation profile that has no sinc wiggles and that can be uniform across the selected frequency range. ... 42

Figure 20. Illustration of spatial regions, called slices, within a) the aqueous phase and b) the organic phase of a biphasic NMR sample. Ω is the respective offset frequency used to select each of the two slices. ..... 45

Figure 21. Slice selection $^{1}H$ NMR spectra: a) An excitation selective pulse (EBurp: 1236 μs) produces spectra of the aqueous (red) and organic (blue, phased negatively for comparison) phases of a model biphasic sample of sucrose in $D_2O$ and 4 chromanone in $CDCl_3$. b) An excitation EBurp pulse followed by a refocusing pulse (ReBurp, 1600 μs) leads to the spectra of aqueous (red) and organic phases (blue, phased negatively for comparison) of the same model sample. The bandwidth and offset of these pulses are 3915 Hz and ±7500 Hz. c) One-shot double-slice selection spectrum of the model biphasic sample using a ReBurp pulse (1600 μs) with a bandwidth of 3915 Hz and the effective offsets are ±1684 Hz. d) Schematic plot of the biphasic sample tube marked with *z* and Δz, indicating the slices excited by two, separate experiments using different offsets. e) Schematic plot of the biphasic sample tube signifying the two slices excited simultaneously by only one ReBurp pulse that produces two effective excitation profiles with opposite phases. ..... 49

Figure 22. $^{1}H$ NMR spectra of a GNE M2 via standard 1D NMR (top) and one-shot double-slice 1D NMR (bottom). ..... 51

Figure 23. a) Excitation profile for 1200 μs ReBurp pulse, b) visualization of the excitation profile as a function of position along the z-axis; the Reburp pulse offset, Ω, is set to 0 Hz in this case. ..... 52

Figure 24. a) Shaped pulse simulation of ReBurp pulse (1200 μs) shows the trajectories of the magnetizations on-resonance (black) and off-resonance (± 2243 Hz, red). Note that the end points of magnetizations with the effective offsets (± 2243 Hz) are nearly 180° out of phase along the x-axis, enabling the simultaneous excitations. b) Simulated excitation profile shows excitations along ±x at Ω=± 2243 Hz and Δν=660 Hz at 30% of the profile height. c) Experimental excitation profile of ReBurp pulse (1200 μs), obtained by varying the offset frequency, is highly consistent with the simulated effective offsets and bandwidth (red in b). ..... 54

Figure 25. Model compounds used as the a) aqueous solute at Genentech, b) aqueous solute at University of Delaware, c) organic solute at Genentech, and d) organic solute at University of Delaware. ..... 55

Figure 26. One-Shot Double-Slice spectra of GNE M2 model biphasic sample utilizing a) the revise ReBurp Inversion Slice Selection pulse sequence with alternating gradient phase, and b) the original ReBurp Inversion Slice Selection pulse sequence with a single gradient polarity..... 59

Figure 27. One-shot double-slice version of a TOCSY spectrum of the UD M1 model biphasic sample. The 90° excitation hard pulse in the TOCSY is replaced by a ReBurp pulse of 1600 μs along with a rectangular gradient pulse at a strength of 3.43G/cm of the same length. The resulting 2D spectrum is phase-sensitive with color coded cross peaks for sucrose (red) and 4-chromanone (blue). The TOCSY mixing time is 60 ms..... 60

Figure 28. One-shot double-slice NMR signals of the UD M1 model biphasic sample a) as a function of pulse width from 800 μs (left) to 2600 μs (right) with an increment of 200 μs at a gradient strength of 3.43 G/cm, and b) as a function of gradient strength from 4% (left) to 10% (right) with a step length of 1%. The pulse width was set to 1200 μs and the gradient strength at 100% is 51.1 G/cm..... 63

Figure 29. $^{1}H$ spectrum of the BGT biphasic sample; the large water signal from the aqueous layer was suppressed via presaturation. ..... 70

Figure 30. $^{1}H$ spectrum of the CHT biphasic sample; the large water signal from the aqueous layer was suppressed via presaturation. (? indicates unidentified resonances.)..... 71

Figure 31. Pictures of biphasic $CDCl_3/D_2O$ samples of a) CHT and b) BGT. One-shot double-slice NMR spectra acquired with a gradient strength of 3.43 G/cm and a ReBurp pulse width of 1600 μs for c) CHT and d) BGT. Conventional presat $^{1}H$ spectra of the biphasic samples for e) CHT and f) BGT. The presat $^{1}H$ spectra of pure g) CHT $D_2O$ extract and h) BGT $D_2O$ extract are shown, along with the standard $^{1}H$ spectra of pure i) CHT $CDCl_3$ extract and j) BGT $CDCl_3$ extract. ..... 74

Figure 32. $^{1}H$ spectrum of the HBC biphasic sample; the large water signal from the aqueous layer was suppressed via presaturation. ..... 76

Figure 33. Classic 1D presat $^{1}H$ spectra for a) CBC and b) HBC. One-shot double-slice NMR spectra for c) biphasic CBC and d) HBC acquired with a pulse field gradient strength of approximately 3.43 G/cm, and a ReBurp pulse width of 1000 µs. One-shot double-slice TOCSY spectra (mixing times of 60 ms) for e) CBC and f) HBC. Dark red and dark green cross peaks respectively represent chemical species from the $D_2O$ and $CDCl_3$ layers. ..... 79

## ABSTRACT

Slice selection NMR spectroscopy is a method that enables the chemical analysis of specific, selected regions of an NMR sample along the z-axis. This type of NMR spectroscopy has applications in metabolomics, kinetics, extractions analyses, and more. The focus of this work is the development of a novel slice selection experiment, called the one-shot double-slice experiment. This experiment enables the simultaneous analysis of two different regions within an NMR tube, with the ability to differentiate between the selected regions, due to the signals from each region being of opposite phase in the resulting NMR spectrum. Slice selection NMR is possible through the combination of pulsed field gradients and shaped pulses. In order to develop this methodology and novel experiment, it was first necessary to develop a deep understanding of those two fundamental components. Pulsed field gradients were investigated through diffusion NMR spectroscopy and one-dimensional NMR imaging. The diffusion experiments were conducted to determine the self-diffusion coefficients of surfactant at various concentrations, in order to further define the system beyond the critical micelle concentration (at which point surface tension no longer can provide insight as to changes in the system). The one-dimensional gradient imaging experiments were employed to determine the location of the receiver coil with respect to the interface of biphasic NMR samples, in order to optimize biphasic sample preparation. Biphasic samples of model compounds were then used to test out classic slice selection NMR experiments, and to test out the novel one-shot double-slice one-dimensional experiment and the two-dimensional TOCSY version that were developed through this work. Once the model compound biphasic sample experiments were proven successful, the experiments were expanded to more complex biphasic

samples that are more representative of real-life samples. The samples used to test these experiments were in-tube extractions of tea leaves and of hot and cold brewed coffees. The result of this research is a novel experiment that provides information about two different regions (or phases, in the case of biphasic samples) simultaneously in a single experiment. This experiment was proven to be robust and easy to implement, and it presents new opportunities for the field of slice selection NMR spectroscopy.

# Chapter 1

# INTRODUCTION

In Nuclear Magnetic Resonance (NMR) spectroscopy, a constant magnetic field is applied across a sample in the z-direction. This applied magnetic field causes the nuclear spins to precess at frequencies that correspond to the unique chemical environments of the nuclei; this is the underlying principle that enables scientists to use NMR as a tool for identifying and measuring chemical species containing atoms with nuclear spins.

Due to the fact that the frequencies of precession are unique for a given chemical environment, combined with characteristic "splitting" of frequency signals that results from coupling with the spins of other magnetically susceptible nuclei, NMR is most commonly known for its application as a structural characterization technique. In addition to qualitative analysis, NMR is also very useful for quantitation. In general, NMR signal intensity is directly proportional to the concentration of the nuclei responsible for a given signal. The combination of the ability to provide chemical identification along with quantitative information make NMR a very useful technique in the field of analytical chemistry. NMR spectra can be used to analyze mixtures, polymer composition, follow reaction kinetics, study molecular dynamics, and much more.

There are other variations of NMR experiments that can provide additional information about a given sample. For example, NMR can be used to measure self-diffusion coefficients of species, to capture "one-dimensional (1D) images" of a

sample, and to analyze physical “slices” of a sample. The latter of these variations is called slice selection NMR spectroscopy and can be used to examine the chemical composition of a sample as a function of location within the NMR tube. Slice selection NMR spectroscopy has many potential applications, such as measuring concentration gradients, evaluating dissolution, and comparing compositions of biphasic systems.

Most recent work in this NMR field has involved measurement of hydrophilic and hydrophobic metabolites via slice selection NMR performed on biphasic extractions performed directly in NMR tubes [1]. The application of this experiment to in-tube extractions greatly increases the speed and ease with which extractions like this can be analyzed by NMR (as opposed to having to perform such an extraction, and then create a separate NMR tube for each phase of the extract). As such, this approach better enables NMR to be used for metabolomics studies, which require high through-put analyses. While this work provides a great advantage to the application of slice selection NMR of biphasic samples, the classic slice selection experiments still require the acquisition of two separate experiments: one experiment for each phase.

This thesis work focuses on the further development of methodology in slice selective biphasic NMR experiments. The outcome of this work is a new version of slice selection NMR, called the one-shot double-slice (OSDS) experiment, where both phases of a biphasic sample can be observed simultaneously, while being distinguished from one another. This provides the same resolution between hydrophilic and hydrophobic extracts, while also eliminating the need for multiple experiments per sample, ultimately further reducing the experiment time and cutting the number of data sets needed to obtain this information in half. In addition, the slice

selection method described in this thesis also, in principle, enable the kinetic and dynamic studies of phase equilibria using NMR spectroscopy.

Since slice selective NMR experiments involve shaped radio frequency pulses and pulsed field gradients; this thesis is focused on those two aspects, which will ultimately be combined for slice selection applications. Chapter 2 discusses pulsed field gradients and related applications. The measurement of diffusion properties of surfactant using NMR spectroscopy is demonstrated in Chapter 2. The Stokes-Einstein equation and the Sutherland model for dynamic viscosity enable the interpretation of the measured diffusion coefficients for the surfactant across the critical micelle concentration (CMC). In Chapter 3, the general concepts of shaped pulses are first introduced. The special phenomena of spatial selection of spins when shaped pulses and pulsed field gradients are combined is then discussed. The OSDS method, a new slice selection experiment, that simultaneously detects and separates the NMR signals of the two phases of a biphasic sample is described in detail and demonstrated via its application to several model compounds in Chapter 3. Finally in Chapter 4, we apply the OSDS method to biphasic samples of in-tube tea and coffee extractions and demonstrate the unique features of this new experiment method.

## REFERENCES

[1] Seeger, K. Simple and Rapid (Extraction) Protocol for NMR Metabolomics-Direct Measurement of Hydrophilic and Hydrophobic Metabolites Using Slice Selection. *Anal Chem* **2021**, *93* (3), 1451-1457. DOI: 10.1021/acs.analchem.0c03353 From NLM Medline.

# Chapter 2

# APPLICATIONS OF PULSED FIELD GRADIENTS

## 2.1 Background of Pulsed Field Gradients

Variations of standard NMR spectroscopy utilize additional electromagnetic coils through which current can be applied to generate a controlled, homogeneous magnetic field gradient across the z-axis of the sample (along which the external magnetic field is applied), as shown in Figure 1; these are called pulsed field gradients (PFG). The "pulsed" characteristic corresponds to the fact that they are typically applied for very brief periods of around 1-2 ms. The strength of these applied field gradients is very weak relative to the overall applied field, $B_0$, of the NMR magnet.

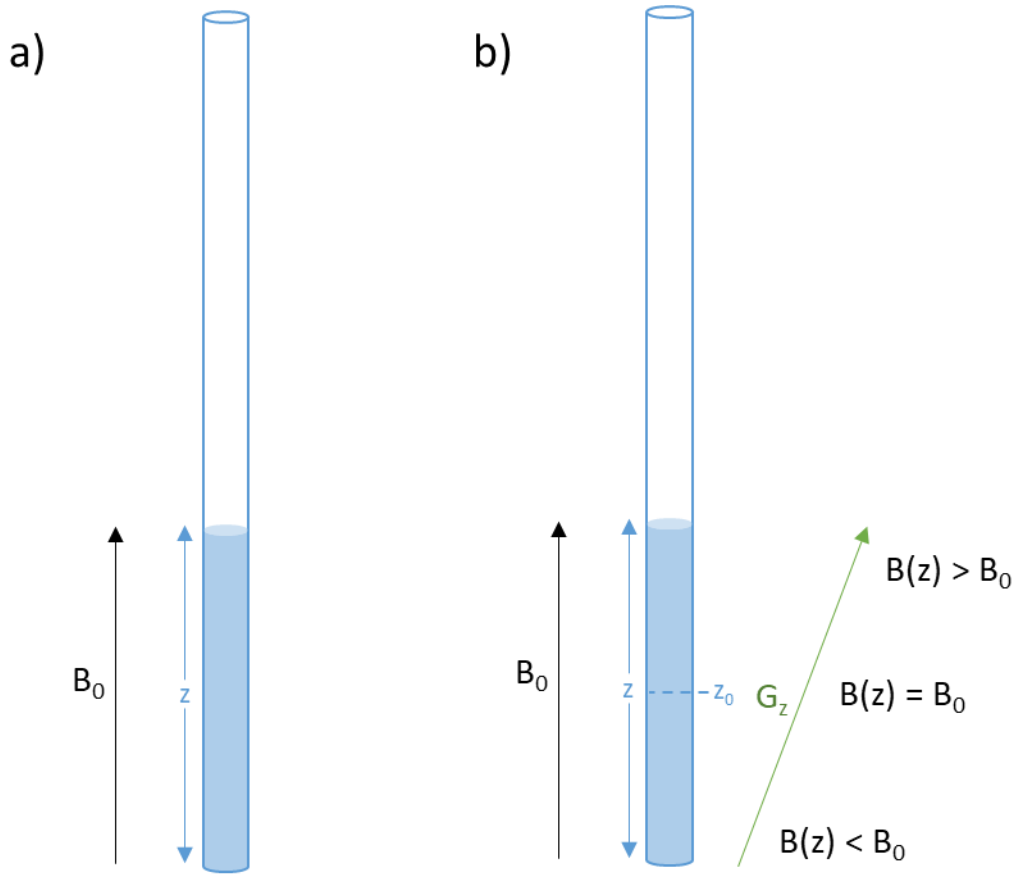


Figure 1. a) An NMR sample tube surrounded by an NMR coil in an external magnetic field, $B_0$, along the z-axis. b) The NMR sample tube subjected to an applied magnetic field gradient, $G_z$, centered at $z_0$.

The resonance frequency, $\nu_0$, of a nuclear spin is dependent on the applied magnetic field strength, $B_0$ according to Equation (2.1)

$$v_0 = \gamma B_0 / 2\pi \tag{2.1}$$

where $\gamma$ is the gyromagnetic ratio of the observed nucleus (4,258 Hz/G in the case of $^1$H). As such, the application of a magnetic field gradient across the sample length (z-axis) with a PFG causes a location-dependence in the resonance frequency for a given

nuclear spin that corresponds to the effective, local magnetic field, B(z). These local magnetic fields, B(z), vary as a function of position of those nuclei along the applied field axis following Equation (2.2)

$$B(z) = B_0 + zG_z \tag{2.2}$$

Where z represents the position and $G_z$ is the strength of the gradient applied along the z-axis. As the frequency of precession for a given nuclei is dependent on the magnetic field strength, the frequencies of the nuclei, $\nu_z$, also become dependent on z-axis position according to Equation (2.3)

$$\nu_z = \nu_0 + \gamma z G_Z/2\pi \tag{2.3}$$

In a typical NMR probe hardware arrangement, at $z_0$, the center of the applied field gradient, B(z) is equivalent to $B_0$. However, above and below the center of that applied field gradient, B(z) increases and decreases, respectively, as the positions of the nuclei move away from the center. This effect is illustrated in Figure 1b). As a result, the nuclear spins precess at frequencies faster than $\nu_0$ when $B(z) > B_0$ (above $z_0$), and at rates slower than $\nu_0$ when $B(z) < B_0$ (below $z_0$).

If the PFG is applied immediately after a radio frequency (r.f.) pulse is imposed, the transverse magnetization created by the r.f. pulse will lose coherence because the resonance spins are precessing at different rates and are no longer aligned along in the x-y plane. As a result, the spins are effectively "fanned out" in the x-y plane across the z-axis after a PFG is applied, such that the net magnetization is zero and no signal is detectable.

One of the important applications of PFGs in NMR is the measurement of diffusional properties of molecules of interest in solution. The experiment designed for this purpose is called Diffusion Ordered SpectroscopY (DOSY). Figure 2 shows the

pulse sequence for the version of the DOSY experiment used in this work, DOSY Bipolar Pulse Pair Stimulated Echo (DBPPSTE) [1]; the DBPPSTE pulse sequence was developed to reduce the effects of eddy currents induced in metal probe and coil components by the gradients. This experiment works by applying a PFG of a given strength across the length of the sample (along the z-axis). After a diffusion delay, Δ, a refocusing gradient pulse is applied. If a molecule does not move (or diffuse) far in that time, its nuclear spins will be "refocused" along the detection axis (x or y). However, if the molecule migrates far from its original position in that time, its nuclear spins will not be effectively refocused, and the signal intensity will be significantly decreased. The extent of signal intensity decrease is affected by multiple factors and can be described by Equation (2.4), called the Stejskal-Tanner formula [2]

$$S(G_z) = S_0 e^{-D\gamma^2\delta^2 {G_z}^2\left(\Delta - \delta/3\right)} \tag{2.4}$$

where $G_z$ is the strength of the gradient that is applied along the z axis, and S is the signal intensity at that gradient strength. $S_0$ is the signal intensity when the gradient strength is 0. γ is the gyromagnetic ratio of the nucleus being observed (4,258 Hz/G for $^1$H). Δ is the diffusion delay (time allowed for molecules to diffuse before refocusing), and δ is the gradient pulse duration. D is the self-diffusion coefficient of the molecules under investigation.

In a DOSY experiment, the gradient strength, $G_z$, is arrayed to produce a series of 1D spectra containing signals that are reduced to varying degrees depending on the diffusion rates of the corresponding molecules. The slower diffusing molecules will be less reduced at higher gradient strengths than the faster diffusing molecules will be. From the 1D series, a "pseudo-2D" plot is generated where the horizontal axis is chemical shift and the vertical axis corresponds to the self-diffusion coefficient.

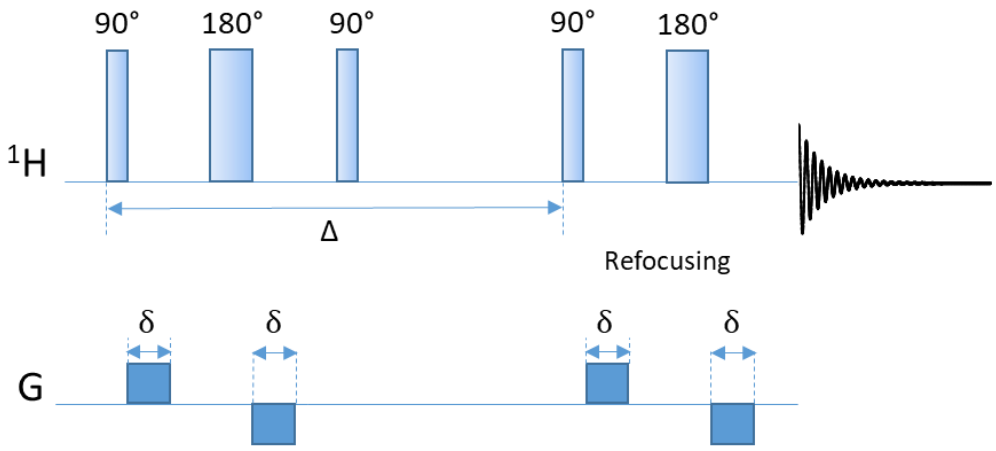


Figure 2. Schematic of the pulse sequence for the DBPPSTE version of DOSY experiments.

Stable temperature and careful calibration of the gradient strength are essential to the accuracy of NMR measurement of diffusion properties. Once these calibrations are carried out, the NMR DOSY experiment can be used to determine self-diffusion coefficients of compounds in experimental samples.

For a surfactant solution, the concentration above which all additional surfactant introduced to a solution will convert to micelles is called the critical micelle concentration (CMC). Since the surface tension of a surfactant solution reduces as micelles form within said solution, monitoring surface tension over a range of surfactant concentrations serves as a traditional method of determining the CMC [3]. One of the interesting applications of PFGs via a DOSY experiment is to measure the molecular diffusion property of a surfactant. The average self-diffusion coefficients are also closely related to the properties of a surfactant in solution. One can apply NMR diffusion measurements to investigate the formation of micelles in surfactant solutions [4]. For example, the self-diffusion coefficient can be an excellent indication

of molecular weight of an entity; the higher the molecular weight, the lower the self-diffusion coefficient should be. Because of that micelles have a significantly different self-diffusion coefficient in comparison to their counterpart surfactant monomers. It is anticipated that the self-diffusion coefficients of the surfactant species will decrease as they form large micelles that travel much slower than the monomers.

Another application of PFGs in NMR is 1D imaging. This technique is based on Magnetic Resonance Imaging (MRI) technology, where PFGs find their origin. In MRI, the instrumentation incorporates gradients along x, y, and z axes, enabling 3D imaging. In contrast, most NMR systems are only set up to generate a field gradient along the z-axis, which can still be utilized for imaging, but is then limited to a "one dimensional" image, also along the z-axis.

Because resonance frequency becomes spatially dependent when a field gradient is applied, in a 1D imaging experiment observing $^{1}H$, the NMR frequencies observed are directly proportional to the location along the sample's z-axis wherever the corresponding $^{1}H$ nuclei are present [5].

The 1D imaging technique has enabled the use of gradient shimming, which has been a great advance for sample shimming in the field. Additionally, it can be used to monitor solvent or water infiltration into various substrates or matrices [6]. It can also be used to calibrate gradient strength as an alternate to other methods.

## 2.2 NMR Diffusion Measurements of Surfactants

Natsurf 265, a product of Croda International Plc, is composed of the two different types of nonionic surfactant molecules shown in Figure 3. The trend in surface tension versus concentration for Natsurf 265 is given in Figure 4. The

inflection point around 0.3 % w/w indicates the CMC. Below the CMC, surface tension decreases as surfactant monomers pack into the liquid surface, until the bulk solution (and surface) concentration approaches a saturation level. Once the bulk solution and surface are saturated with surfactant, any additional surfactant forms micelles while keeping the bulk solution concentration at the CMC. As long as the concentration is above the CMC, surface tension levels remain constant, as the concentration of surfactant at the surface is no longer changing. As such, the surface tension measurements provide less information about changes in the surfactant system at concentrations above the CMC.

One of the goals of this work is to investigate the diffusion properties of the surfactant using the NMR pulsed field gradient method at concentrations above the CMC to provide additional insights based on diffusion properties.

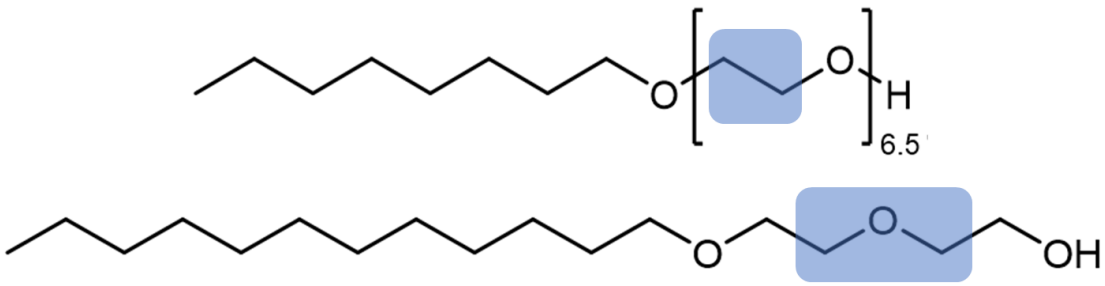


Figure 3. The components of the Natsurf 265 surfactant. The $CH_2$ signals that produce signals at 3.57 ppm are highlighted in blue here.

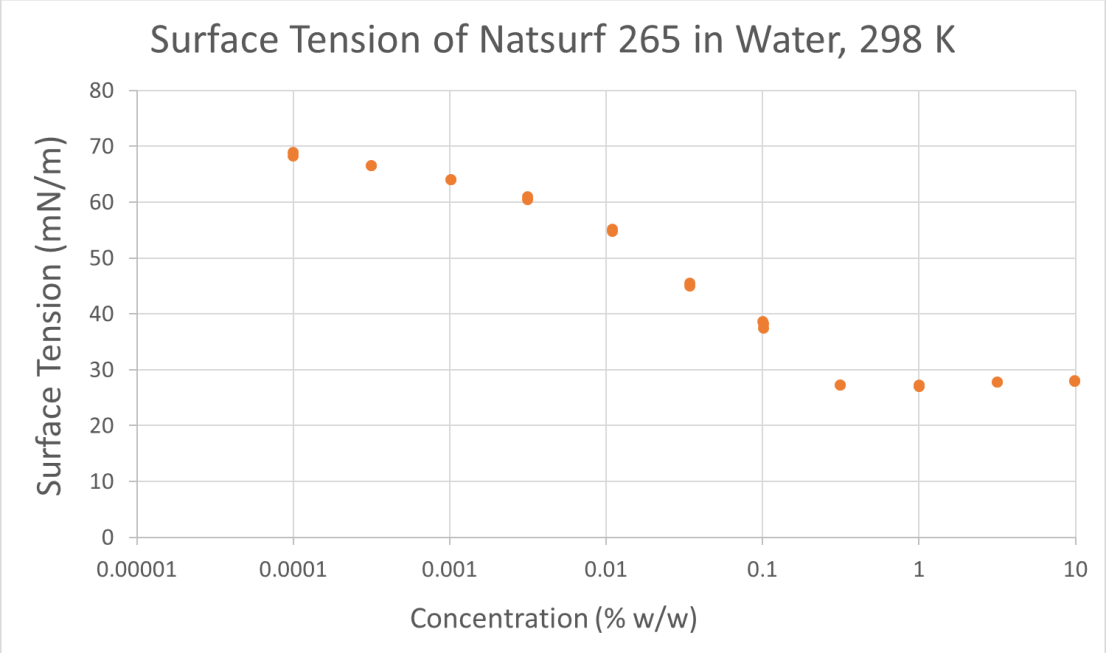


Figure 4. Surface tension measurements vs. concentration of Natsurf 265 in water at 298 K.

There are several challenging aspects to this investigation. First, the concentrations of some systems are very low for NMR experiments. In principle, increasing the number of NMR scans (measurements) can solve this problem. Second, the two types of nonionic surfactants are quite similar, and the chemical shift differences between the structural functional groups will only be slight if visible at all. It is very difficult for the DOSY experiment to differentiate between signals that overlap, and especially those that overlap heavily. The surfactant components with the shorter aliphatic chain and longer ethylene oxide chain both exhibit the unique signal at 3.57 ppm; this signal corresponds to the $CH_2$'s in the inner repeat ethylene oxide

units of these species. This work uses the signal at 3.57 ppm as a benchmark in the investigation (see Figure 3).

### 2.2.1 Experimental Methods

All NMR spectra and experiments were performed on a Varian 500 MHz VnmrS NMR spectrometer with a Performa IV z-gradient amplifier. The spectrometer was equipped with a 5mm $^{1}H$-$^{19}F/^{15}N$-$^{31}P$ PFG Switchable Broadband probe.

Temperature calibration was performed with 100% Ethylene Glycol sample with the variable temperature system set to 298 K. A typical $^{1}H$ spectrum was collected with 1 transient, a recycle delay of 30 sec, and an acquisition time of 4.67 sec. The distance between the two observed peaks was measured manually. The sample temperature can be calculated based on the measured difference between the chemical shifts of the peaks representing the hydroxyl and $CH_2$ groups.

Once the sample temperature is carefully calibrated, the gradient strength and nonlinearity must also be calibrated using a doped 1% $H_2O$ in $D_2O/GdCl_3$ sealed standard sample with a known diffusion coefficient. These calibrations are stored and used by the spectrometer system to correctly calculate self-diffusion coefficients. The nonlinearity calibrations account for any deviations out of a linear gradient across the sample area.

To calibrate the gradient strength, the 90-degree pulse width was first determined to be 10.8 μs. The VnmrJ special built-in macro, Doneshot_nugmap, was then used with the calibrated temperature value from the ethylene glycol calibration. Based on the experiment output, the VnmrJ software calculated the gradient strength and calibrated the nonlinearity variables, storing them for future experiments.

To verify the calibrations, the same standard sample (doped 1% $H_2O$ in $D_2O/GdCl_3$) was analyzed with two different pulse sequences: DOSY Bipolar Pulse Pair Stimulated Echo and DOSY Bipolar Pulse Pair Stimulated Echo with a convection compensation component. The results obtained from both pulse sequences will be discussed later.

A neat sample of Natsurf 265 was provided by Kevin Penfield (Croda). The Naturf 265 sample was diluted (stepwise where appropriate) in $D_2O$ to create solutions of the following weight concentrations (% w/w): 20, 10, 5, 2, 1, 0.6, 0.22, 0.2, 0.15, 0.1, 0.01, and 0.001.

The 90-degree radio frequency (r.f.) pulse width was calibrated on the 1% Natsurf 265 sample and the result was the same as that for the 1% $H_2O$ in $D_2O/GdCl_3$ sealed standard. The DOSY Bipolar Pulse Pair Stimulated Echo (DBPPSTE) pulse sequence (Figure 2) was used to collect DOSY spectra of each surfactant sample. The percent reduction from lowest to highest gradient strengths in the array was checked for each sample, and the diffusion delay and the gradient pulse duration were adjusted such that the signal intensity at the highest gradient strength was reduced to 5-15% of the signal at the lowest gradient strength. In all measurements, the gradient strength maxima/minima were set to the allowed limits. The gradient strength was arrayed across 15 increments for each sample. The number of scans collected per increment was adjusted for each sample based upon concentration and resulting S/N ratios. For the lowest concentration sample tested, 256 transients were collected per increment, resulting in a total experiment time of 12 hours. Table 1 summarizes the experimental parameters for each surfactant sample.

Table 1. DOSY experimental parameters used for each concentration of Natsurf 265 in $D_2O$.

| Natsurf % w/w | transients | Del (Δ, sec) | gt1 (δ*2, sec) | total experiment time (hr:min:sec) |
|---|---|---|---|---|
| 0.001 | 256 | 0.070 | 0.002 | 11:28:59 |
| 0.01 | 128 | 0.065 | 0.002 | 05:45:03 |
| 0.1 | 64 | 0.070 | 0.002 | 02:53:20 |
| 0.15 | 64 | 0.073 | 0.002 | 02:53:23 |
| 0.2 | 64 | 0.075 | 0.002 | 02:53:26 |
| 0.22 | 64 | 0.075 | 0.002 | 02:53:25 |
| 0.6 | 64 | 0.080 | 0.0022 | 02:53:31 |
| 1 | 32 | 0.080 | 0.003 | 01:27:29 |
| 2 | 32 | 0.082 | 0.003 | 01:27:31 |
| 5 | 32 | 0.085 | 0.004 | 01:27:32 |
| 10 | 16 | 0.095 | 0.005 | 00:44:32 |
| 20 | 16 | 0.095 | 0.007 | 00:44:33 |

*The following parameters were constant for all samples: relaxation delay of 6 sec, 15 increments, gzlvl1 min of 1130 DAC, gzlvl1 max of 32500 DAC*

### 2.2.2 Results and Discussion

The ethylene glycol signals had a chemical shift difference of 1.647 ppm between the peaks for the hydroxyl and $CH_2$ groups when the sample temperature was set to 298 K. Based on this chemical shift difference, the calibrated temperature was calculated to be 299.99 K and this temperature was used in the gradient calibrations.

Initially, a convection-compensation diffusion experiment (DOSY Bipolar Pulse Pair Stimulated Echo with convection compensation) was used to check if the calibration was successful using the doped 1% $H_2O$ in $D_2O/GdCl_3$ standard. However, this pulse sequence was giving a self-diffusion value of 21.4 x $10^{-10}$ $m^2/s$ for the HOD signal, which is inconsistent with the reported value of 19.8 x $10^{-10}$ $m^2/s$ at 299.99 K.

However, a standard DOSY Bipolar Pulse Pair Stimulated Echo pulse sequence (shown in experimental section) was then tried and generated a value of 19.7 x $10^{-10}$ $m^2/s$ at 299.99 K. The convection compensation experiments in principle provide improved results when convection is interfering with the diffusion measurements, however they also introduce added complications to the pulse sequence that can lead to errors. Based upon these results, the standard version of the DOSY Bipolar Pulse Pair Stimulated Echo (which has no convection compensation component) was chosen as the pulse sequence to use for the surfactant experiments. Table 2 and Figure 6 below summarize the self-diffusion coefficients measured for the signal at 3.57 ppm corresponding to the long chain ethylene oxide $CH_2$'s as a function of concentration.

Table 2. Calculated Natsurf 265 concentrations (in $D_2O$) and corresponding self-diffusion coefficients for the ethylene oxide group signal (3.57 ppm).

| Natsurf Concentration (% w/w) | D (x $10^{-10}$ $m^2/s$) |
|---|---|
| 0.00101 | 3.3 ±0.2 |
| 0.0102 | 3.3 ±0.2 |
| 0.101 | 3.3 ±0.2 |
| 0.149 | 3.4 ±0.1 |
| 0.218 | 3.3 ±0.1 |
| 0.605 | 2.28 ±0.09 |
| 1.01 | 1.75 ±0.05 |
| 1.94 | 1.26 ±0.04 |
| 5.00 | 0.76 ±0.02 |
| 10.02 | 0.50 ±0.02 |
| 20.03 | 0.30 ±0.01 |

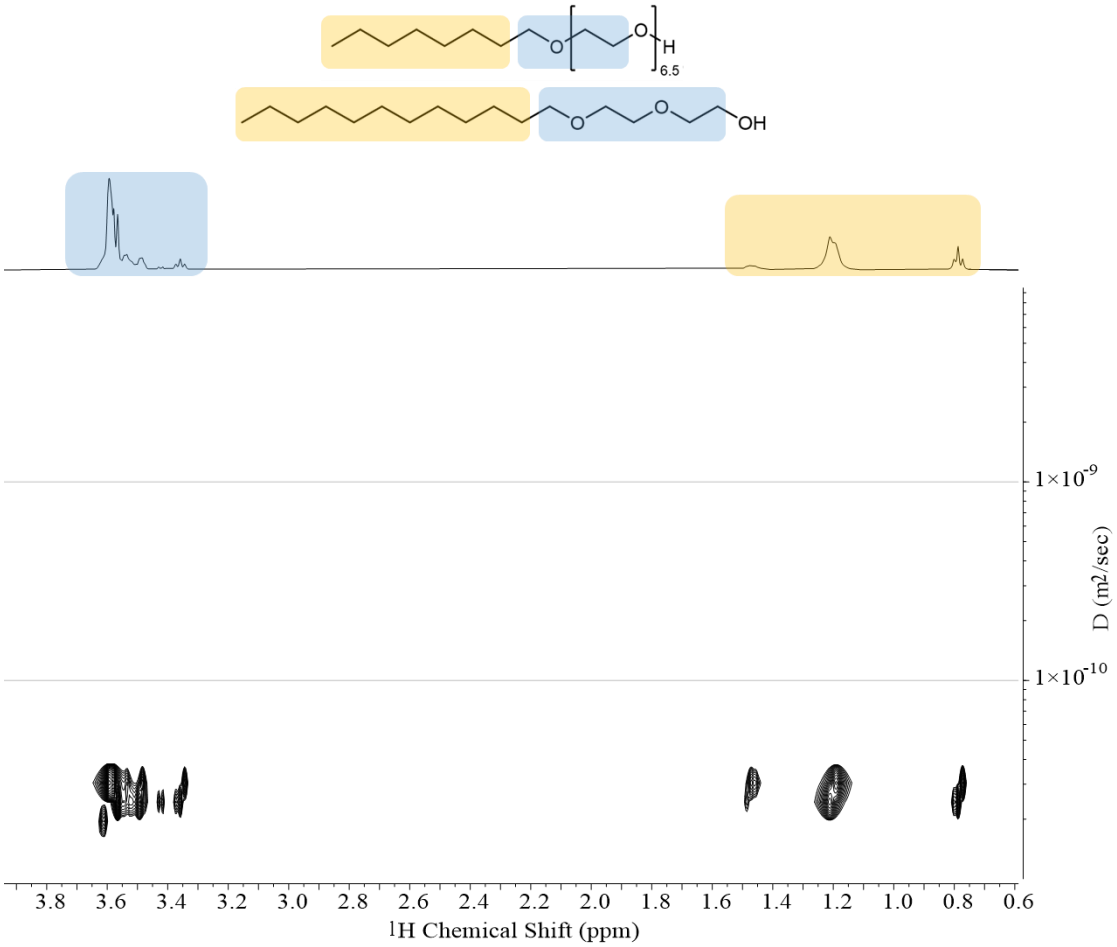


Figure 5. DOSY NMR spectrum of Natsurf 265 at a concentration of 20 % w/w.

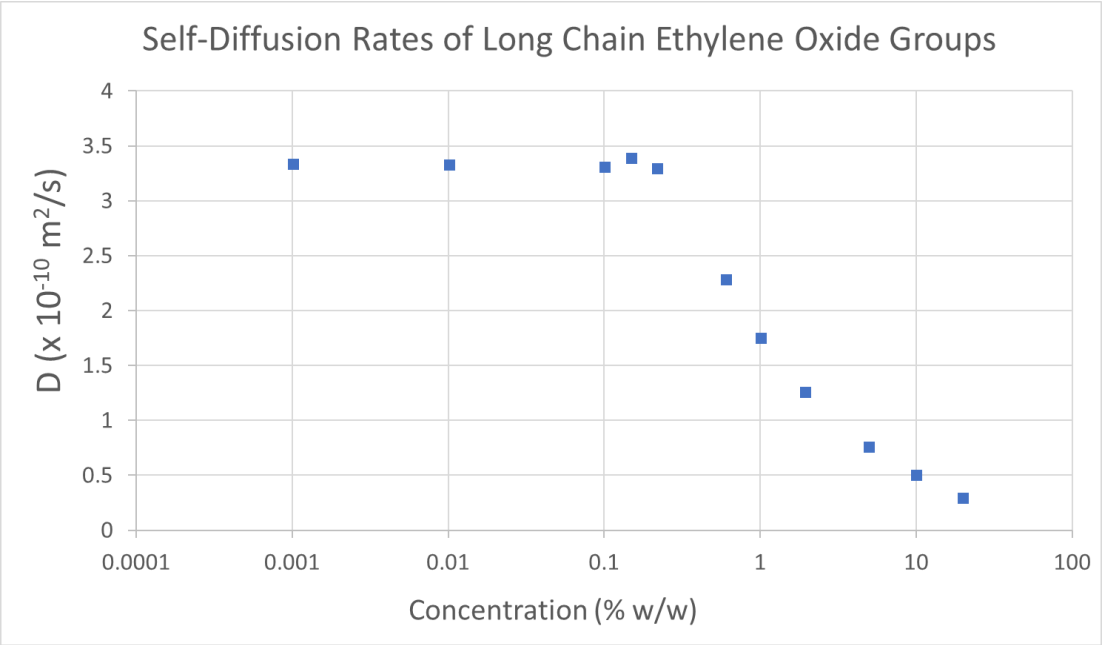


Figure 6. Self-diffusion coefficients for the long chain ethylene oxide signal at 3.57 ppm over a range of concentration of Natsurf 265 in $D_2O$.

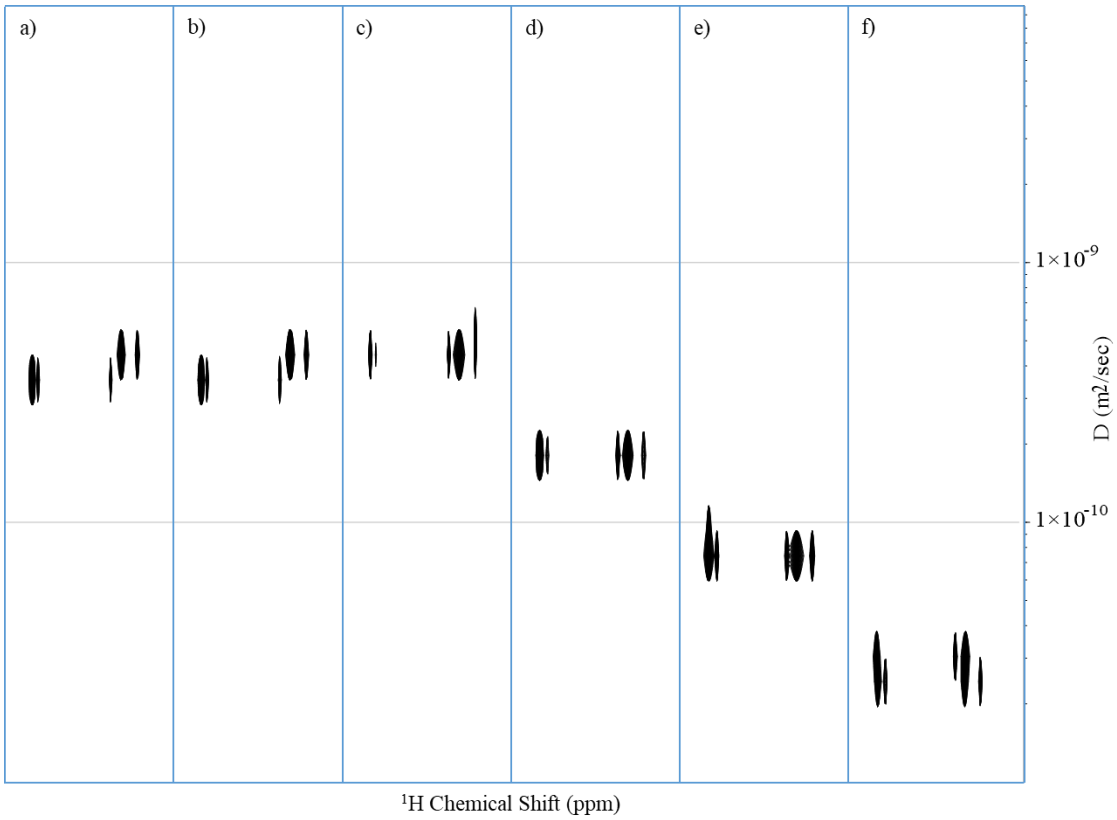


Figure 7. Surfactant region in the DOSY spectra of four Natsurf 265 solutions in $D_2O$ at concentrations of a) 0.01, b) 0.1, c) 0.2, d) 1, e) 5, and f) 20 % w/w.

Figure 5 shows the 2D DOSY NMR spectrum for Natsurf 265 (20 % w/w); the corresponding $^1H$ 1D NMR spectrum is presented as a projection at the top of the 2D DOSY spectrum. The Natsurf 265 structural components are highlighted with yellow and blue to correlate the NMR signals to the corresponding functional groups in the surfactant molecules. The cross peaks indicate the self-diffusion coefficients that correspond to the respective $^1H$ NMR signals. The panel plot in Figure 7 shows the 2D DOSY spectra for Natsurf 265 at the weight concentrations of 0.01, 0.1, 0.2, 1, 5, and

20 %. As is also observed in the graph for the 3.57 ppm ethylene oxide signal (Figure 6), the general trend of the self-diffusion coefficient (D, $m^2$/sec) remains essentially constant when the concentration is equal and below 0.2 % w/w, but begins decreasing at concentrations greater than 0.2 % w/w.

For polydispersed polymers and mixtures with overlapping signals, significant spread and variation in the self-diffusion coefficients is a common observation in corresponding DOSY spectra. However, this is typically not observed for surfactant micelles, due to short residential periods of surfactant monomer within the micelles, which results in a complete time-averaging of the molecular self-diffusion coefficients [4]. There is some polydispersity within the Natsurf 265 (as evidenced from the chemical structures and the fact that there are two components), and there are some regions of varying flexibility within a molecule, so any spread in the self-diffusion coefficients at a given concentration is likely due to this, and it is important to note that for a given concentration, all of the Natsurf 265 signals have very similar diffusion coefficients. It is also observed that the diffusion coefficients of Natsurf 265 below and above the CMC differ by about one order of magnitude. The diffusion coefficients of Natsurf 265 below the CMC is about one order of magnitude smaller than that of water molecules.

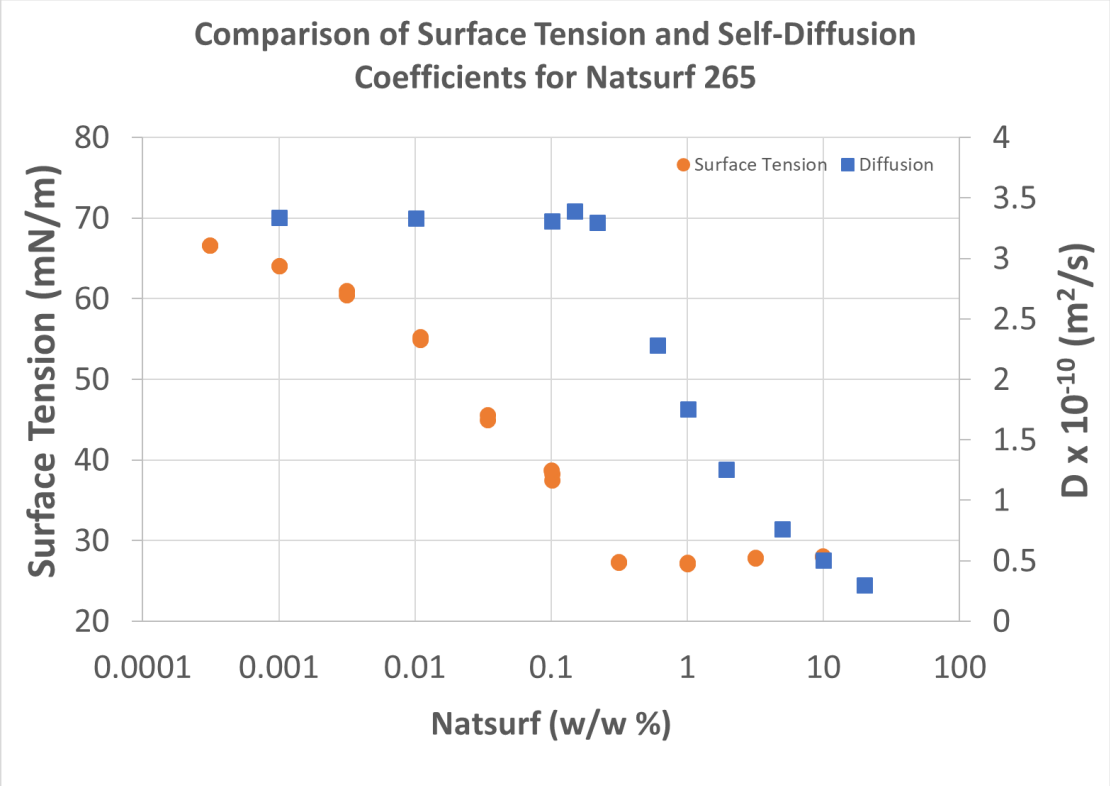


Figure 8. A comparison of surface tension values and self-diffusion coefficients across various concentrations of Natsurf 265.

The self-diffusion coefficients and surface tension values both show distinct inflection points around the same concentration, indicating an agreement as to the CMC (Figure 8). Diffusion NMR data can be used to define the CMC by determining the intersection of the linear sections of self-diffusion coefficients as a function of the inverse of total concentration ($1/C_T$) before and after the CMC [7]. Based upon the experimental NMR diffusion data, the CMC for Natsurf 265 was determined to be 0.359 % w/w from the intersection of the two linear functions that fit the data before

and after the inflection point of the diffusion data (Figure 9). This agrees with the CMC determined similarly from the surface tension data, which was found to be 0.408 % w/w, based on the intersection of the logarithmic function representing the concentrations just below the CMC and the linear function representing the concentrations just above the CMC, at which point the surface tension should be relatively constant (Figure 10). The discrepancy between the two values could be partially attributable to the different techniques for the CMC determination having been employed with a slight difference in temperature. It is well-known that the CMC also depends on the sample temperatures.

a)

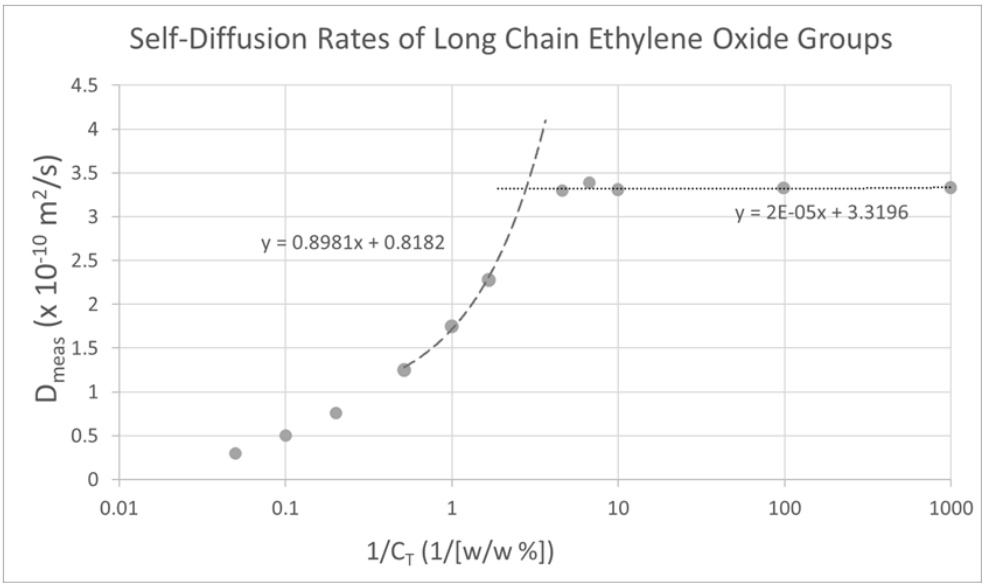


b)

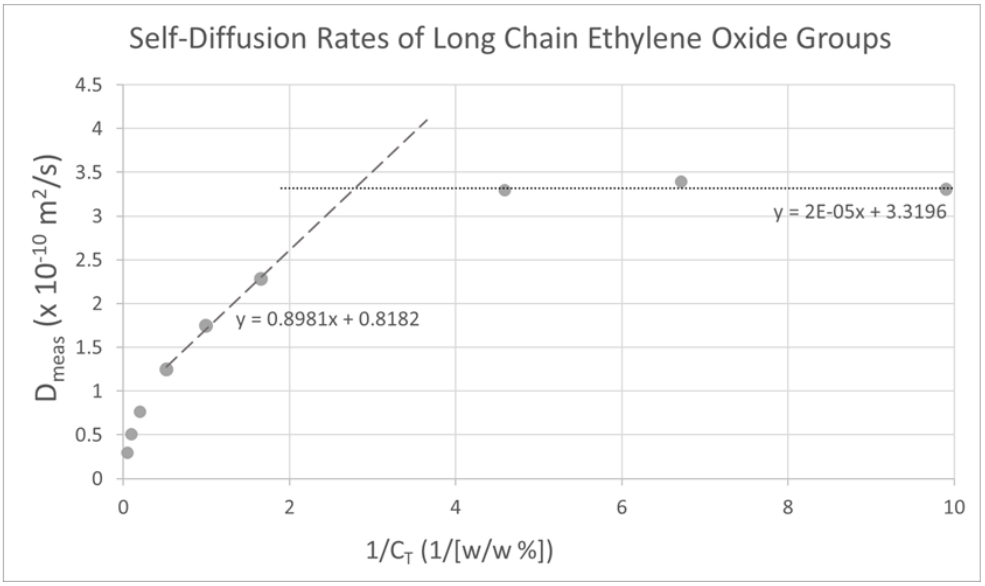


Figure 9. Plots of the measured self-diffusion coefficients for Natsurf 265 as a function of the inverse of the total concentration a) on a logarithmic scale, showing all concentration data collected, and b) on a linear scale, zoomed in to show the region for concentrations above the CMC (with low $1/C_T$ values). The linear segments above and below the CMC are fit to equations to determine their intersection.

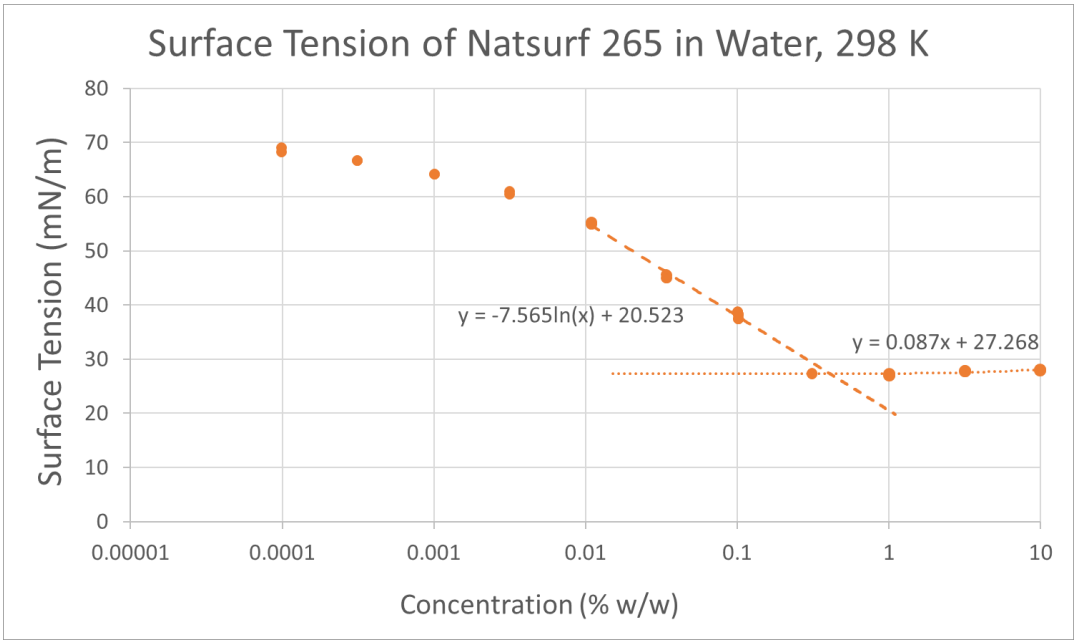


Figure 10. Plot of the measured surface tension for Natsurf 265 as a function of the total concentration on a logarithmic scale, showing all concentration data collected. The linear segment above and the logarithmic segment below the CMC are fit to equations to determine their intersection.

Depending on whether the system in question is above or below the CMC, the measured diffusion coefficient, $D_{meas}$, is defined differently, per the following two equations [7]. When the total surfactant concentration, $C_T$, is less than or equal to the CMC ($C_T \leq CMC$), $D_{meas}$ is described as

$$D_{meas} = D^{mon} \tag{2.5}$$

where $D^{mon}$ is the self-diffusion coefficient of the monomer. When the total surfactant concentration surpasses the CMC ($C_T > CMC$), $D_{meas}$ becomes [7]

$$D_{meas} = D^{mic} + \frac{CMC}{C_T}\left(D^{mon} - D^{mic}\right) \tag{2.6}$$

where $D^{mic}$ is the self-diffusion coefficient of the micelle; this equation assumes the residential period of the monomers within the micelles is sufficiently fast as that the observed diffusion coefficient is a weighted average of the monomer and micelle, as proposed previously.

Based on Equation (2.5), and the linear trend for the diffusion data when the concentrations are below the CMC (Figure 9), the NMR measurements indicate that $D^{mon}$ for Natsurf 265 is 3.32 x $10^{-10}$ $m^2/s$.

Under the assumption that the concentration of surfactant in the monomer form remains constant and equal to the CMC once the system is at concentrations above the CMC, $D_{meas}$ would be expected to have a linear relationship to the inverse of $C_T$ at that point, based on Equation (2.6). However, it is evident that this is not the case for Natsurf 265.

When the $D_{meas}$ for Natsurf 265 concentrations above the CMC are fit to a power function (Figure 11), the exponent is -0.57. When experimental error is factored in, this exponent is essentially -1/2, indicating that the diffusion coefficient may be inversely proportional to $\sqrt{C_T}$.

To understand the implications of this relationship, the Stokes-Einstein equation is first be considered:

$$D = \frac{k_B T}{6\pi\eta \mathrm{r}} \tag{2.7}$$

Here, η is the dynamic viscosity, *r* is the micellar radius, T is sample temperature, and $k_B$ is the Boltzmann constant. It is assumed that the shape of the micelle is essentially spherical with the hydrophobic tails pointing towards the core of the micelle and the hydrophilic heads pointing out towards the aqueous environment. If the radius of the micelle is also assumed to stay constant as more surfactant is added to solution, the

volume of the micelles can be considered constant. Under those assumptions, the addition of further surfactant only increases the mass of the micelle without changing the apparent volume (see Figure 12).

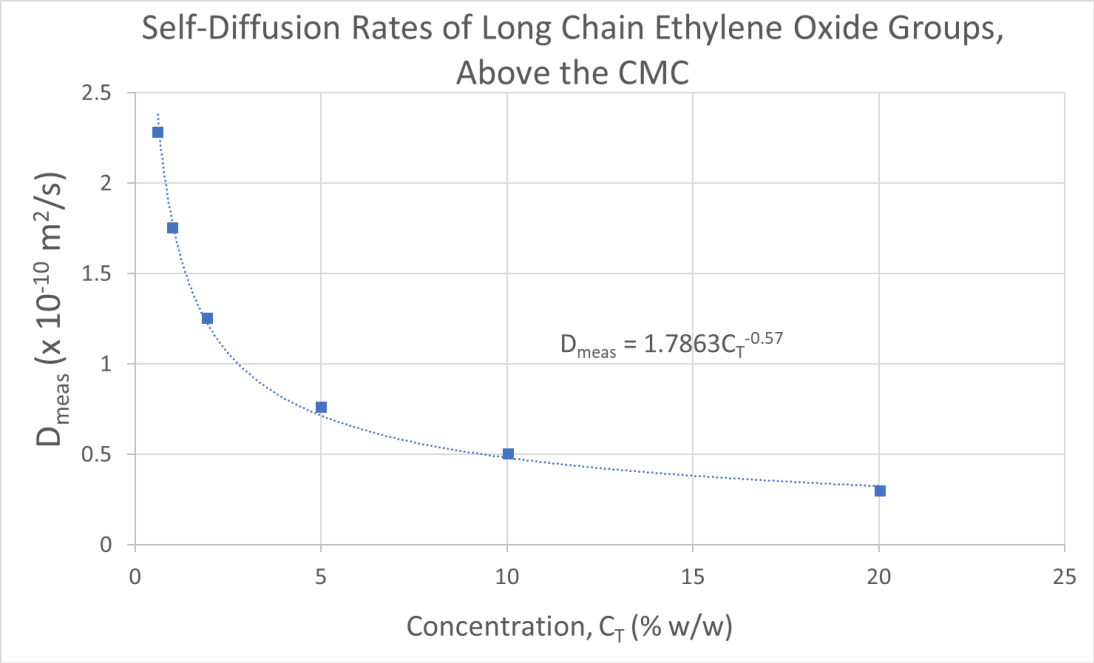


Figure 11. The experimental diffusion coefficients of Natsurf 265 above the CMC fit a power function with a -1/2 exponent (within experimental error).

Under these considerations, the Sutherland equation can be used to model the dynamic viscosity of the solution [8]:

$$\eta = k_S\sqrt{T} \tag{2.8}$$

where

$$k_s = \frac{\sqrt{k_B m}}{4\pi^3 r^2} \tag{2.9}$$

In Equation (2.9), *m* is the mass of the micelle. If the effective volume of the micelles ($V_{micelle}$) does not change significantly as previously discussed,

$$m = C_T V_{micelle} \tag{2.10}$$

The effective micelle volume $V_{micelle}$, is related to the effective radius of the micelle:

$$V_{micelle} = \frac{3}{4}\pi r^3 \tag{2.11}$$

Rearrangements of these equations leads to the following relationship:

$$D = \frac{\sqrt{3\pi}}{3\pi}\frac{\sqrt{k_B r T}}{\sqrt{C_T}} \tag{2.12}$$

Equation (2.12) indicates that the diffusion coefficient is inversely proportional to $\sqrt{C_T}$ if the size of the micelle does in fact remain constant. The experimental diffusion data for Natsurf 265, as shown in Figure 11, appears to support this model. A schematic of this model is depicted in Figure 12c and 12d. Figure 12 also portrays the system at concentrations below (a) and just at (b) the CMC, where monomers partition between the surface and the solution until the CMC is reached, after which point micelle formation begins, keeping the surface and solution concentrations constant.

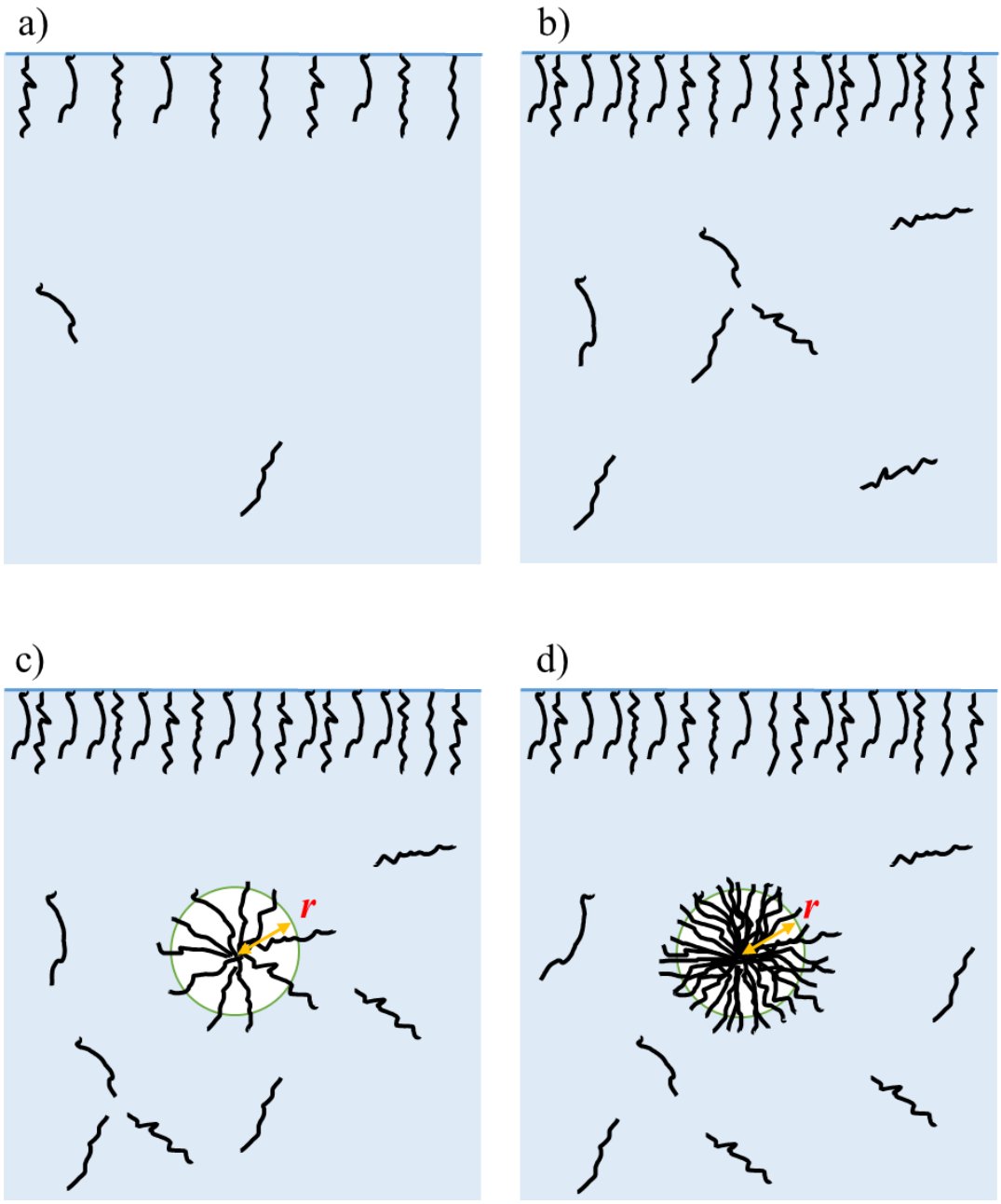


Figure 12. Schematic of Natsurf 265 in solution at concentrations a) below the CMC, b) at the CMC, c) just above the CMC where additional surfactant molecules start to form micelles, and d) further above the CMC, at which point the micelle mass increases, but the volume and the radius, r, stay constant.

### 2.2.3 Conclusions

The NMR diffusion property measurements of Natsurf 265 presented here demonstrate that diffusion NMR serves as a complimentary method to the surface tension measurement for the investigation of the surfactants, particularly when the total concentration of surfactant is above the CMC. In the Natsurf 265 solutions, it appears that micelles form as spherical entities, while the effective volume is kept constant. The Stokes-Einstein equation for diffusion properties, along with the Sutherland model for dynamic viscosity, can be used to interpret the NMR diffusion data for Natsurf 265 solution.

## 2.3 One-Dimensional Imaging of Biphasic Samples Using Pulsed Field Gradients

The 1D NMR image for a sample is a projection of the profile of that sample along the z-axis, where the location along z is represented by a frequency, and the intensity of the signal at a given location represents the density of the population of spins of the observed nucleus at that location. The portion of the sample that is observed is the portion that is located within the excitation range of the receiver coil, and in this work, the observed nucleus is $^{1}H$.

A 1D NMR image of a monophasic sample will essentially look like a sideways image, or profile, of the tube, with near equal intensity across the NMR receiver coil. Imperfections in this image when collected in real life represent imperfections in the magnetic field homogeneity. The 1D NMR image for a biphasic sample will present in a more interesting way. As the image represents only the density of $^{1}H$ nuclei, the portion containing a greater concentration of $^{1}H$ nuclei will produce a higher-intensity profile, and there will be a clear distinction between the two

phases based on that concentration difference. This image will prove to be very important for optimizing the preparation of biphasic samples for slice selective experiments, as it will help identify the center of the receiver coil with respect to the NMR tube. The center of the receiver coil will be at the center of the 1D image, and this is the optimal location for the interface of the two phases. Examples of this application of 1D-imaging are presented in this chapter.

Figure 13 shows the pulse sequence for the 1D gradient-echo experiment [9] used for the 1D imaging in this work (see Appendix B). This pulse sequence involves a short excitation pulse (in this case, 2 μs), followed by a short dephasing gradient, and then a longer "read" gradient of opposite sign that is applied during the FID acquisition. The application of this read gradient during the acquisition period has the effect of encoding the sample's spatial coordinates along z as frequency components; this is ultimately what produces the 1D image of the sample.

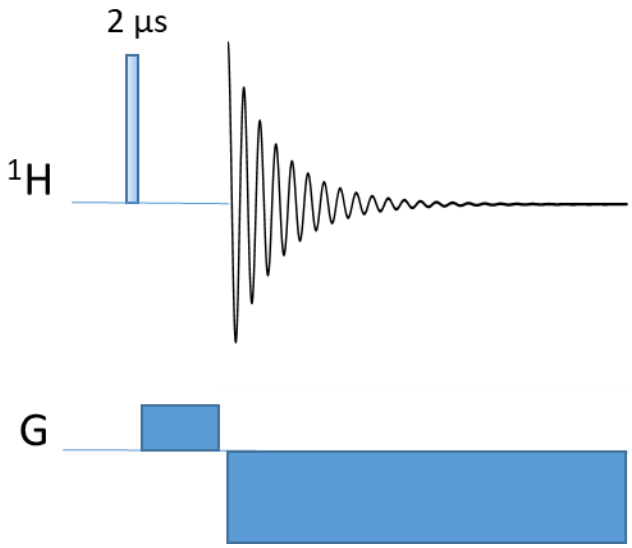


Figure 13. Schematic of the pulse sequence for the 1D gradient-echo experiment used for 1D NMR imaging in this work.

### 2.3.1 Experimental Methods

A homogeneous sample of at 1% (w/w) Natsurf 265 in $D_2O$ was prepared following the methodology described in 2.2.1.

Two biphasic model samples were prepared at Genentech using $D_2O$ from Cambridge Isotope Labs, $CDCl_3$ also from Cambridge Isotope Labs, D-Glucose from Sigma Life Science, and 2,3-Dichloro-1,4-naphthoquinone from Alfa Aesar. The solutions were prepared in separate scintillation vials at desired concentrations, and long glass pipette tips were used to carefully transfer approximately equal amounts of the organic and aqueous solutions into the NMR tubes, attempting to avoid getting solution on the tube sidewalls and minimize mixing of the two phases (both of which would cause issues in the resulting spectra for later experiments). The organic solution was transferred into the NMR tube first, as chloroform has a higher density than water

and will settle as the lower layer. The two samples prepared were Genentech Model Biphasic Sample #1 (GNE M1) and Genentech Model Biphasic Sample #2 (GNE M2). GNE M1 was prepared to match standard NMR sample amounts used in the Genentech lab of 600 μL, and approximately 300 μL of each solution were added to the tube; concentrations were 10,000 μg/mL each of 2,3-dichloro-1,4-naphthoquinone in $CDCl_3$ and D-glucose in $D_2O$. Based on experimental observations for GNE M1 (discussed in the results and conclusions below), GNE M2 was prepared by physically marking on the outside of the NMR tube the location of the center of the receiver coil and adding approximately equal amounts of the each solution such that the interface of the two phases sat at/near the receiver coil center (physically marked on the tube); the resultant sample contained approximately 500 μL total and 250 μL of each solution. Concentrations for the GNE M2 sample were also lowered by an order of magnitude to 1,000 μg/mL each of 2,3-dichloro-1,4-naphthoquinone in $CDCl_3$ and D-glucose in $D_2O$.

### 2.3.2 Results and Discussion

As expected, the 1D NMR image of the monophasic 1% Natsurf sample in $D_2O$ is a homogeneous profile of the NMR tube along the z-axis (Figure 14). The 1D NMR image of GNE M1 (Figure 15a) is primarily composed of a profile corresponding to the organic $CDCl_3$ layer, with the interface and aqueous $D_2O$ layer evident at the right side of the image. In contrast, the interface between the organic and aqueous layers is observed at the center of the 1D NMR image of GNE M2 (Figure 15b).

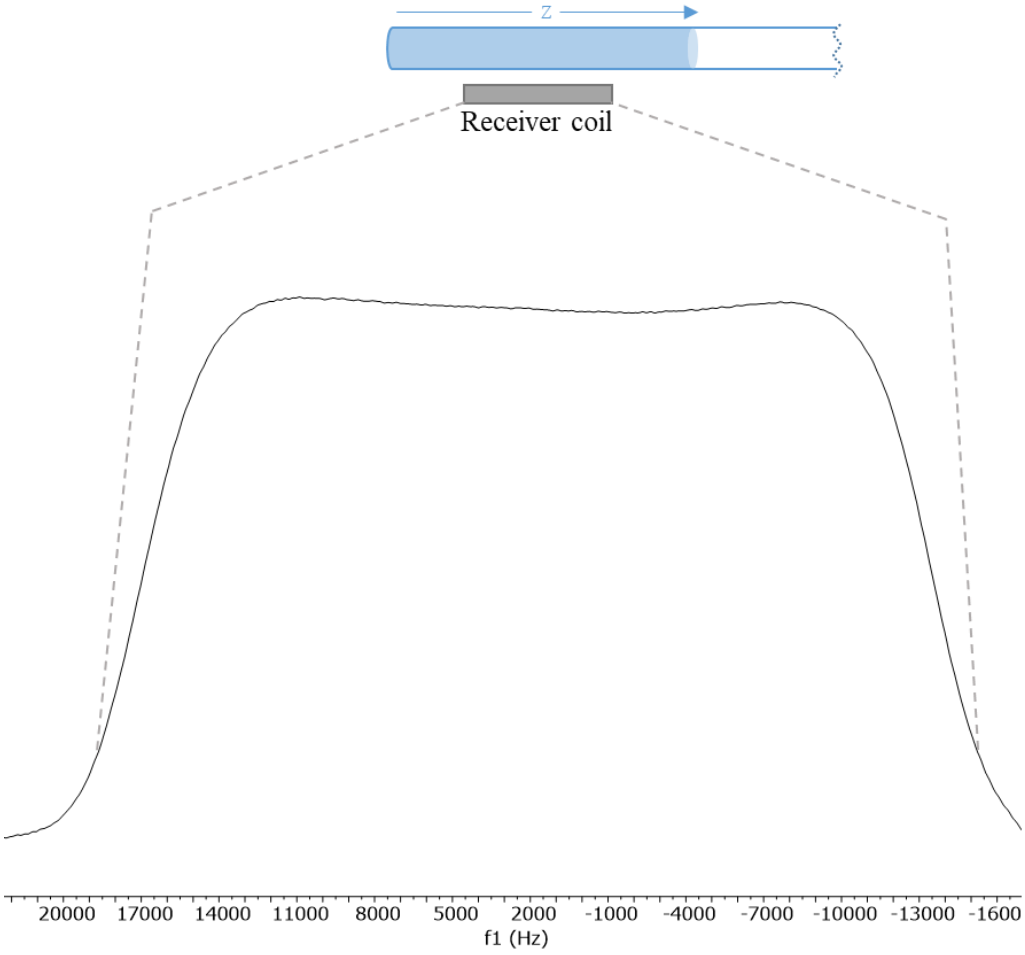


Figure 14. 1D NMR image of a homogeneous sample of 1% Natsurf in $D_2O$.

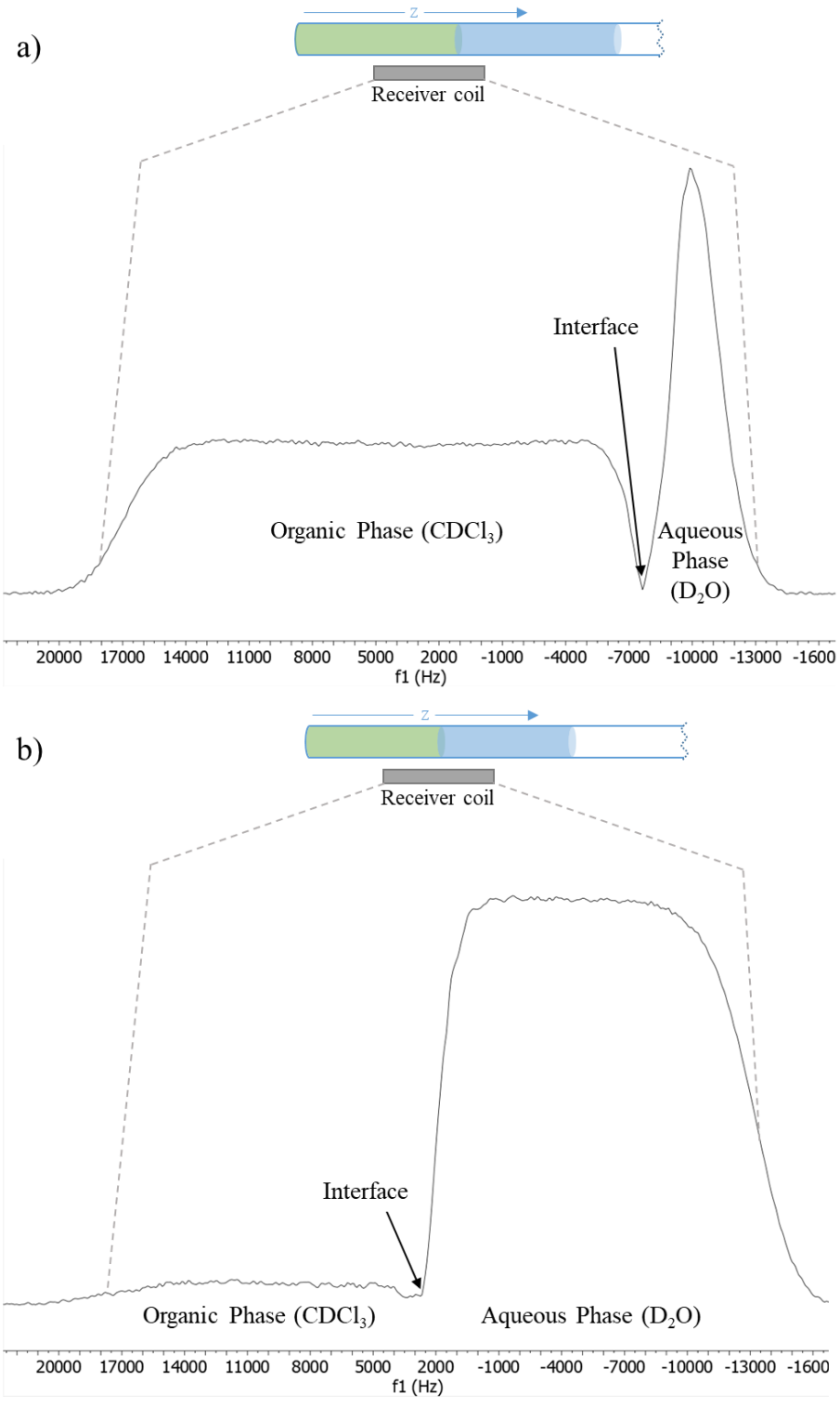


Figure 15. 1D NMR images of biphasic samples a) GNE M1 and b) GNE M2.

The 1D NMR image of the monophasic 1% Natsurf sample shown in Figure 14 indicates that the imaging experiment is working properly. The edges of the image profile indicate the edges of the receiver coil. However, this does not provide very much information as to the location of the receiver coil with respect to the edges or center of the sample volume within the NMR tube (as the receiver coil is smaller than the sample volume).

In the 1D $^{1}H$ NMR images of GNE M1 and GNE M2 (Figure 15), the organic $CDCl_3$ layer has significantly lower signal intensity as compared to the aqueous $D_2O$ layer. The intensity difference between the two phases is greater than the difference that would be expected based on the model compounds alone. If the relative concentrations and number of hydrogens per each unit weight of solute are the only factors to be considered, the intensity ratio between aqueous and organic phases should be on the order of 3.8:1. The additional intensity observed experimentally in the aqueous phase is likely due to a relatively large amount of $H_2O$ present as an impurity in the $D_2O$ solvent.

In the image of GNE M1 (Figure 15a), the fact that the aqueous signal and the interface are evident at the right side of the image provides spatial orientation in that going from the left side to the right side of the images represents going from the bottom of the tube to the top. This is based on the signal intensity of the aqueous layer combined with the knowledge that $CDCl_3$ is actually higher density than $D_2O$, and as such, would sit as the bottom layer in the NMR tube.

The location of the interface observed in the 1D NMR image of GNE M1 also provided insight that adding 300 μL of each phase to the tube placed the interface of

the two phases at the edge of the receiver coil, and most of the aqueous phase outside of the receiver coil. This was confirmed by placing the GNE M1 sample in a Bruker sample gauge (Figure 16a) and observing the approximate location of a Bruker 5mm receiver coil relative to the NMR tube; this was then used to estimate where the interface should be in order for it to be located close to the center of the receiver coil (Figure 16b).

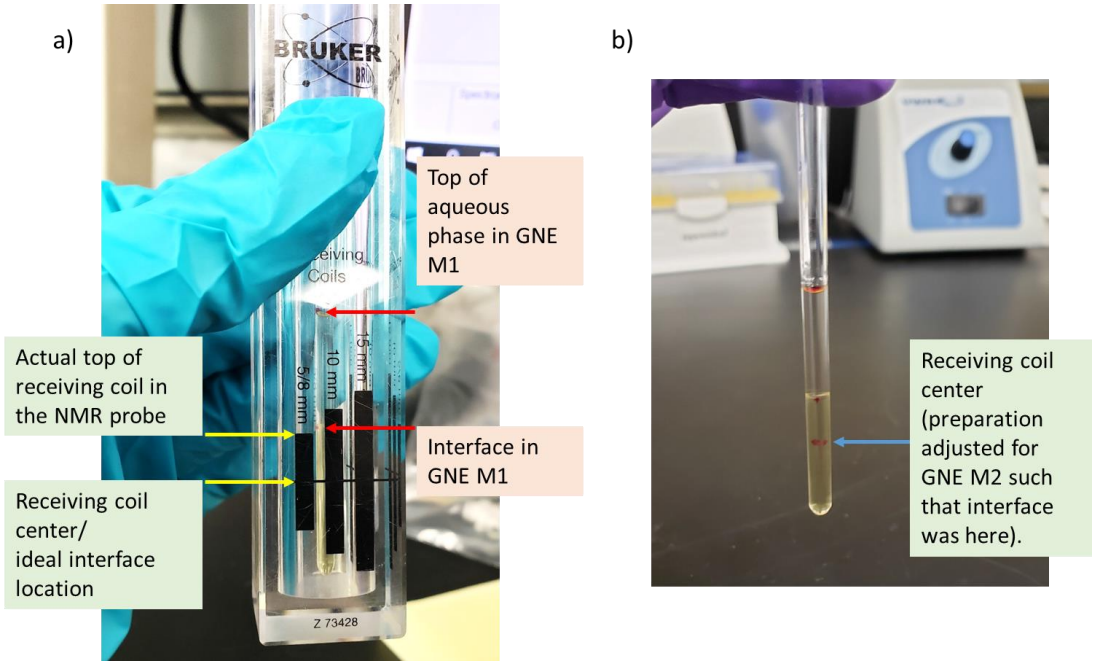


Figure 16. a) GNE M1 NMR tube inside sample gauge, confirming that the interface is much higher than the center of the receiving coil, and that the majority of the aqueous phase is not within the receiving coil; b) GNE M1 NMR tube marked with the proper biphasic interface for reference during preparation of GNE M2

This information was used to prepare GNE M2, with the hopes that the interface would be near the center of the receiver coil and optimized for slice selection NMR experiments. The 1D image of GNE M2 (Figure 15b), showed an interface at the center of the image profile, indicating it was in fact centered in the receiver coil. Based upon these 1D image results, the sample volumes and heights within the GNE M2 NMR tube were then used for the preparation of all further biphasic samples.

### 2.3.3 Conclusions

The 1D image NMR experiment can be used to profile biphasic NMR samples quickly and effectively, which enables an accurate assessment of biphasic samples used for the methodology development in the slice selection NMR experiments. The experiment, which is very easy and robust, demonstrates the powerful application when pulse field gradient is included in a NMR experiment.

## REFERENCES


[1] Wu, D. H.; Chen, A.; Johnson, C. S. An Improved Diffusion-Ordered Spectroscopy Experiment Incorporating Bipolar-Gradient Pulses. *Journal of Magnetic Resonance, Series A* **1995**, *115* (2), 260-264. DOI: 10.1006/jmra.1995.1176.

[2] Stejskal, E. O.; Tanner, J. E. Spin Diffusion Measurements: Spin Echoes in the Presence of a Time-Dependent Field Gradient. *The Journal of Chemical Physics* **1965**, *42* (1), 288-292. DOI: 10.1063/1.1695690.

[3] Burlatsky, S. F.; Atrazhev, V. V.; Dmitriev, D. V.; Sultanov, V. I.; Timokhina, E. N.; Ugolkova, E. A.; Tulyani, S.; Vincitore, A. Surface tension model for surfactant solutions at the critical micelle concentration. *J Colloid Interface Sci* **2013**, *393*, 151-160. DOI: 10.1016/j.jcis.2012.10.020 From NLM Medline.

[4] Söderman, O.; Stilbs, P. NMR studies of complex surfactant systems. *Progress in Nuclear Magnetic Resonance Spectroscopy* **1994**, *26*, 445-482. DOI: 10.1016/0079-6565(94)80013-8.

[5] Levitt, M. H. *Spin Dynamics: Basics of Nuclear Magnetic Resonance*; John Wiley & Sons, Inc., 2001.

[6] Le Feunteun, S.; Diat, O.; Guillermo, A.; Poulesquen, A.; Podor, R. NMR 1D-imaging of water infiltration into mesoporous matrices. *Magn Reson Imaging* **2011**, *29* (3), 443-455. DOI: 10.1016/j.mri.2010.10.001 From NLM Medline.

[7] Denkova, P. S.; Van Lokeren, L.; Verbruggen, I.; Willem, R. Self-Aggregation and Supramolecular Structure Investigations of Triton X-100 and SDP2S by NOESY and Diffusion Ordered NMR Spectroscopy. *Journal of Physical Chemistry B* **2008**, *112* (35), 10935-10941. DOI: 10.1021/jp802830g.

[8] Dybowski, D.; Teplyakov, A. *Essential Data and Equations for a Course in Physical Chemistry*; D&T Publishing Company.

[9] *NMR Tips for Shimming, Part III. Gradient Shimming: Principles and Practical Aspects.*

# Chapter 3

# APPLICATION OF RADIO FREQUENCY SHAPED PULSES TO SLICE SELECTIVE NMR SPECTROSCOPY

## 3.1 Background of Shaped Radio Frequency Pulses

The Fourier transform of a rectangular function is sin (x)/x, which is called the sinc function. As such, when a rectangular radio frequency pulse undergoes a Fourier transform, it generates a sinc wiggle shape [1], such as those shown in Figure 17. When this pulse is short with high power, the result is a broad excitation bandwidth with relatively uniform excitation, as the spectral region is encompassed by a wide sinc wiggle (Figure 17a). These high-power, short-duration pulses are the basic NMR pulse, utilized to excite the chemical shifts across an entire spectrum with as much uniformity as possible [1]. These types of pulses are often called non-selective, hard pulses. In contrast, if a rectangular pulse is applied with low power for a relatively long time, the resulting excitation bandwidth is narrower and can be set so that it is right on resonance (Figure 17b); this can be referred to as a selective pulse. However, this latter case will also produce side sinc wiggles that could result in excitation of other signals, especially as the pulse gets longer and the power gets lower in an attempt to make the selected frequency range smaller (Figure 17c) [1]. These sinc wiggles can produce undesired side effects, such as spectral artifacts or excitation of unwanted resonances, etc.

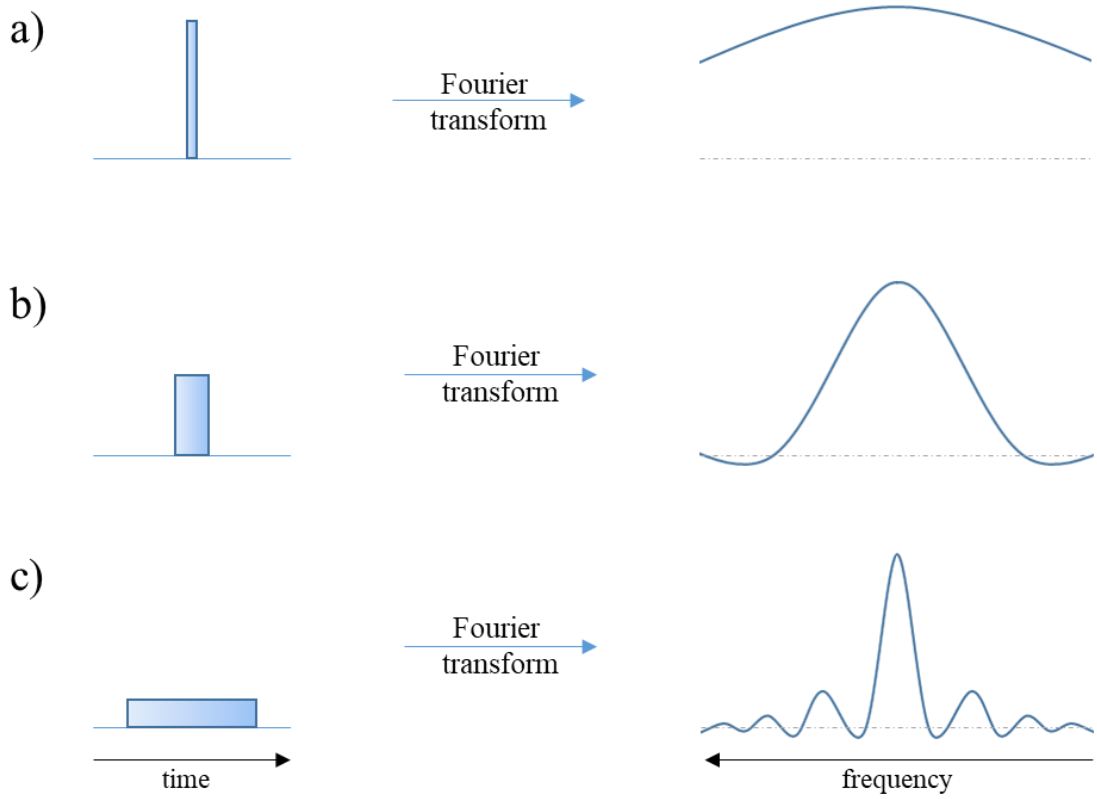


Figure 17. Fourier transforms of rectangular pulses with a) high power and short duration, b) slightly lower power and slightly longer duration, and c) much lower power and much longer duration.

Shaped pulses arise from trying to selectively excite (or otherwise selectively interact with) a given spin with a specific and often narrow frequency range, while avoiding the side sinc wiggles that result from a rectangular selective pulse. For example, a Gauss-shaped pulse has a Gauss excitation profile (Figure 18) and a sinc-shaped pulse has a square excitation profile (Figure 19) via the Fourier transformation [1]. These shapes are made by stringing together a long series of very short rectangular pulses. It is worthwhile to note that, in addition to the Gaussian and sinc shapes, various shaped pulses are available for a variety of applications in NMR experiments.

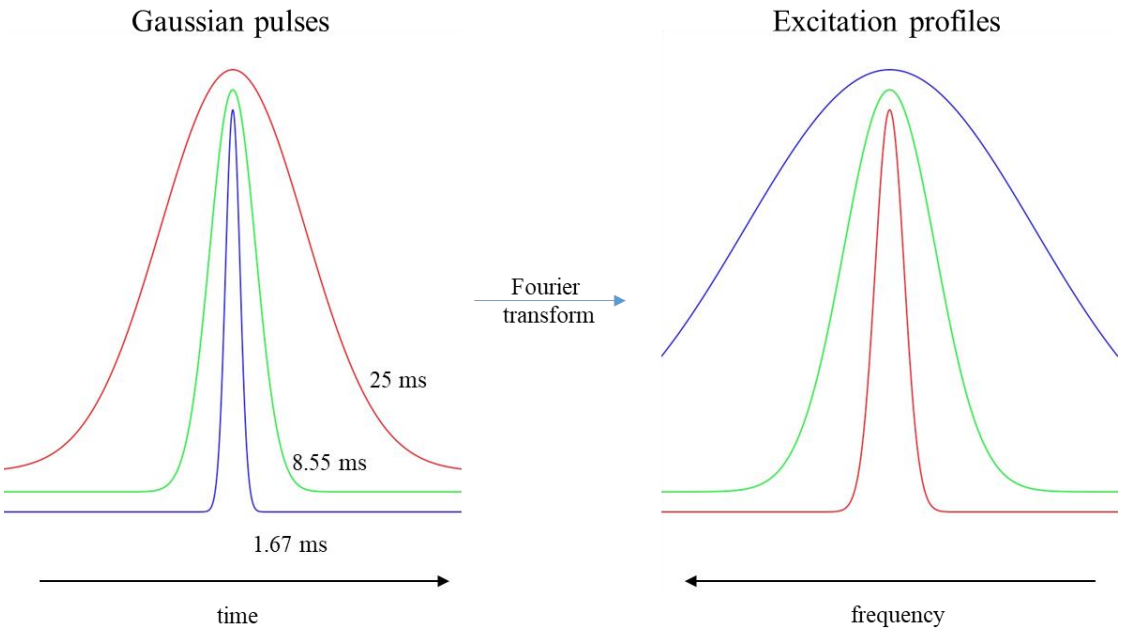


Figure 18. The Fourier transform of a Gaussian pulse will also generate a Gaussian excitation profile; the narrower the pulse width, the broader the resultant excitation profile will be, as indicated by the color coding in the figure. In addition, the Gaussian shaped pulses do not generate the sinc wiggles that square pulses do.

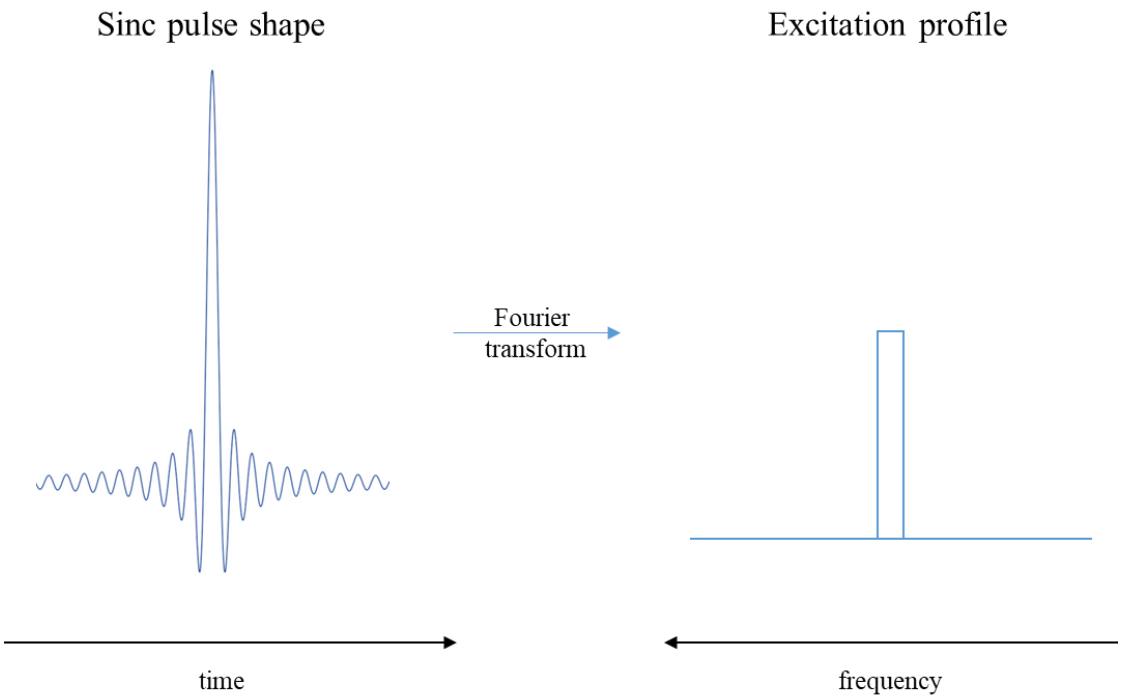


Figure 19. The Fourier transform of a sinc pulse will generate a square shape excitation profile. This results in an excitation profile that has no sinc wiggles and that can be uniform across the selected frequency range.

Shaped pulses have a large number of applications as selective pulses. They can be used to suppress singular and multiple signals in a spectrum, such as large solvent signals which could effectively reduce spectral dynamic range or interfere with signals of interest [2]. Relationships that might typically be probed through multidimensional NMR (such as through-bond or through-space interactions) can be investigated in a 1D NMR spectrum with the use of shaped pulses; this can reduce the overall experiment time required and provide further simplification or improved resolution over a multidimensional NMR experiment [2]. Shaped pulses can also be used for selectively decoupling nuclei, such as for homonuclear decoupling [3]. There

are endless applications for shaped pulses in 1D and multidimensional NMR, as well as in magnetic resonance imaging. In fact, it is the application of shaped pulses for selection of image "slices" for the purpose of magnetic resonance imaging that is the foundation of slice selective NMR experiments.

## 3.2 The Combination of Shaped Pulses with Pulsed Field Gradients for Slice Selection NMR

Though shaped radio frequency pulses present a number of useful and unique applications, they suffer from issues such as phase distortions when employed on their own. However, when utilized in combination with pulsed field gradients (PFGs), these issues can be resolved, as the PFGs are able to eliminate unwanted, out-of-phase magnetization by jumbling undesired excitation at the selected frequency [1].

There is another unique advantage to combining shaped pulses and PFGs, given the ability of PFGs to encode position dependencies as demonstrated by equations (2.1), (2.2), and (2.3) in Chapter 2. When applied simultaneously with a PFG, shaped pulses can be used to selectively excite nuclei with specified frequencies or frequency ranges, which in this case are also at specified locations along the z-axis. When the shaped pulse bandwidth, $\Delta\omega$, is larger than the entire spectral region of interest, the combined application of PFGs and shaped pulses can be used to selectively probe different spatial regions, called slices, within a sample [4].

A number of pulse sequences that combine gradients and shaped pulses exist for the purpose of spatially selective or spatially encoded experiments, and many of these are well known and have been reviewed in the past [5].

Spatially selective experiments utilize only one slice, or a subset of slices, of the sample to generate a spectrum, whereas spatially encoded experiments typically involve varying an experimental parameter across an entire set of slices of the whole sample in parallel to generate a spectrum. This work focuses on spatially selective experiments, so spatially encoded experiments will not be further discussed here.

Slice selective NMR methods [6] enable one to obtain a $^{1}H$ spectrum (or that of other NMR-active nuclei) that represents only the chemical species present within a selected region, or "slice," of an NMR sample tube. When applied to a biphasic system in which aqueous and organic layers coexist, representative spectra of organic and aqueous phases can be obtained by choosing two different frequency offsets ($\Omega$) for the selective r.f. pulses (Figure 20).

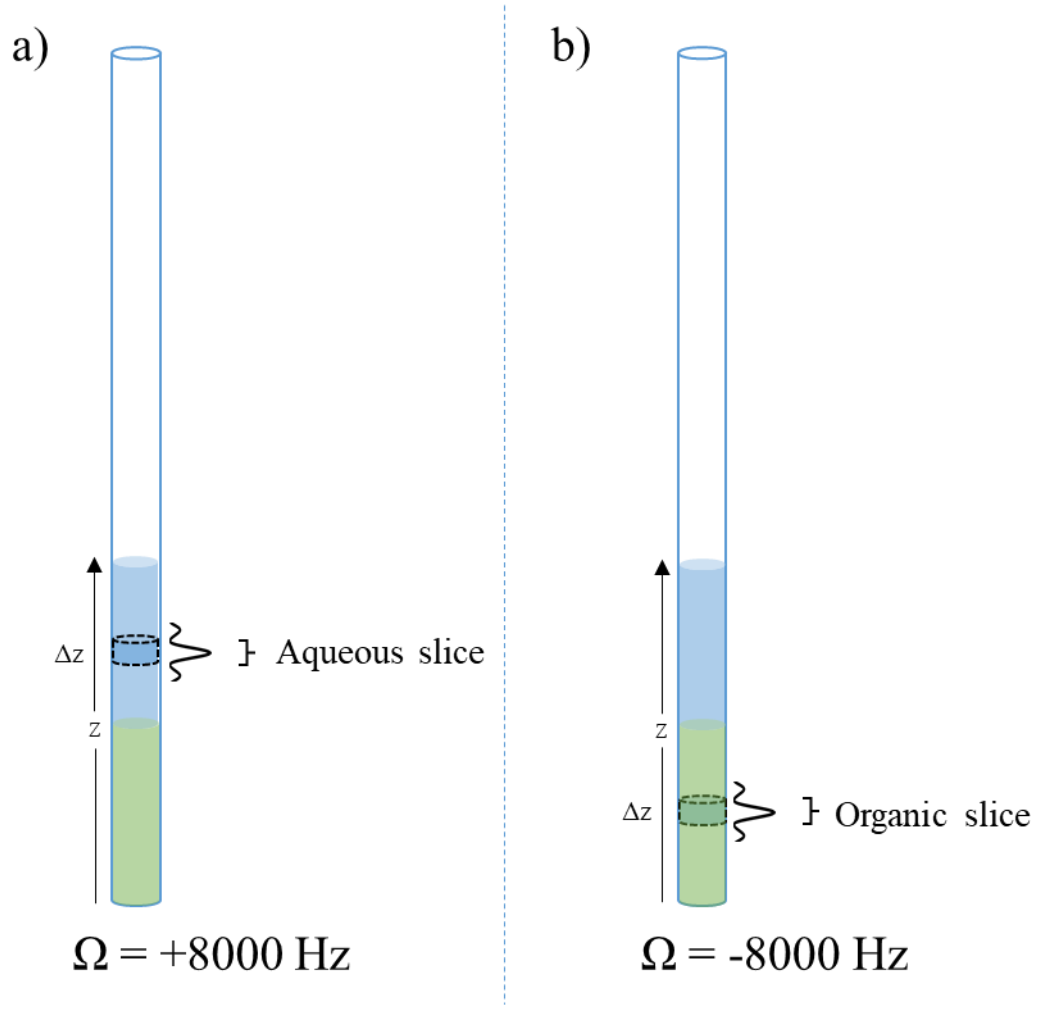


Figure 20. Illustration of spatial regions, called slices, within a) the aqueous phase and b) the organic phase of a biphasic NMR sample. Ω is the respective offset frequency used to select each of the two slices.

The ability to tune the width and location of slices, and the prospect of quantitative NMR applications make slice selective NMR a very interesting experiment for industrial and academic purposes. Slice selective NMR spectroscopy has been utilized in the analyses of diffusion properties [7-10], liquid-liquid interfaces [11-13], rapid reaction kinetics [14-16], biofuel [17] and crude oil emulsions [18],

hydrophilic/hydrophobic metabolites [19], and ion-transportation in lithium-ion battery electrolytes [20]. Sensitivity enhancement using simultaneous multiple slice excitation [21] and development of quantitative methodology [4] of the slice selection NMR have both been proposed. Implementation of slice selective 2D homo-nuclear correlation spectroscopy has also been reported [22]. In these cases, slice selective NMR provides the unique ability to observe the spatial distribution of chemical species across a sample non-destructively and rapidly.

In classic slice selection NMR spectroscopy [6], a z-axis gradient pulse is applied along with a selective r.f. excitation pulse (Fig. 21a) to achieve selective excitation of the nuclear spins occupying a targeted spatial location. As demonstrated previously by Equation (2.2), when applying a pulsed field gradient ($G_z$), the magnetic field strength, B(z), is dependent on the coordinate, z, along the axial direction of the NMR tube. Consequently, the resonance frequency ($\nu_z$) of nuclear spins is also dependent on z:

$$\nu_z = \nu_0 + \gamma z G_Z / 2\pi \tag{2.3}$$

A z-axis field gradient can be applied along an NMR sample such that the magnetic field strength stays at $B_0$ at the center of the NMR coil but increases and decreases gradually above and below the center coordinate. In this case, the frequency range ($\Delta\nu_{\pm z}$) induced by the gradient pulse within a defined distance of ±z along the NMR tube is

$$\Delta\nu_{\pm z} = \nu_z - \nu_{-z} = z\gamma G_z / \pi \tag{3.1}$$

A selective excitation pulse can be characterized by its offset frequency ($\Omega$) and bandwidth ($\Delta\nu$) [23]. If the offset of the selective pulse is chosen such that

$$\Omega = \nu_z - \nu_0 = z\gamma G_z / 2\pi \tag{3.2}$$

only the spins with $\nu_z$ at point z will be, in principle, excited or selected (Figure 21d). If a finite cross-section with a thickness

$$\Delta z = z_1 - z_2 \tag{3.3}$$

centered around z is considered, the frequency range induced by the gradient pulse is

$$\nu_1 - \nu_2 = (z_1 - z_2)\gamma G_z/2\pi \tag{3.4}$$

Thus, a selective pulse with the offset of Ω and bandwidth of $\nu_1$-$\nu_2$ can excite the spins confined within Δz at point z. In other words, the slice thickness

$$\Delta z = (2\pi/\gamma G_z)\Delta\nu \tag{3.5}$$

depends on $G_z$ and Δν of the excitation pulse. In the case of a strong magnetic field gradient and a sufficiently large r.f. bandwidth, all $^1$H chemical shift offsets can be virtually manipulated in the same slice [5].

For example, two slice selective NMR spectra of aqueous (red) and organic (blue) layers of a model biphasic NMR sample, consisting of sucrose in $D_2O$ and 4-chromanone in $CDCl_3$, were obtained by choosing two offsets of the selective r.f. excitation pulse (Figure 21a). This scenario of utilizing a shaped excitation pulse in parallel with a PFG affords minimal reduction in signal due to diffusion or relaxation, as it consists of only one pulse. However, deficient spectral selectivity and poor spectral phasing are noted in both spectra. To address this, the excitation pulse is often appended with a refocusing pulse incorporated with a gradient pulse to suppress the magnetic susceptibility artifacts [4, 24]. The modified pulse scheme produces spectra with improved spectral selectivity (Figure 21b); though the resultant spectrum takes a slight hit in signal to noise ratio, it is producing a much cleaner spectrum for visual interpretation and for quantitation.

There are a number of variations of selective excitation and refocusing pulses that can be employed in these classic slice selection experiments [24]. In the case of a biphasic sample, however, at least two NMR experiments with different offset frequencies are required to obtain two spectra representing the chemical species in two phases of the biphasic sample, respectively (Figures 21a, 21b, and 21d). This poses a concern especially in the case of kinetics experiments, for which the data points should be collected simultaneously. It also requires the set up and execution of two, separate experiments.

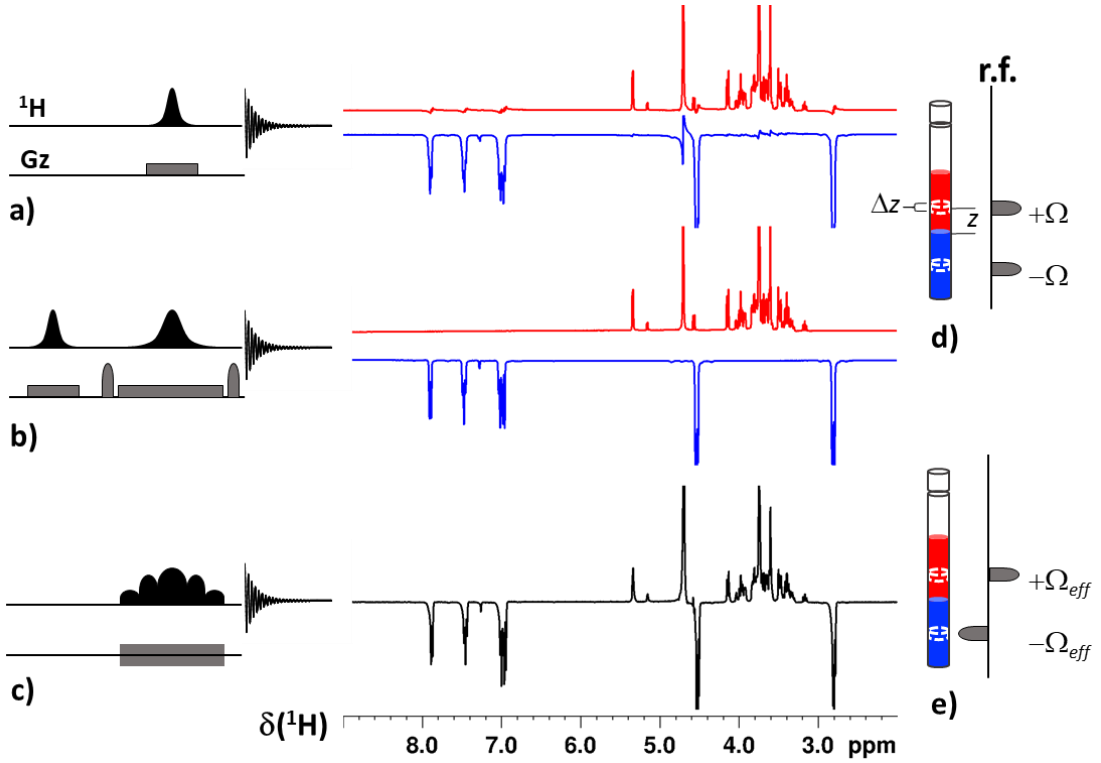


Figure 21. Slice selection $^{1}$H NMR spectra: a) An excitation selective pulse (EBurp: 1236 μs) produces spectra of the aqueous (red) and organic (blue, phased negatively for comparison) phases of a model biphasic sample of sucrose in $D_2O$ and 4 chromanone in $CDCl_3$. b) An excitation EBurp pulse followed by a refocusing pulse (ReBurp, 1600 μs) leads to the spectra of aqueous (red) and organic phases (blue, phased negatively for comparison) of the same model sample. The bandwidth and offset of these pulses are 3915 Hz and ±7500 Hz. c) One-shot double-slice selection spectrum of the model biphasic sample using a ReBurp pulse (1600 μs) with a bandwidth of 3915 Hz and the effective offsets are ±1684 Hz. d) Schematic plot of the biphasic sample tube marked with *z* and Δ*z*, indicating the slices excited by two, separate experiments using different offsets. e) Schematic plot of the biphasic sample tube signifying the two slices excited simultaneously by only one ReBurp pulse that produces two effective excitation profiles with opposite phases.

### 3.3 The Design of One-Shot Double-Slice Experiments

A new “one-shot double-slice” (OSDS) experiment was employed on biphasic samples of model compounds and in-tube extractions, enabling visualization of these biphasic systems in a single shot. This pulse sequence (Figure 21c, Appendix C) employs an established and well-known refocusing pulse, called ReBurp (REfocusing, Band-selective, Uniform response, Pure-phase) [25], as the excitation pulse. It was found that when this pulse sequence was applied with the offset frequency set to 0 Hz (the center of the receiving coil), all signals from both the organic and aqueous phases were observed in the spectrum, but with opposite phases (Figure 22). This pulse sequence presents opportunities for “one shot” slice-selective experiments that would be extremely useful in kinetics studies, as data points could be collected in half that time that it would take to run the spin echo version (which requires two experiments to observe each phase), and where data for two phases would be from the exact same time point. Utilization of alternating phases of pulsed field gradients was found to improve spectral quality, so was incorporated into the pulse sequence.

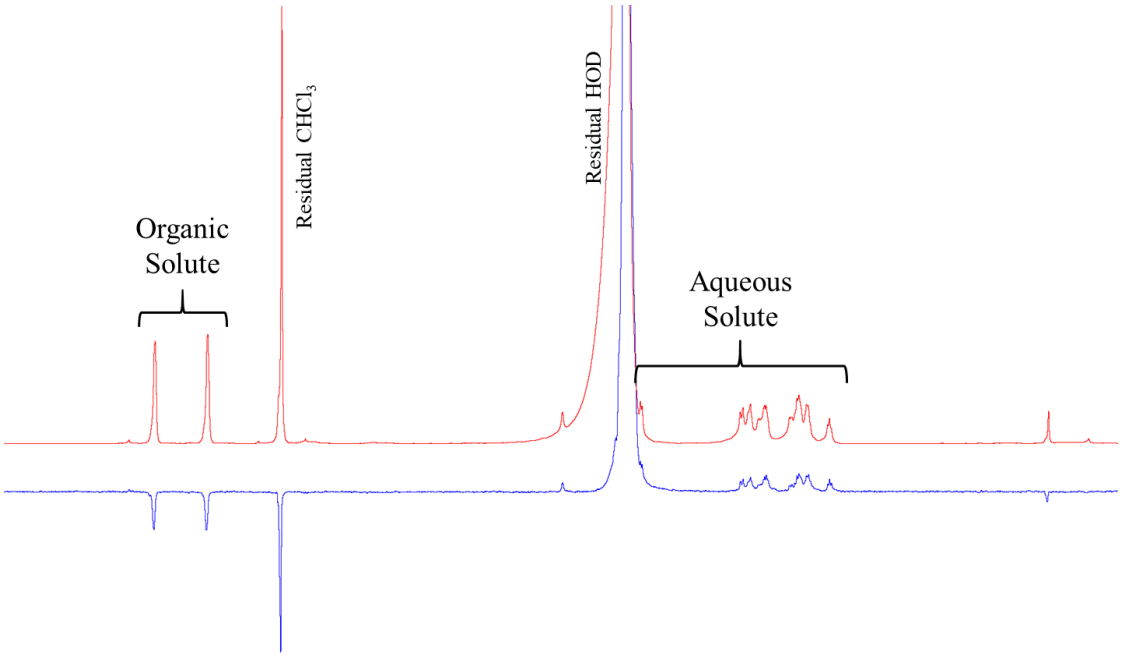


Figure 22. $^{1}$H NMR spectra of a GNE M2 via standard 1D NMR (top) and one-shot double-slice 1D NMR (bottom).

The OSDS experiment works by applying a specific excitation profile across the entire NMR coil, which results in signal that is concentrated in two "slices" - one from the top phase in the tube, and one from the bottom phase in the tube, with the signals corresponding to those slices having opposite phases from each other (Figure 23).

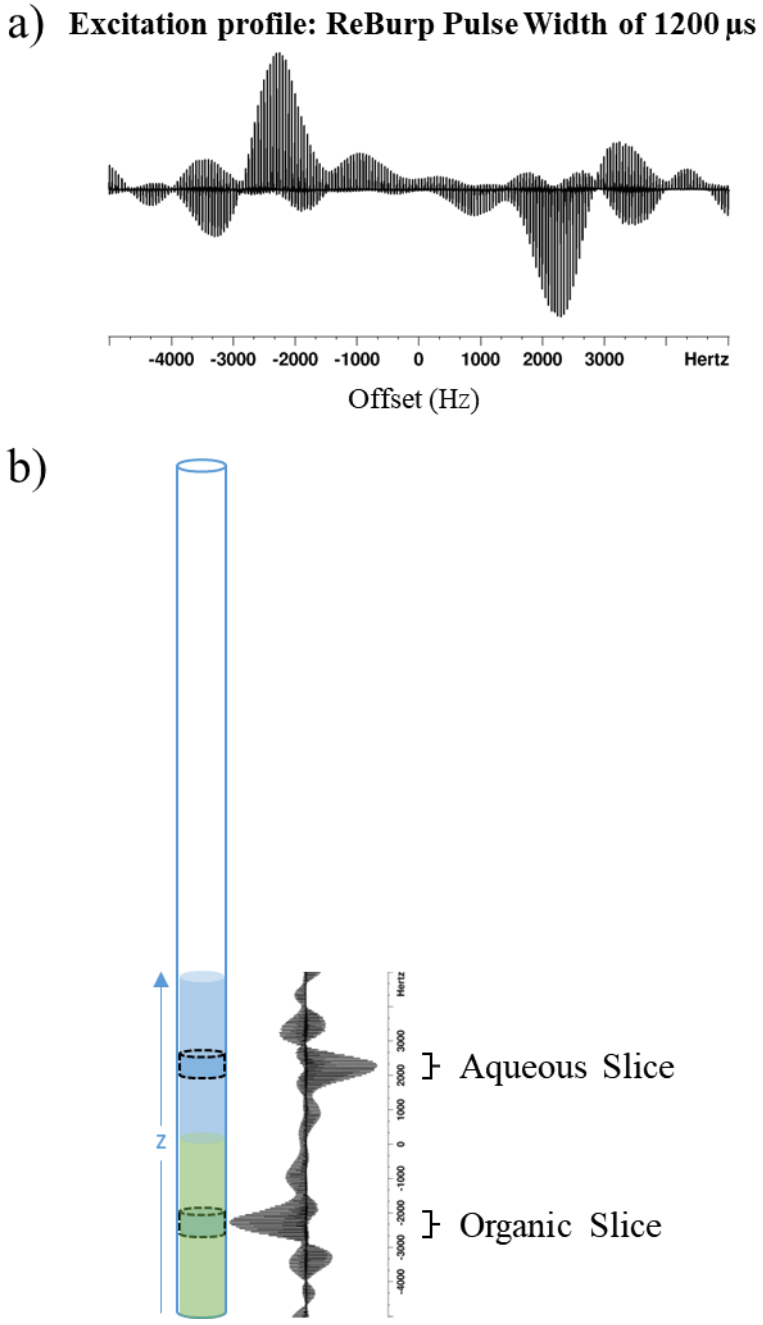


Figure 23. a) Excitation profile for 1200 µs ReBurp pulse, b) visualization of the excitation profile as a function of position along the z-axis; the Reburp pulse offset, Ω, is set to 0 Hz in this case.

This effect can be clearly seen in ReBurp pulse simulations (Figure 24a), in which the trajectory of the magnetization shows an inversion (black arrow) for the on-resonance spins ($\Omega$=0). If the offsets of the ReBurp pulse are set to characteristic effective frequencies ($\pm\Omega_{eff}$), the magnetization trajectories (red arrows) end in nearly opposite phases along the x-axis, indicative of simultaneous effective excitation of the nuclear spins with $\pm\Omega_{eff}$. The simulated ReBurp pulse excitation profiles (Figure 24b) also show an inversion of the on-resonance spins (black curve) and two simultaneous, opposite-phase side-lobes (red curve) with the effective bandwidth $\Delta\nu_{eff}$ centered around $\pm\Omega_{eff}$. The experimental excitation profile (Figure 24c) of the ReBurp pulse confirms a near-zero excitation in the vicinity of zero offset ($\Omega$=0) while imposing opposite-phase excitations at $\pm\Omega_{eff}$, highly consistent with the simulated results. Due to their opposite r.f. polarities, the effects of these two side lobes cancel each other in the absence of a field gradient. However, in the presence of said gradient pulse, the two r.f. excitation side lobes (Figures 24b and 24c) simultaneously select the signals of chemical species above and below the interface (Figure 21e) corresponding to $\Omega_{eff}$.

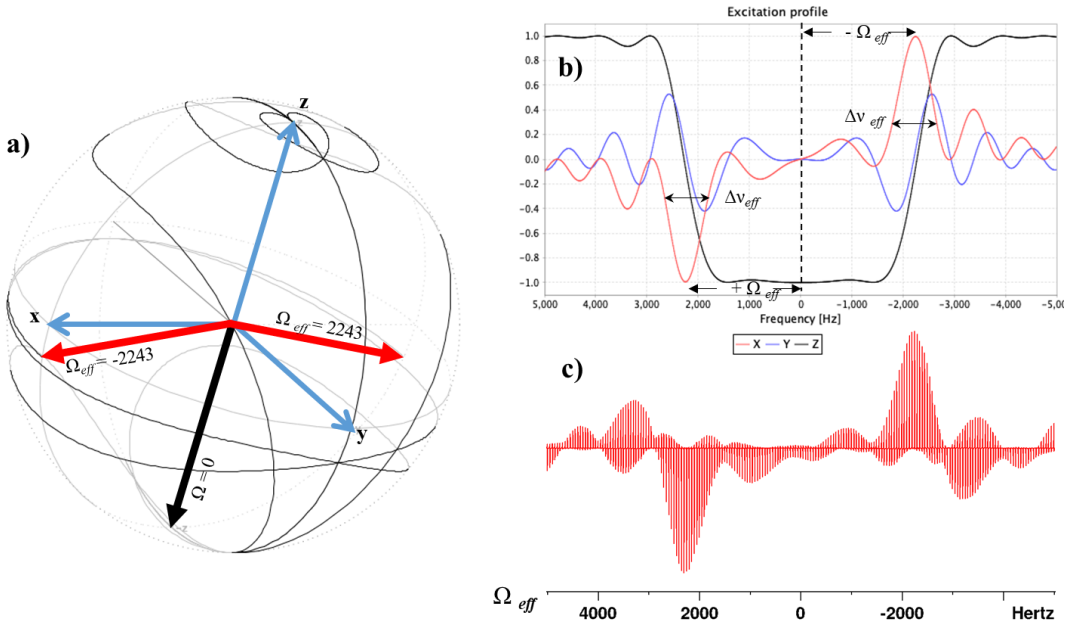


Figure 24. a) Shaped pulse simulation of ReBurp pulse (1200 μs) shows the trajectories of the magnetizations on-resonance (black) and off-resonance (± 2243 Hz, red). Note that the end points of magnetizations with the effective offsets (± 2243 Hz) are nearly 180° out of phase along the x-axis, enabling the simultaneous excitations. b) Simulated excitation profile shows excitations along ±x at Ω=± 2243 Hz and Δν=660 Hz at 30% of the profile height. c) Experimental excitation profile of ReBurp pulse (1200 μs), obtained by varying the offset frequency, is highly consistent with the simulated effective offsets and bandwidth (red in b).

### 3.4 Application to Model Biphasic Samples

The first goal of this slice selection NMR work was to successfully implement the modified pulse scheme containing a refocusing pulse incorporated with a gradient pulse on NMR systems of two different magnetic field strengths at University of Delaware and Genentech. The model biphasic samples were prepared with $CDCl_3$ and $D_2O$ as the solvents for the organic and aqueous phases, respectively. D-Glucose (Figure 25a) was the aqueous analyte used at Genentech, while sucrose (Figure 25b) was used at University of Delaware; 2,3-dicholoro-1,4-naphthoquinone (Figure 25c)

and 4-chromanone (Figure 25d) were used as the organic analyte at Genentech and University of Delaware, respectively.

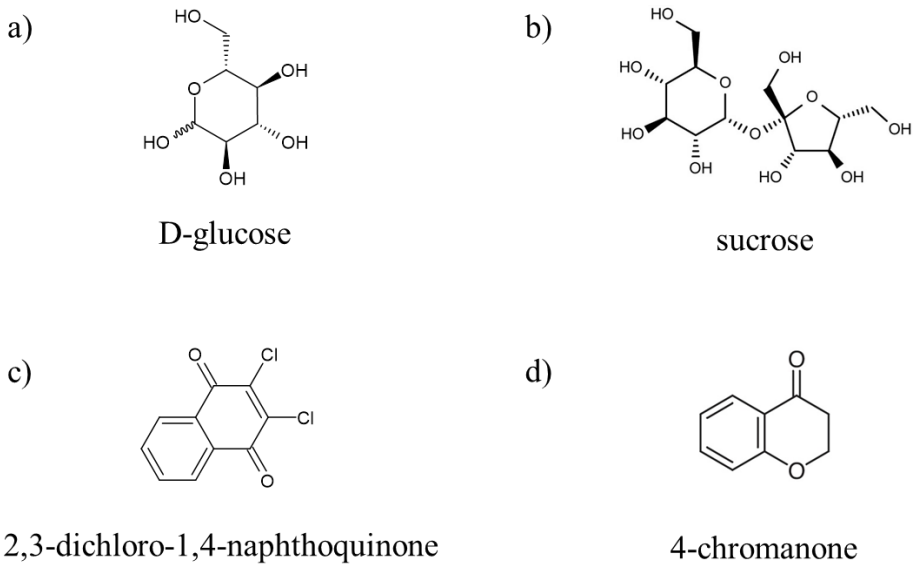


Figure 25. Model compounds used as the a) aqueous solute at Genentech, b) aqueous solute at University of Delaware, c) organic solute at Genentech, and d) organic solute at University of Delaware.

### 3.4.1 Experimental Methods

The two model biphasic samples used for slice selective NMR experiments were Genentech Model Biphasic Sample #2 (GNE M2) and University of Delaware Model Biphasic Sample #1 (UD M1).

As described previously, for GNE M2, 1,000 μg/mL solutions were prepared of 2,3-dichloro-1,4-naphthoquinone in $CDCl_3$ and D-glucose in $D_2O$, respectively. These solutions were then carefully transferred to the NMR tube, avoiding getting sample on the tube walls, and adding the $CDCl_3$ solution first to minimize any mixing

of the two layers. The amounts added were approximately 250 μL of each solution, and were based on physical markings on the tube indicating the location of the receiver coil.

For preparation of UD M1, 50 mg of sucrose and 53 mg of 4-chromanone were dissolved in 1 ml of $D_2O$ and 1 ml of $CDCl_3$, respectively. First, 250 μL of the 4-chromanone-$CDCl_3$ solution was transferred to a 5-mm NMR tube. Then, 250 μL of 4-chromanone-$D_2O$ solution was carefully and slowly added to the tube to form a biphasic sample.

A Bruker AVIII 400 MHz NMR spectrometer with a BBFO probe (University of Delaware) and Bruker NEO 600 MHz spectrometer with a TCI CryoProbe (Genentech) were used in this study. The number of scans to be collected were determined based upon obtaining sufficient signal-to-noise. For the model biphasic samples, the number of scans ranged between 8 and 16.

Standard $^1H$ NMR spectra, classic slice selection spectra, one-shot double-slice selection spectra, and 2D OSDS TOCSY spectra were collected for the model biphasic samples.

In the OSDS selection experiment, alternative polarity of the gradient pulses (±3.43 G/cm) were used to improve the spectral properties such as phasing and baseline line integrity.

A presat TOCSY pulse with the MLEV spin-lock scheme (see Appendix D) was used by replacing the 90° pulse for magnetization preparation with a selective ReBurp pulse in our investigation.

The r.f. power of ReBurp.1000 pulse for a given pulse width can be calculated by the spectrometer software or calibrated by observing the minimum signal at the

zero-offset frequency. There was very minimal discrepancy observed between these two methods, so the software-calculated power level was used for most of the measurements, unless otherwise noted.

The ReBurp.1000 excitation profile was measured by selecting a $CH_2$ group of 4-chromanone in $CDCl_3$ using a Bruker "selzg" pulse program and ramping the offset frequency from -5000 Hz to +5000 Hz with a step length of 50 Hz.

The Shaped Pulse Tool of Bruker's TopSpin software was used to calculate the excitation profiles and simulate magnetization trajectories of the ReBurp pulses. To generate a ReBurp pulse for the simulation, the excitation mode was set to Universal 180, the excitation type was set to Refocusing, the rotation was set to 180°, the bandwidth factor was set to 5.81, and the size was set to 1024. First, the excitation profile of a ReBurp pulse at a given pulse width was calculated, then the positive and negative effective offsets were obtained from the profile. The magnetization trajectories were simulated by setting a three-step simulation from the negative offset to the positive offset.

### 3.4.2 Results and Discussion

In the original application of the Spin Echo Slice Selective pulse sequence, the shaped excitation pulse used was a G4 gauss-cascade, and the shaped refocusing pulse used was Rsnob [4]. EBurp and ReBurp were also suggested [26] for the excitation and refocusing shaped pulses, respectively, and were utilized in this work. While trying to optimize the resultant pulse sequence, it was observed that changes to the excitation pulse had minimal impact on the resulting spectra, whereas changes to the refocusing pulse, ReBurp, had the most impact. This led to experimenting with a pulse

sequence (Figure 21c) that excluded the excitation pulse, and ultimately to the discovery of an unusual and interesting effect of the ReBurp shaped pulse, when essentially applied as a universal inversion pulse instead of a refocusing pulse. It was found that when this pulse sequence was applied with the offset frequency, Ω, set to 0 Hz (the center of the receiving coil), all signals from both the organic and aqueous phases were observed in the spectrum, but with opposite phases. This pulse sequence presents opportunities for "one shot" slice-selective experiments that would be extremely useful in kinetics studies, as data points could be collected in half that time that it would take to run the spin echo version (which requires two experiments to observe each phase), and where data for two phases would be from the exact same time point.

The original version of the ReBurp Inversion Slice Selection (One-Shot Double-Slice) pulse sequence executes a PFG of only a single phase. In an attempt to further enhance the quality of the experiment output, the pulse sequence was edited to have alternating PFG pulse polarities. The resulting spectra were notably improved over those from the original pulse sequence version (Figure 26), and this became the pulse sequence of choice for the OSDS experiment.

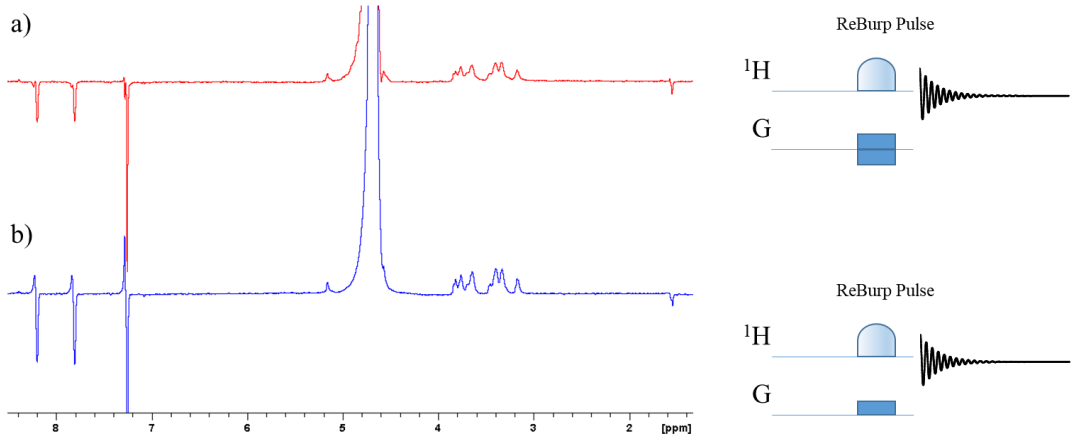


Figure 26. One-Shot Double-Slice spectra of GNE M2 model biphasic sample utilizing a) the revise ReBurp Inversion Slice Selection pulse sequence with alternating gradient phase, and b) the original ReBurp Inversion Slice Selection pulse sequence with a single gradient polarity.

It is interesting to note that the one-shot double-slice scheme (Figure 21c) can be readily incorporated to a 2D experiment to acquire through-bond correlations with spatial-specificity. For example, when the 90° pulse of a 2D TOCSY sequence is replaced by a ReBurp selective pulse combined with a magnetic field gradient pulse, the result is a OSDS phase-sensitive TOCSY spectrum. Such a TOCSY spectrum of a model biphasic sample (Figure 27) allows immediate differentiation of through-bond correlations between sucrose and 4-chromanone based on phases of their cross-peaks in just one 2D spectrum.

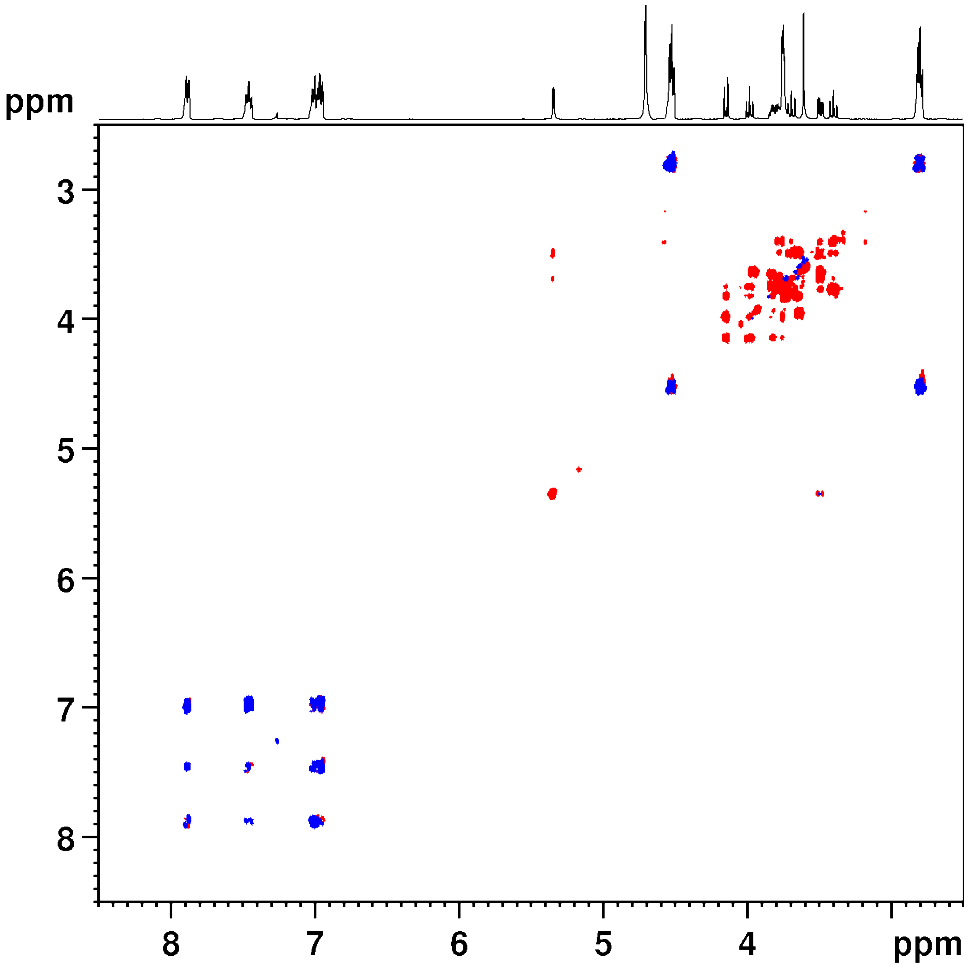


Figure 27. One-shot double-slice version of a TOCSY spectrum of the UD M1 model biphasic sample. The 90° excitation hard pulse in the TOCSY is replaced by a ReBurp pulse of 1600 μs along with a rectangular gradient pulse at a strength of 3.43G/cm of the same length. The resulting 2D spectrum is phase-sensitive with color coded cross peaks for sucrose (red) and 4-chromanone (blue). The TOCSY mixing time is 60 ms.

Some results of the ReBurp Pulse simulations are captured in Table 3. These simulations show that as the ReBurp pulse width is increased, the band width, slice thickness ($\Delta z$) and effective offset from the center of the receiver coil ($\Omega_{eff}$) all decrease. This shows that these aspects of the OSDS experiment are tunable by

adjusting the ReBurp pulse width used. However, they are not independently tunable in this experiment, unlike for a classical slice selection experiment.

Table 3. Bandwidths, Effective offsets, Effective bandwidths of the ReBurp[a] Pulse

| Pulse width (μs) | Band width (Hz) | $\Omega_{eff}$ (Hz) | $\Delta\nu_{eff}$ (Hz) | $z$ (mm) | $\Delta z$ (mm) |
|---|---|---|---|---|---|
| 1000 | 6264 | ±2700 | 1030 | 1.8 | 0.7 |
| 1200 | 5220 | ±2243 | 860 | 1.5 | 0.6 |
| 1400 | 4474 | ±1928 | 737 | 1.3 | 0.5 |
| 1600 | 3915 | ±1684 | 645 | 1.2 | 0.4 |
| 1800 | 3483 | ±1498 | 573 | 1.0 | 0.4 |
| 2000 | 3132 | ±1346 | 516 | 0.9 | 0.4 |

[a]Effective ReBurp pulse offsets and bandwidth for excitation are obtained from simulations using the shaped pulse tool (Bruker TopSpin). $z$ and $\Delta z$ are estimated using the calibrated gradient strength of 3.43 G/cm and $\Omega_{eff}$and $\Delta\nu_{eff}$.

There is an inherent cost with slice selective NMR vs. standard NMR in terms of signal to noise, as only a small portion of the sample is being excited to generate signal. The thickness of the selected slice depends on the bandwidth of the shaped pulse. It is also inversely propositional to strength of the applied pulsed field gradient. As the signal to noise ratio of these NMR measurements is proportional to the fraction of the sample volume observed, in principle, the sensitivity of slice NMR experiment can be tuned by selecting shaped pulse bandwidth and by altering gradient strength to a certain degree.

Experimental observations show that the NMR signal intensity and quality is dependent on the ReBurp pulse width and on the applied gradient strength, as is demonstrated in Figure 28. The signal intensity decreases with both increasing pulse width and with increasing gradient strength. At the same time, spectral quality appears to improve as both pulse width and gradient strength increase within the range tested.

This experimental observation supports the simulation output, in that as the pulse width increases, the slice thickness is getting smaller; this results in spectra with less sensitivity, but also with fewer spectral artifacts (perhaps due to things like less diffusion within a slice). The experimental data shows that this is also true for gradient strength. These results indicate that the pulse width and gradient strength can both be adjusted to optimize for the spectral quality and sensitivity needed for a given experiment, and that there is a slight sacrifice needed of either spectral quality or sensitivity.

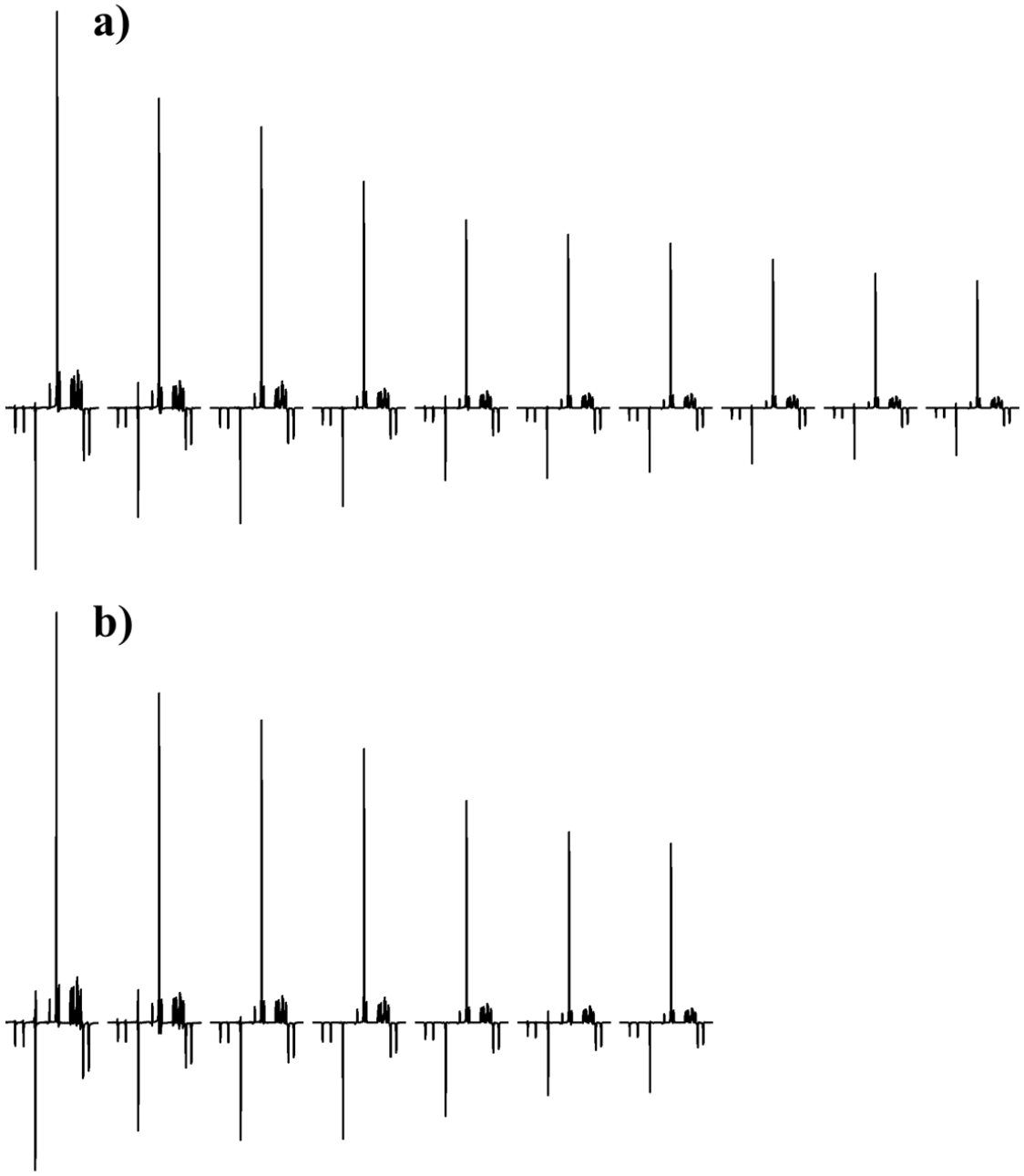


Figure 28. One-shot double-slice NMR signals of the UD M1 model biphasic sample a) as a function of pulse width from 800 μs (left) to 2600 μs (right) with an increment of 200 μs at a gradient strength of 3.43 G/cm, and b) as a function of gradient strength from 4% (left) to 10% (right) with a step length of 1%. The pulse width was set to 1200 μs and the gradient strength at 100% is 51.1 G/cm

### 3.4.3 Conclusions

The classical slice selection experiment can be easily employed on biphasic samples. The OSDS experiment, developed and proposed in this thesis, is a reliable experiment when applied to biphasic model samples. This new experiment enables the collection of the same information in a single experiment that would require two experiments by a classic slice selective NMR method. Additionally, the OSDS experiment can be integrated into a 2D TOCSY NMR experiment, enabling spectral resolution by cross-peak phases, while simultaneously collecting molecular connectivity data.

## REFERENCES


[1] Jacobsen, N. E. NMR Spectroscopy Explained: Simplified Theory, Applications and Examples for Organic Chemistry and Structural Biology; John Wiley & Sons, Inc., 2007.

[2] Freeman, R. Selective Excitation in High-Resolution NMR. Chemical Reviews **1991**, 91 (7), 1397-1412. DOI: 10.1021/cr00007a006.

[3] Castañar, L.; Parella, T. Broadband 1H homodecoupled NMR experiments: recent developments, methods and applications. Magn Reson Chem **2015**, 53 (6), 399-426. DOI: 10.1002/mrc.4238 From NLM PubMed-not-MEDLINE.

[4] Mitrev, Y. N. Slice selective NMR approach for investigation of distribution phenomena in biphasic samples. Bulgarian Chemical Communications **2017**, 49 (F), 65-69.

[5] Dumez, J. N. Spatial encoding and spatial selection methods in high-resolution NMR spectroscopy. Progress in Nuclear Magnetic Resonance Spectroscopy **2018**, 109, 101-134. DOI: 10.1016/j.pnmrs.2018.08.001 From NLM PubMed-not-MEDLINE.

[6] Koźmiński, W. Application of spatially resolved NMR spectroscopy for high resolution spectra of heterogeneous samples. Polish Journal of Chemistry **2000**, 74, 1185-1189.

[7] Allen, J.; Damodaran, K. High-resolution slice selection NMR for the measurement of CO2 diffusion under non-equilibrium conditions. Magn Reson Chem **2015**, 53 (3), 200-202. DOI: 10.1002/mrc.4176 From NLM Medline.

[8] Pantoja, C. F.; Bolanos, J. A.; Bernal, A.; Wist, J. Mutual Diffusion Driven NMR: a new approach for the analysis of mixtures by spatially resolved NMR spectroscopy. Magn Reson Chem **2017**, 55 (6), 519-524. DOI: 10.1002/mrc.4561 From NLM PubMed-not-MEDLINE.

[9] Poppler, A. C.; Frischkorn, S.; Stalke, D.; John, M. Toluene and lithium amide diffusion into polystyrene: a slice-selective NMR-spectroscopic study. Chemphyschem **2013**, 14 (13), 3103-3107. DOI: 10.1002/cphc.201300609 From NLM PubMed-not-MEDLINE.

[10] Wisniewska, M. A.; Seland, J. G. Investigating structure-dependent diffusion in hydrogels using spatially resolved NMR spectroscopy. J Colloid Interface Sci **2019**, 533, 671-677. DOI: 10.1016/j.jcis.2018.08.112 From NLM Medline.

[11] Lambert, J.; Hergenroder, R.; Suter, D.; Deckert, V. Probing liquid-liquid interfaces with spatially resolved NMR spectroscopy. Angew Chem Int Ed Engl **2009**, 48 (34), 6343-6345. DOI: 10.1002/anie.200901389 From NLM Medline.

[12] Mantel, C.; Bayle, P. A.; Hediger, S.; Berthon, C.; Bardet, M. Study of liquid-liquid interfaces by an easily implemented localized NMR sequence. Magn Reson Chem **2010**, 48 (8), 600-606. DOI: 10.1002/mrc.2628 From NLM Medline.

[13] Martin, B. T.; Chingas, G. C.; McDougal, O. M. Origin and correction of magnetic field inhomogeneity at the interface in biphasic NMR samples. J Magn Reson **2012**, 218, 147-152. DOI: 10.1016/j.jmr.2012.02.012 From NLM Medline.

[14] Kind, J.; Thiele, C. M. Still shimming or already measuring?--Quantitative reaction monitoring for small molecules on the sub minute timescale by NMR. J Magn Reson **2015**, 260, 109-115. DOI: 10.1016/j.jmr.2015.09.008 From NLM PubMed-not-MEDLINE.

[15] Niklas, T.; Stalke, D.; John, M. Single-shot titrations and reaction monitoring by slice-selective NMR spectroscopy. Chem Commun (Camb) **2015**, 51 (7), 1275-1277. DOI: 10.1039/c4cc08329f From NLM Medline.

[16] Wagner, G. E.; Sakhaii, P.; Bermel, W.; Zangger, K. Monitoring fast reactions by spatially-selective and frequency-shifted continuous NMR spectroscopy: application to rapid-injection protein unfolding. Chem Commun (Camb) **2013**, 49 (30), 3155-3157. DOI: 10.1039/c3cc39107h From NLM Medline.

[17] Evans, R.; Sandhu, A.; Bridgwater, T.; Chong, K. Slice-Selective NMR: A Noninvasive Method for the Analysis of Separated Pyrolysis Fuel Samples. Energy & Fuels **2017**, 31 (4), 4135-4142. DOI: 10.1021/acs.energyfuels.7b00223.

[18] Hjartnes, T. N.; Sørland, G. H.; Simon, S.; Sjöblom, J. Demulsification of Crude Oil Emulsions Tracked by Pulsed Field Gradient (pfg) Nuclear Magnetic Resonance (nmr). Part I: Chemical Demulsification. Industrial & Engineering Chemistry Research **2019**, 58 (6), 2310–2323. DOI: 10.1021/acs.iecr.8b05165.

[19] Seeger, K. Simple and Rapid (Extraction) Protocol for NMR Metabolomics-Direct Measurement of Hydrophilic and Hydrophobic Metabolites Using Slice Selection. Anal Chem **2021**, 93 (3), 1451-1457. DOI: 10.1021/acs.analchem.0c03353 From NLM Medline.

[20] Krachkovskiy, S. A.; Pauric, A. D.; Halalay, I. C.; Goward, G. R. Slice-

Selective NMR Diffusion Measurements: A Robust and Reliable Tool for In Situ Characterization of Ion-Transport Properties in Lithium-Ion Battery Electrolytes. The Journal of Physical Chemistry Letters **2013**, 4 (22), 3940-3944. DOI: 10.1021/jz402103f.

[21] Castañar, L.; Nolis, P.; Virgili, A.; Parella, T. Full sensitivity and enhanced resolution in homodecoupled band-selective NMR experiments. Chemistry **2013**, 19 (51), 17283-17286. DOI: 10.1002/chem.201303235 From NLM PubMed-not-MEDLINE.

[22] Vega-Vazquez, M.; Cobas, J. C.; Martin-Pastor, M. Fast multidimensional localized parallel NMR spectroscopy for the analysis of samples. Magn Reson Chem **2010**, 48 (10), 749-752. DOI: 10.1002/mrc.2659 From NLM Medline.

[23] Freeman, R. Shaped radiofrequency pulses in high resolution NMR. Progress in Nuclear Magnetic Resonance Spectroscopy **1998**, 32 (1), 59-106.

[24] Trigo-Mourino, P.; Merle, C.; Koos, M. R.; Luy, B.; Gil, R. R. Probing spatial distribution of alignment by deuterium NMR imaging. Chemistry **2013**, 19 (22), 7013-7019. DOI: 10.1002/chem.201300254 From NLM Medline.

[25] Geen, H.; Freeman, R. Band-Selective Radiofrequency Pulses. Journal of Magnetic Resonance **1991**, 93, 93-107.

[26] In Private Communication with Clemens Anklin from Bruker BioSpin, 2021.

# Chapter 4

# THE APPLICATION OF ONE-SHOT DOUBLE-SLICE NMR EXPERIMENTS TO COMPLEX BIPHASIC SAMPLES

## 4.1 Background on Recent Applications of Slice Selection NMR to Real-life Biphasic Samples

There has been some recent work done applying classic slice selective sequences to extractions performed directly in NMR tubes as an approach to perform quick and simplified metabolomics analyses on the extracted samples [1]. The NMR spectra of these samples are more complex than for a model biphasic system with only one or two solutes. If the one-shot double-slice experiment works well on complicated systems like biphasic in-tube extracts from a complex mixture, this experiment would enable the further elimination of an additional step (acquiring two spectra) and reduce the already large amount of data needed for a metabolomics sample set by a factor of two.

For this reason, we evaluate the feasibility of applying the OSDS experiment to several in-tube extraction biphasic samples to explore the possible implementation of this experiment to real issues in the analytical chemistry field.

## 4.2 Biphasic Tea Extracts

The first goal of these efforts was to test the functionality of the 1D OSDS experiment on real, in-tube extractions containing insoluble materials, similar to those analyzed with classic slice selection by Seeger in 2021 [1]. The tests were performed on NMR systems at University of Delaware and at Genentech with different samples

of tea leaves that were extracted with $D_2O$ and $CDCl_3$. However, spectral assignment of the $^1H$ signals was only performed for the tea samples analyzed at University of Delaware, and as such, the tea samples analyzed at Genentech will not be discussed further here.

The two tea samples that were extracted and analyzed at University of Delaware were Benner green tea (BGT) and Celestial herbal tea (CHT). The $^1H$ NMR spectra (collected using presaturation to suppress the water signal) of the biphasic extracts of these teas are shown in Figure 29 for BGT and Figure 30 for CHT, with the assignments summarized in Table 4 and Table 5, respectively. CHT does not contain caffeine, while BGT does.

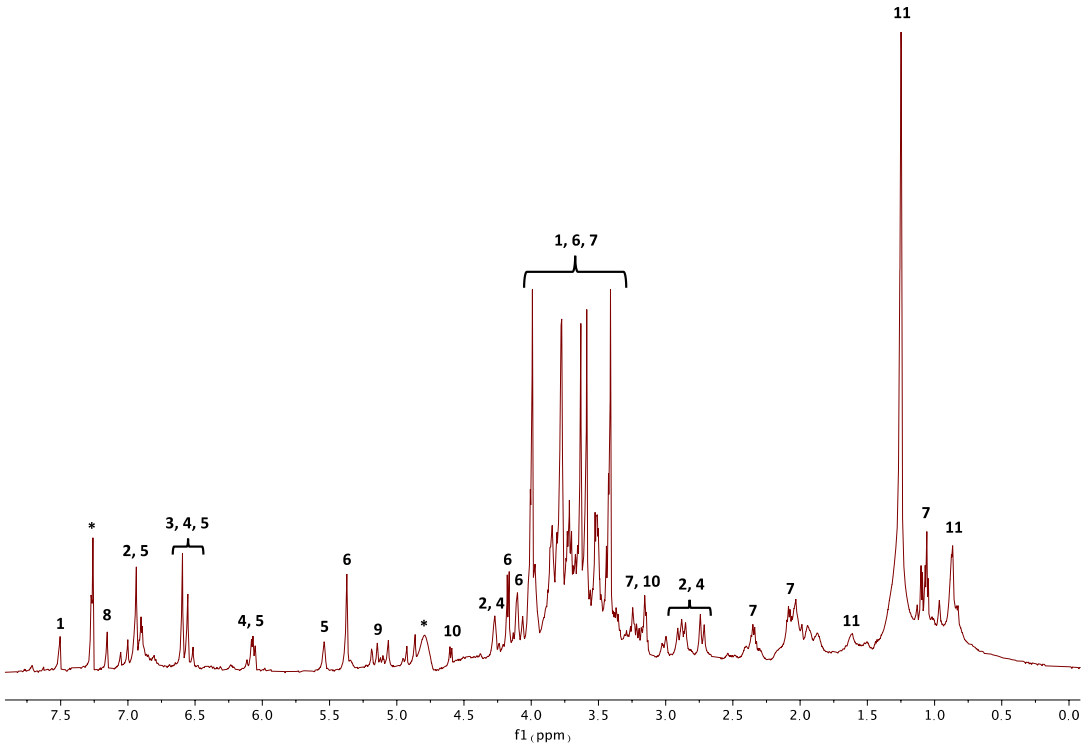


Figure 29. $^{1}$H spectrum of the BGT biphasic sample; the large water signal from the aqueous layer was suppressed via presaturation.

Table 4. $^{1}$H Chemical shift assignments for BGT.

| Peak Label | Assignment | Chemical shift, δ (ppm) |
|---|---|---|
| 1 | Caffeine [2, 3] | 7.50 (s), 3.99 (s), 3.59 (s), 3.41 (s) |
| 2 | Epicatechin (EC) [4] | 6.95, 4.27, 2.87, 2.73 |
| 3 | Gallocatechin (GC) [5] | 6.52 (s) |
| 4 | Epigallocatechin (EGC) [5] | 6.59 (s), 6.07, 4.27, 2.87, 2.73 |
| 5 | Epigallocatechin gallate (EGCG) [5] | 6.90, 6.55 (s), 6.07, 5.54 |
| 6 | Sucrose [2, 5] | 5.37 (d), 4.17, 4.06, 3.85 (m), 3.78, 3.63, 3.51 (m) |
| 7 | Theanine [2, 3] | 3.72 (t), 3.16 (m), 2.33 (m), 2.08 (m), 1.06 (t) |
| 8 | Gallic acid [3] | 7.15 (s) |
| 9 | α-glucose [2, 3] | 5.18 (d) |
| 10 | β-glucose [3] | 4.60 (d), 3.23 (m) |
| 11 | Unsaturated fatty acid [6] | 1.61, 1.25 (s), 0.87 (m) |

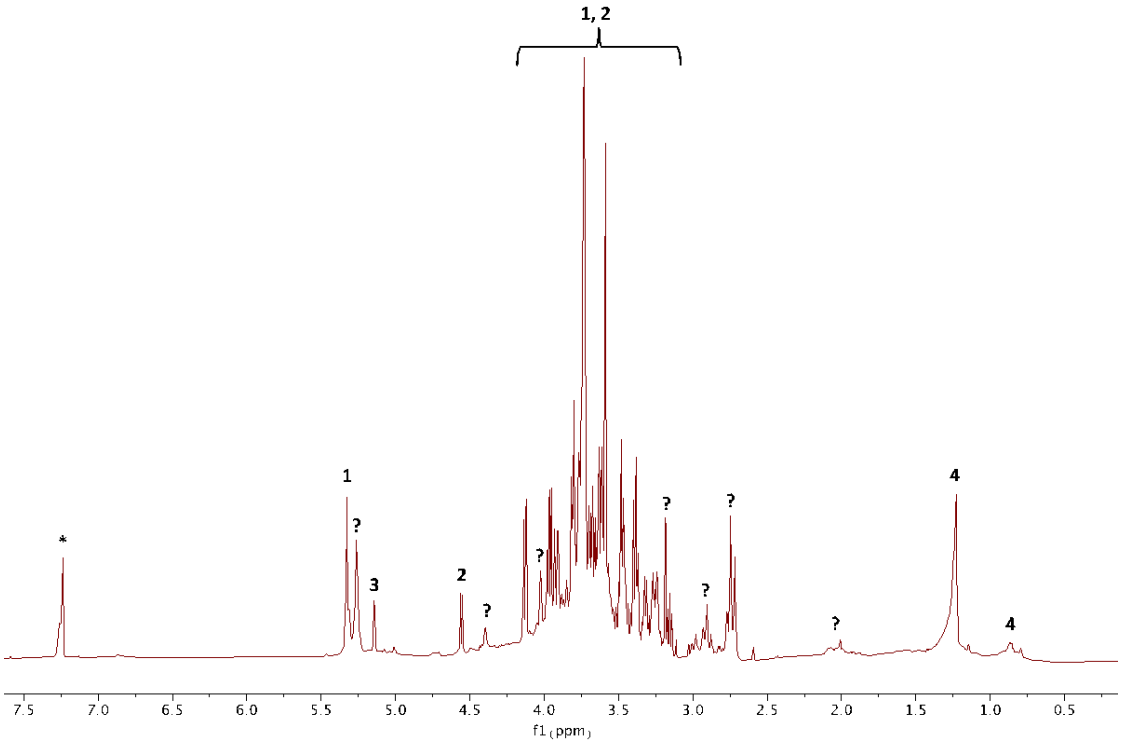


Figure 30. $^{1}$H spectrum of the CHT biphasic sample; the large water signal from the aqueous layer was suppressed via presaturation. (? indicates unidentified resonances.)

Table 5. $^{1}$H Chemical shift assignments for CHT.

| Peak Label | Assignment | Chemical shift, δ (ppm) |
|---|---|---|
| 1 | Sucrose [2, 3, 6] | 5.34 (m), 4.15 (d), 3.82 (m), 3.76, 3.61 |
| 2 | β-glucose [4] | 4.58 (d), 3.18 (m) |
| 3 | α-glucose [2-4] | 5.17 |
| 4 | Saturated fatty acid [7] | 1.27 (s), 0.86 (m) |

### 4.2.1 Experimental Methods

For the tea pure solvent extraction samples, 25 mg of cryo-ground tea leaves (Watermelon Lime Zinger Caffeine Free Herbal Tea made by Celestial Seasonings, Inc. Boulder CO, USA and Benner Green Tea Original by Aldi, Inc. Batavia, IL) were added to 3 ml of $D_2O$ and $CDCl_3$, respectively. These were mixed well. The mixtures were then filtered using a 45 μm sterile syringe filter before transferring to a 5-mm NMR tube.

For the biphasic tea samples, 250 μL $CDCl_3$ and 250uL of $D_2O$ were added into a 5-mm NMR tube, then ~6.5mg of cryo-ground tea leaves were transferred into the tube and mixed well with the solvents by shaking. The NMR tube containing the biphasic sample was centrifuged with a hand crank centrifuge until a well separated biphasic sample formed.

A Bruker AVIII 400 MHz NMR spectrometer with a BBFO probe was used in this study.

The number of scans to be collected were determined based upon obtaining sufficient signal-to-noise. For the tea extract biphasic samples, the number of scans ranged between 16 and 32.

Standard $^1H$ NMR spectra were collected for the pure solvent extractions of the teas (with and without presaturation for the aqueous and organic extractions, respectively).

Standard $^1H$ NMR spectra (with presaturation on water) and one-shot double-slice selection spectra were collected for the biphasic, in-tube tea extraction samples. In the one-shot double-slice selection experiment, alternative polarity of the gradient pulses (±3.43 G/cm) were used to improve the spectral properties such as phasing and baseline line shapes.

### 4.2.2 Results and Discussion

The pure tea solvent extraction samples were used for experiment set up and sample shimming, for clarification around $^{1}H$ signal assignments, and for comparison against the in-tube biphasic extraction samples. The OSDS experiment was applied to the biphasic NMR samples obtained via in-tube extractions of tea leaves. Pictures of the biphasic NMR samples (Figures 31a and 31b) show insoluble tea leaf particulate settled near the interface of the aqueous and organic phases (the $D_2O$ phase is the top layer, while the $CDCl_3$ phase is the bottom layer).

In the OSDS spectra of these samples (Figures 31c and 31d), all $^{1}H$ signals corresponding to the organic phase appear as negative peaks, whereas the aqueous phase have positive peaks. First of all, we note that the spectral resolution of the one-shot double-slice spectra of the CHT and GBT biphasic samples (Figures 31c and 31d) is comparable to that of their presaturation (presat) $^{1}H$ spectra (Figures 31e and 31f). To make a comparison, NMR spectra of monophasic samples of the $D_2O$ and $CDCl_3$ extracts are given for CHT in Figures 31g and 31i, respectively, and for BGT in Figures 31h and 31j, respectively. As expected, the spectra of the pure $D_2O$ extracts (Figures 31g and 31h) contain various amino acids, saccharides, and catechins [2, 3]. The corresponding signals of these components in the aqueous phase of the biphasic samples are clearly evident as positive peaks (Figures 31c and 31d). The spectra of the pure $CDCl_3$ extracts (Figures 31i and 31j) primarily contain unsaturated fatty acids, represented by the peaks at 0.9 and 1.2 ppm [6]. The BGT sample also contains significant levels of caffeine, as indicated by the signals at 7.5, 4.0, 3.6, and 3.4 ppm [3]. These spectral features of the organic solubles are also well-preserved in the one-

shot double-slice spectra (Figures 31c and 31d) as the negative peaks. It is worth noting that the signature peaks of caffeine in the BGT biphasic sample demonstrate the greater solubility of caffeine in $CDCl_3$ than in $D_2O$.

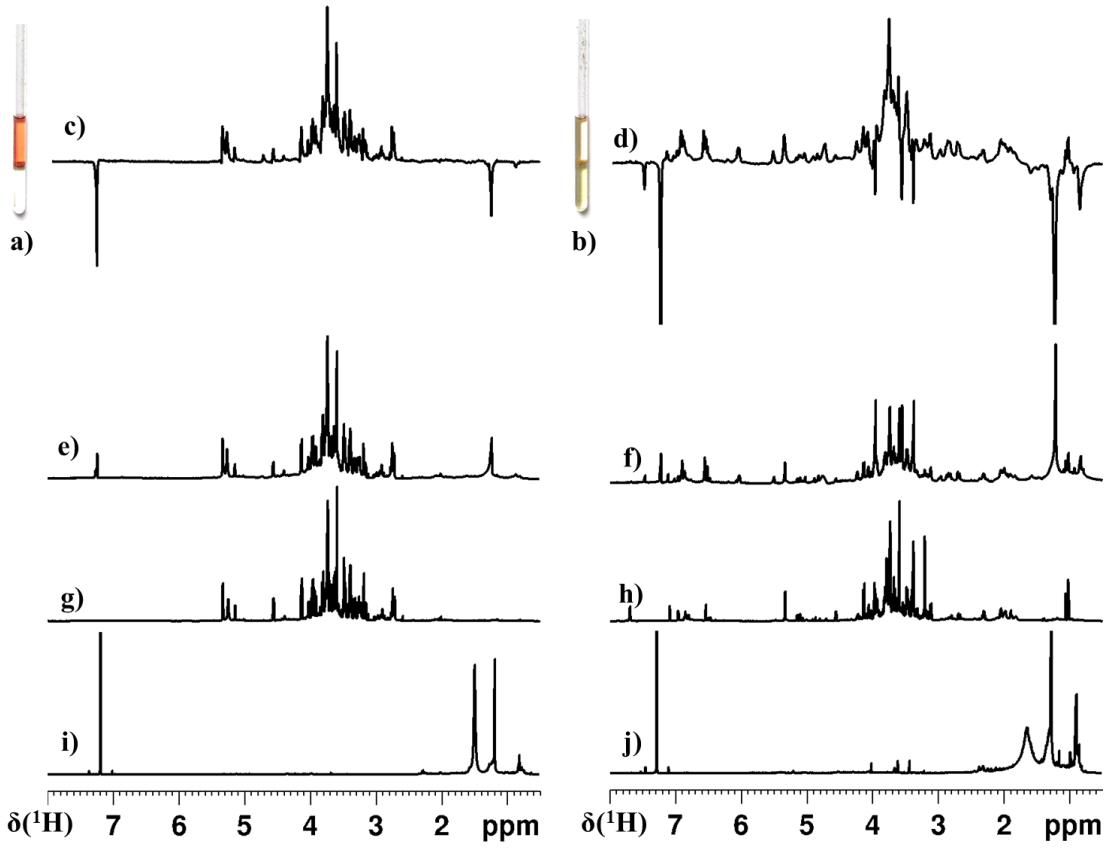


Figure 31. Pictures of biphasic $CDCl_3/D_2O$ samples of a) CHT and b) BGT. One-shot double-slice NMR spectra acquired with a gradient strength of 3.43 G/cm and a ReBurp pulse width of 1600 µs for c) CHT and d) BGT. Conventional presat $^1H$ spectra of the biphasic samples for e) CHT and f) BGT. The presat $^1H$ spectra of pure g) CHT $D_2O$ extract and h) BGT $D_2O$ extract are shown, along with the standard $^1H$ spectra of pure i) CHT $CDCl_3$ extract and j) BGT $CDCl_3$ extract.

### 4.2.3 Conclusions

This application clearly demonstrates that the OSDS $^{1}$H experiment is robust and has high selectivity and sensitivity, even when applied to biphasic samples containing insoluble materials which may, in principle, affect magnetic field homogeneity across that sample. It is conceivable that NMR signals arising from insoluble materials near the center of the NMR coil are effectively eliminated by the inversion of the ReBurp pulse.

## 4.3 Biphasic Coffee Extracts

As cold brew coffee is a popular new trend, it is a point of interest to understand the chemical differences between cold and hot brew coffees. These compositional variations can explain differences observed in flavor profiles, as well as potential implications for health benefits. To investigate these differences, we applied the OSDS selection experiment to biphasic NMR samples composed of in-tube extractions of cold brew coffee (CBC) and hot brew coffee (HBC).

The $^{1}$H NMR spectrum (collected using presaturation to suppress the water signal) of the biphasic HBC extract sample is shown in Figure 32, with the assignments summarized in Table 6. The HBC assignments are representative for the CBC biphasic sample as well.

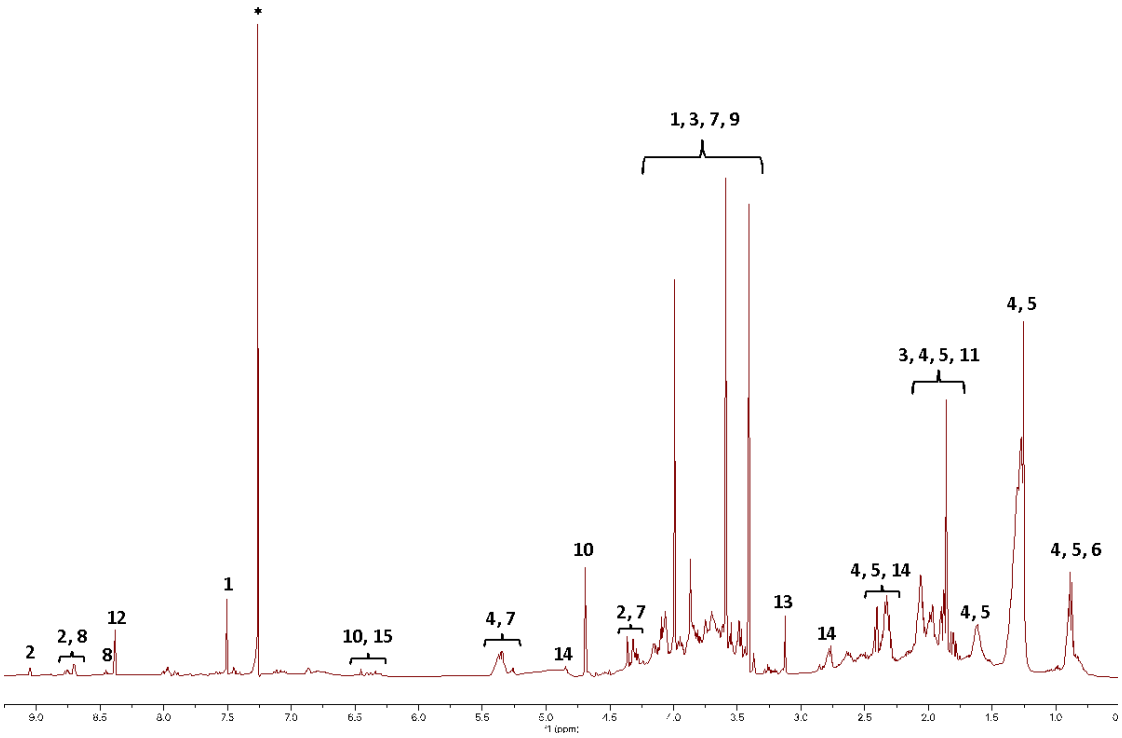


Figure 32. $^{1}$H spectrum of the HBC biphasic sample; the large water signal from the aqueous layer was suppressed via presaturation.

Table 6. $^{1}$H Chemical shift assignments for HBC.

| Peak Label | Assignment | Chemical shift, δ (ppm) |
|---|---|---|
| 1 | Caffeine | 7.50 (s), 3.99 (s), 3.59 (s), 3.41 (s) |
| 2 | Trigonelline [7] | 9.05 (s), 8.76 (t), 4.36 (s) |
| 3 | Quinic acid [8] | 4.07 (m), 3.95 (td), 3.48 (m) |
| 4 | Linoleic acid | 5.35 (m), 2.77 (m), 2.33 (m), 2.06 (m), 1.60, 1.28, 0.88 |
| 5 | Palmitic acid | 2.33 (m), 1.60, 1.28, 0.88 |
| 6 | Lactic acid [7] | 4.07 (m) |
| 7 | Glycerol ester | 4.29 (dd), 4.14 (m), 2.33 (m) |
| 8 | *N*-methylpyridinium [9] | 8.70 (d), 8.45 |
| 9 | *myo*-inositol [8] | 3.44 |
| 10 | 2-furylmethanol [9] | 6.41 (d), 4.69 (s) |
| 11 | Acetic acid [8][6] | 1.86 (s) |
| 12 | Formic acid [7] | 8.38 (s) |
| 13 | Choline [8] | 3.13 (s) |
| 14 | *γ*-quinide [9] | 4.84, 2.42 (d) |

| | | |
|---|---|---|
| 15 | 5-caffeoylquinic acid [9] | 6.29 |

### 4.3.1 Experimental Methods

For the coffee extractions, two vials were prepared by combining ~500 mg of ground coffee beans (Organic Rainforest Blend Whole Bean Coffee by San Francisco Bay Coffee, Lincoln, CA, USA) with 10 mL of $D_2O$; the vials were shaken/swirled to ensure contact of the $D_2O$ and the coffee grounds. The cold brew coffee vial was then left at room temperature for 24 hours with occasional swirling. The hot brew coffee vial was brought to a boil, and left to boil with occasional swirling for two minutes. The contents of both vials were transferred to polystyrene centrifuged tubes and centrifuged at ~3000 RCF for 25 minutes. The liquid contents were decanted into fresh containers, leaving the coffee grinds behind in the tubes. 250 μL of $CDCl_3$ were added to two NMR tubes, followed by the addition of 250 μL of the $D_2O$ coffee samples (separate tubes for each brew method). The samples were gently inverted and shaken repeatedly to perform the extraction. The tubes were then placed in centrifuge tubes with home-made foam inserts and centrifuged at ~3000 RCF for 30 minutes until well-separated biphasic samples formed.

A Bruker NEO 600 MHz spectrometer with a TCI cryoprobe was used in this study.

The number of scans to be collected were determined based upon obtaining sufficient signal-to-noise. For the coffee extract biphasic samples, the number of scans ranged between 16 and 64.

Standard $^1H$ NMR spectra, 1D OSDS spectra, and 2D OSDS TOCSY spectra were collected for the coffee extract biphasic samples.

In the OSDS experiment, alternative polarity of the gradient pulses (±3.43 G/cm) were used to improve the spectral properties such as phasing and baseline line shapes.

A presat TOCSY pulse with the mlev spin-lock scheme was used by replacing the 90° pulse for magnetization preparation with a selective ReBurp pulse in our investigation.

### 4.3.2 Results and Discussion

Compared with classic presat $^{1}$H spectra (Figures 33a and 33b) of the biphasic CBC and HBC samples, the 1D one-shot double-slice spectra of CBC (Figure 33c) and HBC (Figure 33d) allow an immediate identification of the signals in the aqueous (positive peaks) and organic (negative peaks) layers. It is clear that the organic layer contains caffeine (peaks at 7.5, 4.0, 3.6, and 3.4 ppm) for both CBC and HBC, as expected. The subtle spectroscopic differences between CBC and HBC are revealed by combining one-shot double-slice scheme with a 2D TOCSY experiment (Figures 33e and 33f). While the spectral “fingerprints” of the aqueous layers (dark red) of CBC and HBC are very similar, the greater intensity of the dark green cross peaks in the HBC one-shot double-slice TOCSY spectrum (Figure 33f) indicate much higher levels of triglyceride fatty acid components- such as linoleic acid (5.4, 2.8, 2.3, 2.1, 1.6, 1.3, and 0.9 ppm) and palmitic acid (2.3, 1.6, 1.3, and 0.9 ppm)- in the HBC organic layer than in the CBC organic phase.

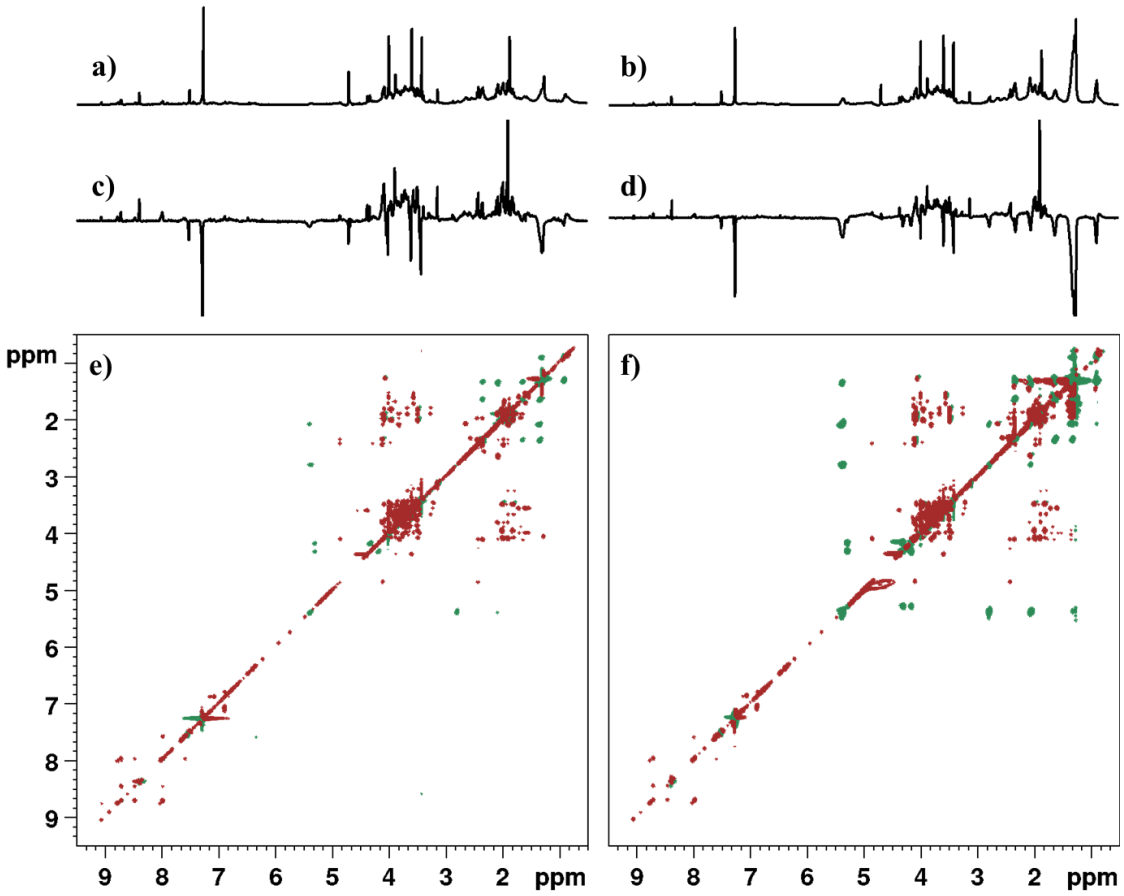


Figure 33. Classic 1D presat $^{1}H$ spectra for a) CBC and b) HBC. One-shot double-slice NMR spectra for c) biphasic CBC and d) HBC acquired with a pulse field gradient strength of approximately 3.43 G/cm, and a ReBurp pulse width of 1000 µs. One-shot double-slice TOCSY spectra (mixing times of 60 ms) for e) CBC and f) HBC. Dark red and dark green cross peaks respectively represent chemical species from the $D_2O$ and $CDCl_3$ layers.

### 4.3.3 Conclusions

Our results suggest that cold brew coffee preserves the same major water-soluble ingredients as those in hot brew coffee. However, the levels of organic-soluble triglyceride-like components are greatly reduced by using the cold brew method. The OSDS 2D TOCSY proved to be a very useful tool for identifying these differences

## REFERENCES


[1] Seeger, K. Simple and Rapid (Extraction) Protocol for NMR Metabolomics-Direct Measurement of Hydrophilic and Hydrophobic Metabolites Using Slice Selection. *Anal Chem* **2021**, *93* (3), 1451-1457. DOI: 10.1021/acs.analchem.0c03353 From NLM Medline.

[2] Rubel Mozumder, N. H. M.; Lee, Y.-R.; Hwang, K. H.; Lee, M.-S.; Kim, E.-H.; Hong, Y.-S. Characterization of tea leaf metabolites dependent on tea (Camellia sinensis) plant age through 1H NMR-based metabolomics. *Applied Biological Chemistry* **2020**, *63* (1). DOI: 10.1186/s13765-020-0492-7.

[3] Yuan, Y.; Song, Y.; Jing, W.; Wang, Y.; Yang, X.; Liu, D. Simultaneous determination of caffeine, gallic acid, theanine, (−)-epigallocatechin and (−)-epigallocatechin-3-gallate in green tea using quantitative1H-NMR spectroscopy. *Anal. Methods* **2014**, *6* (3), 907-914. DOI: 10.1039/c3ay41369a.

[4] Elmi, A.; Spina, R.; Risler, A.; Philippot, S.; Merito, A.; Duval, R. E.; Abdoul-Latif, F. M.; Laurain-Mattar, D. Evaluation of Antioxidant and Antibacterial Activities, Cytotoxicity of Acacia seyal Del Bark Extracts and Isolated Compounds. *Molecules* **2020**, *25* (10). DOI: 10.3390/molecules25102392 From NLM Medline.

[5] Zhang, M.; Otake, K.; Miyauchi, Y.; Yagi, M.; Yonei, Y.; Miyakawa, T.; Tanokura, M. Comprehensive NMR analysis of two kinds of post-fermented tea and their anti-glycation activities in vitro. *Food Chem* **2019**, *277*, 735-743. DOI: 10.1016/j.foodchem.2018.11.028 From NLM Medline.

[6] Munz, E.; Jakob, P. M.; Borisjuk, L. The potential of nuclear magnetic resonance to track lipids in planta. *Biochimie* **2016**, *130*, 97-108. DOI: 10.1016/j.biochi.2016.07.014 From NLM Medline.

[7] Toci, A. T.; de Moura Ribeiro, M. V.; de Toledo, P.; Boralle, N.; Pezza, H. R.; Pezza, L. Fingerprint and authenticity roasted coffees by (1)H-NMR: the Brazilian coffee case. *Food Sci Biotechnol* **2018**, *27* (1), 19-26. DOI: 10.1007/s10068-017-0243-7 From NLM PubMed-not-MEDLINE.

[8] Rocha Baqueta, M.; Coqueiro, A.; Henrique Marco, P.; Mandrone, M.; Poli, F.; Valderrama, P. Integrated (1)H NMR fingerprint with NIR spectroscopy, sensory properties, and quality parameters in a multi-block data analysis using ComDim to evaluate coffee blends. *Food Chem* **2021**, *355*, 129618. DOI: 10.1016/j.foodchem.2021.129618 From NLM Medline.

[9] Wei, F.; Furihata, K.; Hu, F.; Miyakawa, T.; Tanokura, M. Two-dimensional 1H-13C nuclear magnetic resonance (NMR)-based comprehensive analysis of roasted coffee bean extract. *J Agric Food Chem* **2011**, *59* (17), 9065-9073. DOI: 10.1021/jf201716w From NLM Medline.

# Chapter 5

## CONCLUSIONS AND FUTURE WORK

I started the journey of the development of a new experimental method in slice selection NMR spectroscopy with the measurement of self-diffusion properties of special surfactants. Through these basic measurements, the pulsed field gradient technique, a key component in slice selection NMR methodology, was utilized and understood to a new level. This paved the way for me to further apply this understanding to the development of the new technique in slice selection NMR. In the meantime, we proposed to use the Sutherland dynamic viscosity model to interpret the NMR self-diffusion coefficient data measured for Natsurf 265 solutions. The experimental findings that the self-diffusion coefficient for Natsurf 265 solutions is proportional to $1/\sqrt{C_T}$ can be seemingly explained through a model that contains a spherical micelle structure. The proposed model also predicts that the diffusion coefficient is proportional to $\sqrt{T}$, which was not verified in this thesis. In the future, experimental NMR diffusion measurements of the Natsurf 265 at various temperatures would be helpful for validation of the model for the micelle structures.

This thesis next utilizes pulsed field gradients for one-dimensional NMR imaging, which was crucial to establishing proper biphasic sample preparation techniques for slice selection NMR experiments. Biphasic samples of model compounds were used to establish experimental parameters for classic slice selection NMR. As part of the optimization of these classic slice selection NMR methods, a deeper understanding of shaped NMR pulses was ascertained through experimental findings and review of the literature. This laid the fundamental groundwork for the core development presented in this thesis, a OSDS selection NMR experiment for

biphasic systems. Unlike previously used slice selective experiments, the OSDS experiment allows detection of NMR signals from both phases of a biphasic sample simultaneously as oppositely phased peaks in a single spectrum. It has been demonstrated that this method is robust, easy to implement, and can be combined with 2D TOCSY experiments for structural characterization with spatial-specificity. It is readily applicable to not only well-defined, model biphasic systems, but also to practical chemical separation problems involving in-tube extractions. The high selectivity of the OSDS selective $^{1}H$ experiment has been demonstrated via examples of in-tube tea and coffee extractions. Because of the nature of simultaneous excitations with opposite r.f. phases, the OSDS experiment has the potential to monitor chemical kinetic and dynamic processes occurring between two phases when "real time" kinetic data are essential.

As indicated previously, the ReBurp pulse used in the OSDS experiment has a major limitation: the pulse offsets and bandwidths, which are predetermined by the pulse width, cannot be adjusted independently. This could limit the location and thickness of the selected slices, thus limiting its applications to more complex biphasic systems. The limitation in the ability to tune the slice thickness may also prevent the improvement in sensitivity enhancement through the increase of the slice size. New engineering and design of shaped pulses to produce offsets and bandwidths relatively independently is essential to further improve spectral quality and/or sensitivity. There are also possibilities for incorporating the one-shot double-slice pulse sequence into other multidimensional NMR experiments, and these should be investigated as well. As far as practical applications, this experiment should be tested on a dynamic process, such as a biphasic chemical reaction, to test its ability to track the species in

the two phases simultaneously, as well as its performance for kinetics measurements. The application of this experiment should also be tested on a large set of in-tube extractions for metabolomics, to see how the single spectra perform in terms of differentiation and information density when compared to either monophasic samples of extractions or classic slice selection experiments performed on in-tube extractions. These future directions provide opportunities for further advancement of the OSDS experiment, and for the continued development of the slice selection NMR field.

# Appendix A

## PERMISSIONS

Reproduced from *Phys. Chem. Chem. Phys*., 2022, 24, 17961 with permission from the PCCP Owner Societies.

## Appendix B

## PULSE SEQUENCE: 1D GRADIENT IMAGING

*(Bruker NEO Version)*

```
;imgegp1d
;avance-version (16/07/18)
;1D Gradient Echo for gradshim-procedure
;
;$CLASS=HighRes
;$DIM=1D
;$TYPE=
;$SUBTYPE=
;$COMMENT=

#include<Avance.incl>
#include<Grad.incl>
#include<De.incl>

"d11=30m"
"p0=2u"
"plw0=plw1/6.3095"

1 ze
  d11 UNBLKGRAD
2 d1
```

```
  20u pl0:f1
  p0:f1 ph1
  d27 gron1
  5u groff
  d15
  d21 gron2
  ACQ_START(ph30,ph31)
  aq DWELL_GEN:f1
  5u groff
  rcyc=2
  400m wr #0
  d11 BLKGRAD
exit

ph1=0
ph30=0
ph31=0

;pl0: f1 channel : pl1+8dB
;pl1 : f1 channel - power level for pulse (default)
;p0 : f1 channel -  small flip angle              2 usec]
;d1 : relaxation delay
;d11: delay for disk I/O                        [30 msec]
;d15: echo time
```

;d21: gradient stabilisation delay

;d27: length of dephasing gradient (phase encode time)

;ns: 1

;ds: 0

;$Id: imgegp1d,v 1.7 2016/11/11 13:43:39 ber Exp $

## Appendix C

## PULSE SEQUENCE: 1D ONE-SHOT DOUBLE-SLICE

*(Bruker Avance NMR Spectrometer)*

```
;one-shot double-slice
;avance-version
;1D sequence
;
;$CLASS=HighRes
;$DIM=1D
;$TYPE=
;$SUBTYPE=
;$COMMENT=

#include <Avance.incl>
#include <Grad.incl>

"acqt0=-p1*2/3.1416"
"spw2=plw1/((p12*90.0)/(p1*totrot2))*((p12*90.0)/(p1*totrot2))*(integfac2*integfac
2)"
"spoffs2=cnst11"
"l0=1"

1 ze
2 30m
```

```
 20u pl1:f1
 d1
 50u UNBLKGRAD
if "l0%2==1"
{
 5u gron0
 (p12:sp2 ph1):f1
 5u groff
}
else
{
 5u gron1
 (p12:sp2 ph1):f1
 5u groff
}
 50u BLKGRAD
 d20
 "l0=l0+1"
 go=2 ph31
 30m mc #0 to 2 F0(zd)
 20u BLKGRAD
exit

ph1=0 0 2 2 1 1 3 3
```

ph31=0 2 2 0 1 3 3 1

;pl1 : f1 channel - power level for pulse (default)

;p1 : f1 channel -  high power pulse

;p12 : f1 channel - Reburp.1000 pulse [1 - 2ms]

;d1 : relaxation delay; 1-5 * T1

;NS: 1 * n, total number of scans: NS * TD0

;$Id: zg,v 1.9 2006/11/10 10:56:44 ber Exp $

## Appendix D

## PULSE SEQUENCE: 2D OSDS-TOCSY

*(Bruker Avance NMR Spectrometer)*

```
;osds-mlevphpr
;avance-version (12/01/11)
;homonuclear Hartman-Hahn transfer using MLEV17 sequence
;   for mixing
;using two power levels for excitation and spinlock
;phase sensitive
;
;A. Bax & D.G. Davis, J. Magn. Reson. 65, 355-360 (1985)
;
;$CLASS=HighRes
;$DIM=2D
;$TYPE=
;$SUBTYPE=
;$COMMENT=

#include <Avance.incl>
#include <Delay.incl>
#include <Grad.incl>

"p5=p6*.667"
"p7=p6*2"
```

"d11=30m"

"d12=20u"

"d13=4u"

"in0=inf1"

"d0=in0/2-p1*2/3.1416-4u"

"spw2=plw1/(((p12*90.0)/(p1*totrot2))*((p12*90.0)/(p1*totrot2))*(integfac2*integfa
c2))"

"spoffs2=cnst12"

"SCALEF=p7*2/p5"

"FACTOR1=((d9-p17*2)/(p6*64+p5))/SCALEF"

"l1=FACTOR1*SCALEF"

1 ze

2 d11

3 d12 pl9:f1

 d1 cw:f1 ph29

 d13 do:f1

 50u UNBLKGRAD

 d12 pl1:f1

 5u gron0

 (p12:sp2 ph1):f1

 5u groff

 d0

 4u pl10:f1

(p17 ph26)

;begin MLEV17

4 (p6 ph22 p7 ph23 p6 ph22)

(p6 ph24 p7 ph25 p6 ph24)

(p6 ph24 p7 ph25 p6 ph24)

(p6 ph22 p7 ph23 p6 ph22)

(p6 ph24 p7 ph25 p6 ph24)

(p6 ph24 p7 ph25 p6 ph24)

(p6 ph22 p7 ph23 p6 ph22)

(p6 ph22 p7 ph23 p6 ph22)

(p6 ph24 p7 ph25 p6 ph24)

(p6 ph22 p7 ph23 p6 ph22)

(p6 ph22 p7 ph23 p6 ph22)

(p6 ph24 p7 ph25 p6 ph24)

(p6 ph22 p7 ph23 p6 ph22)

(p6 ph22 p7 ph23 p6 ph22)

(p6 ph24 p7 ph25 p6 ph24)

(p6 ph24 p7 ph25 p6 ph24)

(p5 ph23)

lo to 4 times l1

;end MLEV17

(p17 ph26)

50u BLKGRAD

go=2 ph31

d11 mc #0 to 2 F1PH(calph(ph1, +90) & calph(ph29, +90), caldel(d0, +in0))

exit

ph1=0 2 2 0 1 3 3 1

ph22=3 1 3 1 0 2 0 2

ph23=0 2 0 2 1 3 1 3

ph24=1 3 1 3 2 0 2 0

ph25=2 0 2 0 3 1 3 1

ph26=0 2 0 2 1 3 1 3

ph29=0

ph31=0 2 2 0 1 3 3 1

;pl1 : f1 channel - power level for pulse (default)

;pl9 : f1 channel - power level for presaturation

;pl10: f1 channel - power level for TOCSY-spinlock

;p1 : f1 channel - 90 degree high power pulse

;p5 : f1 channel - 60 degree low power pulse

;p6 : f1 channel - 90 degree low power pulse

;p7 : f1 channel - 180 degree low power pulse

;p12 : f1 channel - Reburp.1000 ulse [1-2ms]

;p17: f1 channel - trim pulse [2.5 msec]

;d0 : incremented delay (2D)

;d1 : relaxation delay; 1-5 * T1

;d9 : TOCSY mixing time

;d11: delay for disk I/O [30 msec]

;d12: delay for power switching [20 usec]

;d13: short delay [4 usec]

;l1: loop for MLEV cycle: (((p6*64) + p5) * l1) + (p17*2) = mixing time

;inf1: 1/SW = 2 * DW

;in0: 1/(1 * SW) = 2 * DW

;nd0: 1

;ns: 8 * n

;ds: 16

;td1: number of experiments

;FnMODE: States-TPPI, TPPI, States or QSEQ

;Processing

;PHC0(F1): 180

;PHC1(F1): -180

;FCOR(F1): 1

;$Id: mlevphpr,v 1.12 2012/01/31 17:49:27 ber Exp $

## Appendix E

## PUBLISHED WORK

PCCP

ROYAL SOCIETY OF CHEMISTRY

COMMUNICATION

Check for updates

Cite this: *Phys. Chem. Chem. Phys.*, 2022, **24**, 17961

Received 1st June 2022,
Accepted 15th July 2022

DOI: 10.1039/d2cp02497g

rsc.li/pccp

# A one-shot double-slice selection NMR method for biphasic systems†

Kaitlyn Doolittle Catlin, ‡ Julia Simmons and Shi Bai *

**We propose a new and robust one-shot double-slice selection experiment to detect $^1$H NMR signals of biphasic systems simultaneously. The resultant spectrum contains opposite-phased peaks representing the chemical species from the two phases, respectively.**

## 1. Introduction

Slice selective NMR methods,[1] which combine a selective radio frequency (r.f.) pulse with pulsed field gradients, enable one to obtain a $^1$H spectrum that represents only the chemical species present within a selected region, or "slice," of an NMR sample tube. Slice selective NMR spectroscopy has been utilized in the analyses of diffusion properties,[2] liquid-liquid interfaces,[3] rapid reaction kinetics,[4] biofuel[5] and crude oil emulsions,[6] hydrophilic/hydrophobic metabolites,[7] and ion-transportation in lithium-ion battery electrolytes.[8] Sensitivity enhancement using simultaneous multiple slice excitation[9] and development of quantitative methods[10]of slice selection NMR have both been proposed. Implementation of slice selective 2D homonuclear correlation spectroscopy has also been reported.[11] In these cases, slice selective NMR provides the unique ability to observe the spatial distribution of chemical species across a sample non-destructively and rapidly. When applied to a biphasic system in which aqueous and organic layers coexist, representative spectra of the organic and aqueous phases can be obtained by choosing two different frequency offsets for the selective r.f. pulses.

In classic slice selection NMR spectroscopy,[1] a $z$-axis magnetic gradient pulse is applied along with a selective r.f. excitation pulse (Fig. 1a) to achieve selective excitation of the nuclear spins occupying a targeted spatial location. When applying a pulsed field gradient ($G_z$), the magnetic field strength, $B(z)$, is dependent on the coordinate, $z$, along the axial direction of the NMR tube such that $B(z) = B_0 + zG_z$. Consequently, the resonance frequency ($\nu_z$) of nuclear spins is also dependent on $z$: $\nu_z = \nu_0 + \gamma zG_z/2\pi$, where $\gamma$ is the $^1$H gyromagnetic ratio. A $z$-axis field gradient can be applied along an NMR sample such that the magnetic field strength stays at $B_0$ at the centre of the NMR coil, but increases and decreases gradually above and below the centre coordinate. In this case, the frequency range ($\Delta\nu_{\pm z}$) induced by the gradient pulse within a defined distance of $\pm z$ along the NMR tube is $\Delta\nu_{\pm z} = \nu_z - \nu_{-z} = z\gamma G_z/\pi$.

A selective excitation pulse can be characterized by its offset frequency ($\Omega$) and bandwidth ($\Delta\nu$).[12] If the offset of the selective pulse is chosen such that $\Omega = \nu_z - \nu_0 = z\gamma G_z/2\pi$, only the spins with $\nu_z$ at point $z$ will be excited or selected (Fig. 1d). If a finite cross-section with a thickness ($\Delta z = z_1 - z_2$) centred around $z$ is considered, the frequency range induced by the gradient pulse is $\nu_1 - \nu_2 = (z_1 - z_2)\gamma G_z/2\pi$. Thus, a selective pulse with the offset of $\Omega$ and bandwidth of $\Delta\nu = \nu_1 - \nu_2$ can in principle excite the spins confined within $\Delta z$ at point $z$. In other words, the slice thickness ($\Delta z = (2\pi/\gamma G_z)\Delta\nu$) depends on $G_z$ and $\Delta\nu$ of the excitation pulse. In the case of a strong magnetic field gradient and a sufficiently large r.f. bandwidth, all $^1$H chemical shift offsets can be virtually treated in the same slice.[13]

## 2. Results and discussion

Two slice selective NMR spectra of aqueous (red) and organic (blue) layers of a model biphasic NMR sample, consisting of sucrose in $D_2O$ and 4-chromanone in $CDCl_3$, were obtained by choosing two offsets of the selective r.f. excitation pulse (Fig. 1a). Deficient spectral selectivity and poor spectral phasing are noted in both spectra. The excitation pulse is often appended with a refocusing pulse incorporated with a gradient pulse to suppress the magnetic susceptibility artifacts.[10,14] The modified pulse scheme produces spectra with improved spectral selectivity (Fig. 1b). A schematic plot of the model

*Department of Chemistry and Biochemistry, University of Delaware, Newark, DE 19716, USA. E-mail: bais@udel.edu*

† Electronic supplementary information (ESI) available. See DOI: https://doi.org/10.1039/d2cp02497g

‡ Current address: Protein Analytical Chemistry, Genentech, Inc., South San Francisco, California 94080, USA.

This journal is © the Owner Societies 2022

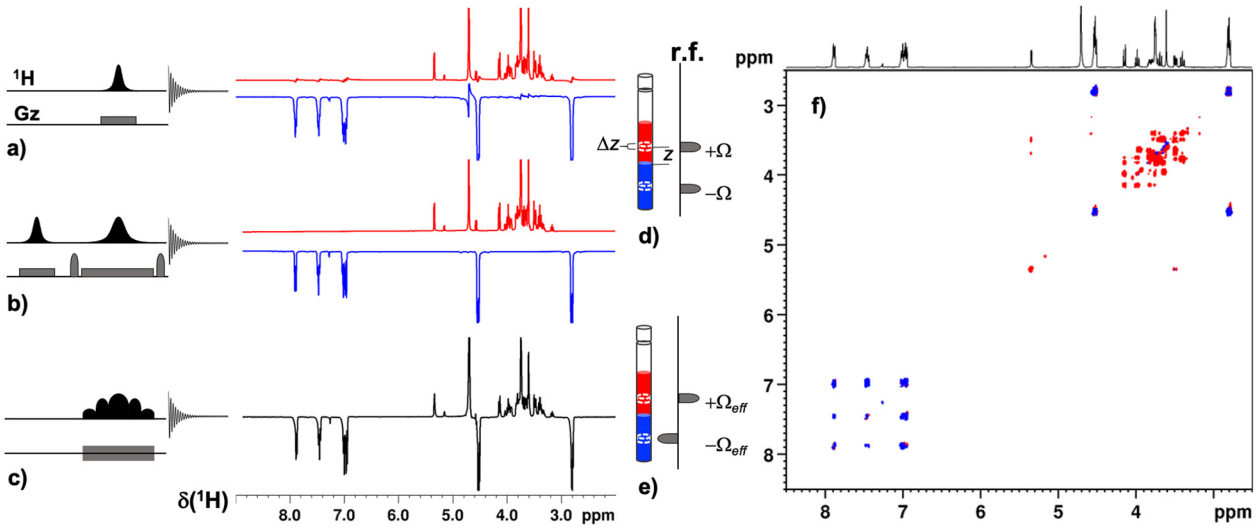


Fig. 1 Slice selection $^{1}$H NMR spectra: (a) An excitation selective pulse (EBurp: 1236 μs) produces spectra of the aqueous (red) and organic (blue, phased negatively for comparison) layers of a model biphasic sample of sucrose in $D_2O$ and 4 chromanone in $CDCl_3$. (b) An excitation Eburp pulse followed by a refocusing pulse (ReBurp, 1600 μs) leads to the spectra of aqueous (red) and organic phases (blue, phased negatively for comparison) of the same model sample. The bandwidth and offset of these pulses are 3915 Hz and ±7500 Hz. (c) One-shot double-slice selection spectrum of the model biphasic sample using a ReBurp pulse (1600 μs) with a bandwidth of 3915 Hz and the effective offsets are ±1684 Hz. (d) Schematic plot of the biphasic sample tube marked with *z* and Δ*z*, indicating the slices excited by two separate experiments using different offsets. This schematic plot represents the cases for both slice selection pulse programs presented in Fig. 1a and b. (e) Schematic plot of the biphasic sample tube signifying the two slices excited simultaneously by only one ReBurp pulse that produces two effective excitation profiles with opposite phases. (f) One-shot double-slice version of a TOCSY spectrum of the model biphasic sample. The 90° excitation hard pulse in the TOCSY pulse sequence is replaced by a ReBurp pulse of 1600 μs along with a rectangular gradient pulse of the same length. The resulting 2D spectrum is phase-sensitive with colour coded cross peaks for sucrose (red) and 4-chromanone (blue). The TOCSY mixing time is 60 ms. The gradient strength used for all experiments is 3.43 G cm$^{-1}$.

biphasic sample (Fig. 1d) and the relative relationship between *z* and Δ*z* are given for the two representative slice selection pulse programs (Fig. 1a and b). Corresponding to the schematic plot of the biphasic sample (Fig. 1d), a 1D $^{1}$H image (Fig. S1, ESI†) shows an interface between the aqueous and organic layers of the model biphasic sample. There are a number of variations of selective excitation and refocusing pulses that can be employed in these classic slice selection experiments.[14] In the case of a biphasic sample, however, at least two NMR experiments with different offset frequencies are required to obtain two spectra representing the chemical species in two phases of the biphasic sample, respectively (Fig. 1a, b and d).

We propose a ''one-shot double-slice'' selection experiment (Fig. 1c), in which the excitation pulse is replaced by a Refocusing Band-selective Uniform-response Pure-phase (ReBurp) pulse.[12] When a ReBurp pulse is applied along with a gradient pulse, the NMR signals from the two phases of a biphasic system can be readily distinguished as opposite-phased peaks in the resulting spectrum of a single experiment (Fig. 1c). In fact, a ReBurp pulse inverts the on-resonance spins near the centre of the NMR coil, while exciting the spins above and below the centre of the coil *simultaneously* with r.f. pulses of opposite phases.

This effect can be clearly seen in ReBurp pulse simulations (Fig. 2a), in which the trajectory of the magnetisation shows an inversion (black arrow) for the on-resonance spins (Ω = 0). If the offsets of the ReBurp pulse are set to characteristic effective frequencies (±$\Omega_{eff}$), the magnetization trajectories (red arrows)

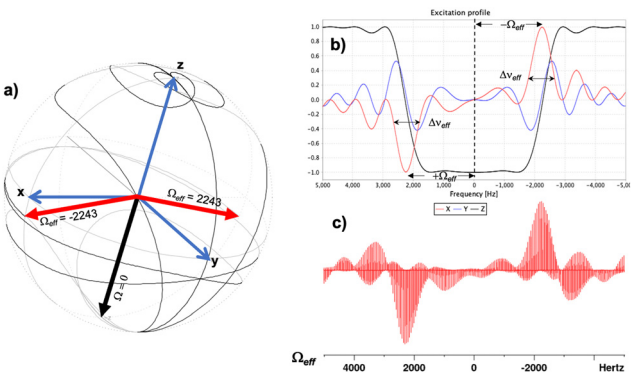


Fig. 2 (a) Shaped pulse simulation of ReBurp pulse (1200 μs) shows the trajectories of the magnetizations on-resonance (black) and off-resonance (± 2243 Hz, red). Note that the end points of magnetizations with the ±$\Omega_{eff}$ (± 2243 Hz) are nearly 180° out of phase along x-axis, enabling the simultaneous excitations. (b) Simulated excitation profile shows excitations along ±*x* at ±$\Omega_{eff}$ = ± 2243 Hz and Δ$\nu$ = 660 Hz at 30% of the profile height. (c) Experimental excitation profile of ReBurp pulse (1200 μs), obtained by varying the offset frequency, is highly consistent with the simulated effective offsets and bandwidth (red curve in b).

end in nearly opposite phases along the *x*-axis, indicative of simultaneous effective excitation of the nuclear spins with ±$\Omega_{eff}$. The simulated ReBurp pulse excitation profiles (Fig. 2b) also show an inversion of the on-resonance spins (black curve) and two simultaneous, opposite-phased side-lobes (red curve) with the effective bandwidth Δ$\nu_{eff}$ centred

 This journal is © the Owner Societies 2022

around $\pm\Omega_{eff}$. The experimental excitation profile (Fig. 2c) of the ReBurp pulse confirms a near-zero excitation in the vicinity of zero offset ($\Omega = 0$) while imposing opposite-phase excitations at $\pm\Omega_{eff}$, which is highly consistent with the simulated results. Due to their opposite r.f. polarities, the effects of these two side lobes cancel each other in the absence of a field gradient. However, in the presence of said gradient pulse, the two r.f. excitation side lobes (Fig. 2b and 2c) simultaneously select the signals of chemical species above and below the interface (Fig. 1e) corresponding to $\pm\Omega_{eff}$.

The resolution of the one-shot double-slice method is comparable to that of the conventional slice selection experiments. Note that the linewidths of the residual water peaks (4.7 ppm) are 3.4 – 3.5 Hz for the slice selection experiments and 3.6 Hz for the one-shot double-slice spectrum.

It is interesting to note that the one-shot double-slice scheme (Fig. 1c) can be readily incorporated to a 2D experiment to acquire through-bond correlations with spatial-specificity. For example, when the 90° pulse of a 2D TOCSY sequence is replaced by a ReBurp selective pulse combined with a field gradient pulse (see ESI† for details), a one-shot double-slice version of a 2D TOCSY spectrum is obtained for the model biphasic sample (Fig. 1f). This allows immediately differentiation of through-bond correlations between sucrose in the aqueous layer (red) and 4-chromanone in the organic layer (blue) based on the phases of their cross-peaks in just one 2D spectrum.

The one-shot double-slice selection NMR signal intensity is proportional to $\Delta z$ if the effects of nuclear spin relaxation and diffusion effects are negligible. As discussed before, $\Delta z$ depends on the bandwidth of the selective r.f. pulse. Further simulations indicate that both the ReBurp pulse bandwidth and its side lobe effective bandwidth decrease with the increase of pulse width (Table S1, ESI†). It is therefore anticipated that the peak intensity decreases as the increase of the pulse width, as verified experimentally (Fig. S2a, ESI†). For similar reasons, the one-shot double-slice NMR intensity decreases when the strength of gradient pulse is increased at a given pulse width (Fig. S2b, ESI†).

We first applied the one-shot double-slice selection experiment to biphasic NMR samples obtained *via* in-tube extractions of tea leaves. The two teas (see ESI† for details) chosen for this study were Celestial herbal tea (CHT) and Benner green tea (BGT). CHT does not contain caffeine, while BGT does. The tea leaves were cryo-ground and added to 5 mm NMR tubes containing 250 μL of $D_2O$ and 250 μL of $CDCl_3$. After mixing the tea leaves with the solvents by inverting and shaking, the NMR tubes were centrifuged with a hand crank centrifuge to form well-separated biphasic samples (see ESI† for details). Pictures of the biphasic NMR samples (Fig. 3a and b) show insoluble tea leaf particulate settled near the interface of the aqueous and organic phases (the $D_2O$ phase is the top layer, while the $CDCl_3$ phase is the bottom layer).

In the one-shot double-slice spectra of the CHT and GBT biphasic samples (Fig. 3c and d), the $^1H$ signals corresponding to the aqueous phase are positive whereas the peaks corresponding to the organic phase are negative. To make a comparison, NMR spectra of monophasic samples of the $D_2O$ and $CDCl_3$ extracts (see ESI† for details) are given for CHT in Fig. 3g and i, respectively. Similarly, spectra for BGT are given in Fig. 3h and j, respectively. As expected, the spectra of the pure $D_2O$ extracts (Fig. 3g and h) contain various amino acids, saccharides, and catechins.[15] The corresponding signals of these components in the aqueous phase of the biphasic samples are clearly evident as positive peaks (Fig. 3c and d). The spectra of the monophasic $CDCl_3$ extracts (Fig. 3i and j) primarily contain unsaturated fatty acids, represented by the peaks at 0.9 and 1.2 ppm.[16] As expected, the BGT sample also contains significant levels of caffeine, as indicated by the signals at 7.5, 4.0, 3.6, and 3.4 ppm.[15a] The spectral features of the organic soluble components are well-preserved in the one-shot double-slice spectra (Fig. 3c and d) as the negative peaks.

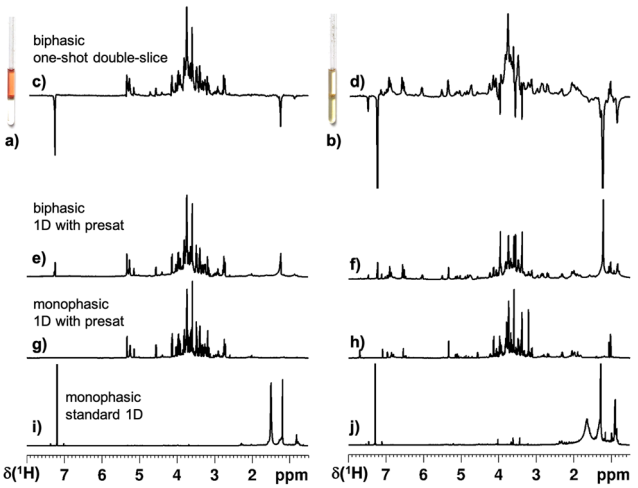


Fig. 3 Pictures of biphasic $CDCl_3/D_2O$ samples of CHT (a) and BGT (b). One-shot double-slice NMR spectra acquired with a gradient strength of 3.43 G $cm^{-1}$ and a ReBurp pulse width of 1600 μs for CHT (c) and BGT (d). $^1H$ presat spectra of the biphasic samples for CHT (e) and BGT (f). $^1H$ presat spectra of the monophasic CHT $D_2O$ extracts (g) and BGT $D_2O$ extracts (h) are shown along with the $^1H$ spectra of monophasic CHT $CDCl_3$ extracts (i) and BGT $CDCl_3$ extracts (j).

Spectral resolution of the one-shot double-slice spectrum is slightly inferior to that of the conventional 1D $^1H$ pre-saturation (presat) spectrum of a real biphasic sample. As an example, the linewidth of a well-resolved peak at 5.5 ppm in the aqueous layer is 14 Hz for the one-shot double-slice spectrum (Fig. 3c) while the linewidth of the same peak is about 11 Hz for a presat spectrum of the same biphasic sample (Fig. 3e). On the other hand, we do not observe a significant correlation between the linewidth and the ReBurp pulse excitation bandwidth.

This example clearly demonstrates that the one-shot double-slice $^1H$ experiment is robust and has high selectivity and sensitivity, even when applied to biphasic samples containing insoluble materials which may, in principle, affect magnetic field homogeneity across that sample.

As cold brew coffee is a popular new trend, it is a point of interest to understand the chemical differences between cold and hot brew coffees. These compositional variations can

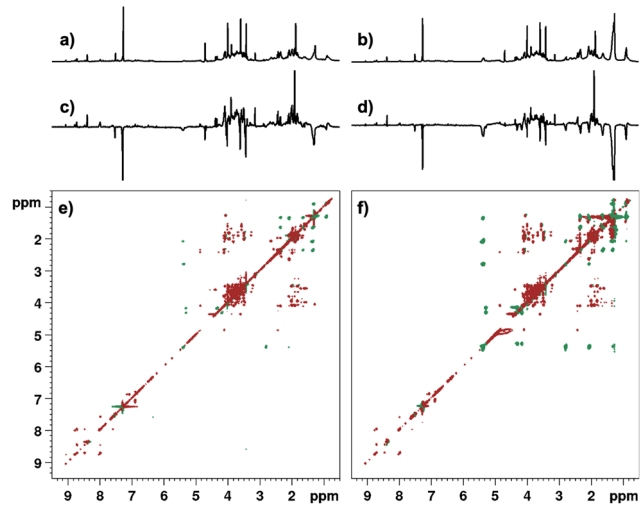


Fig. 4 Classic pre-saturation $^{1}$H spectra for biphasic CBC (a) and HBC (b) samples. One-shot double-slice NMR spectra for biphasic CBC (c) and HBC (d) samples acquired with a pulse field gradient strength of approximately 3.43 G cm$^{-1}$, and a ReBurp pulse width of 1000 μs. One-shot double-slice TOCSY spectra (mixing times of 60 ms) for biphasic CBC (e) and HBC (f). Dark red and dark green cross peaks respectively represent chemical species from the $D_2O$ and $CDCl_3$ layers.

explain differences observed in flavour profiles, as well as have potential implications for health benefits. To investigate these differences, we applied the one-shot double-slice selection experiment to biphasic NMR samples composed of in-tube extractions of cold brew coffee (CBC) and hot brew coffee (HBC).

The organic rainforest whole bean coffee used for these experiments was first brewed in $D_2O$ under both boiling and room temperatures (see ESI† for details). The coffee grounds were removed via centrifugation. 250 μL of the $D_2O$ coffee solution were then transferred to 5 mm NMR tubes containing 250 μL of $CDCl_3$; the samples were inverted and shaken repeatedly to perform the extraction. To ensure optimal separation of the phases, the biphasic tubes were centrifuged in a desktop centrifuge before NMR measurement.

Compared with conventional pre-saturation $^{1}$H spectra (Fig. 4a and b) of the biphasic CBC and HBC samples, the one-shot double-slice 1D spectra of CBC (Fig. 4c) and HBC (Fig. 4d) allow a quick identification of the signals in the aqueous layer (positive peaks) and organic layer (negative peaks). It is obvious that the spectral overlap is alleviated in the one-shot double-slice spectra. The organic layer contains caffeine (peaks at 7.5, 4.0, 3.6, and 3.4 ppm) for both CBC and HBC, as expected. In addition, the triglyceride fatty acid components-such as linoleic acid (5.4, 2.8, 2.3, 2.1, 1.6, 1.3, and 0.9 ppm) and palmitic acid (2.3, 1.6, 1.3, and 0.9 ppm) in both CBC and HBC are identified from the one-shot double-slice spectra (see ESI† for the detailed assignments). The subtle spectroscopic differences between CBC and HBC are further revealed by combining the one-shot double-slice scheme with a 2D TOCSY experiment (Fig. 4e and f). While the spectral "fingerprints" of the aqueous layers (dark red) of CBC and HBC are very similar in terms of cross-peak patterns and intensities, the greater intensity of the dark green crosspeaks in the HBC one-shot double-slice TOCSY spectrum (Fig. 4f) indicate much higher levels of triglyceride fatty acid components in the HBC organic layer than that of the CBC. Our results, thus, suggest that cold brew coffee preserves the same major water-soluble ingredients as those in hot brew coffee. However, the levels of organic-soluble triglyceride-like components are greatly reduced by using the cold brew method.

## 3. Conclusions

In summary, we propose a one-shot double-slice selection NMR experiment for biphasic systems. Unlike previously used slice selective experiments, the one-shot double-slice experiment allows detection of NMR signals from both phases of a biphasic sample *simultaneously* as oppositely phased peaks in one spectrum. We have demonstrated that this method is robust, easy to implement, and can be combined with 2D TOCSY experiments for structural characterisation with spatial-specificity. It is readily applicable to not only well-defined model biphasic systems, but also to practical chemical separation problems involving in-tube extractions. The high selectivity of the one-shot double-slice $^{1}$H experiment has been demonstrated via the examples of in-tube tea and coffee extractions. Because of the nature of simultaneous excitations with opposite r.f. phases, the one-shot double-slice experiment has the potential to monitor chemical kinetic and dynamic processes occurring between two phases when "real time" kinetic data are essential.

KDC and SB designed the experiments, prepared the biphasic samples, optimized NMR parameters, acquired NMR spectra, and wrote the manuscript. JS contributed to this manuscript by preparing biphasic samples, acquiring NMR data, and making $^{1}$H spectral assignments of tea and coffee NMR spectra. All authors discussed the results, analysed the data, commented on the paper, and have given approval to the final version of the manuscript.

## Conflicts of interest

There are no conflicts of interest to declare.

## Acknowledgements

The authors appreciate the helpful discussion with Dr. Clemens Anklin of Bruker BioSpin. The NMR measurements at University of Delaware were made possible by a Delaware COBRE program, supported by a grant from the National Institute of Heath under Award Number P20GM104316.

## Notes and references

1 W. Kozminski, *Pol. J. Chem.*, 2000, **74**, 4.
2 (*a*) J. Allen and K. Damodaran, *Magn. Reson. Chem.*, 2015, **53**, 200–202; (*b*) S. Zhang, *J. Am. Chem. Soc.*, 2006, **128**, 2; (*c*) C. F. Pantoja, J. A. Bolanos, A. Bernal and J. Wist, *Magn. Reson. Chem.*, 2017, **55**, 519–524; (*d*) A. C. Poppler,

 This journal is © the Owner Societies 2022

S. Frischkorn, D. Stalke and M. John, *ChemPhysChem*, 2013, **14**, 3103–3107; (*e*) M. A. Wisniewska and J. G. Seland, *J. Colloid Interface Sci.*, 2019, **533**, 671–677.

3 (*a*) J. Lambert, R. Hergenroder, D. Suter and V. Deckert, *Angew. Chem., Int. Ed.*, 2009, **48**, 6343–6345; (*b*) C. Mantel, P. A. Bayle, S. Hediger, C. Berthon and M. Bardet, *Magn. Reson. Chem.*, 2010, **48**, 600–606; (*c*) B. T. Martin, G. C. Chingas and O. M. McDougal, *J. Magn. Reson.*, 2012, **218**, 147–152.

4 (*a*) T. Niklas, D. Stalke and M. John, *Chem. Commun.*, 2015, **51**, 1275–1277; (*b*) J. Kind and C. M. Thiele, *J. Magn. Reson.*, 2015, **260**, 109–115; (*c*) G. E. Wagner, P. Sakhaii, W. Bermel and K. Zangger, *Chem. Commun.*, 2013, **49**, 3155–3157.

5 R. Evans, A. Sandhu, T. Bridgwater and K. Chong, *Energy Fuels*, 2017, **31**, 4135–4142.

6 T. N. Hjartnes, G. H. Sorland, S. Simon and J. Sjoblom, *Ind. Eng. Chem. Res.*, 2019, **58**, 2310–2323.

7 K. Seeger, *Anal. Chem.*, 2021, **93**, 1451–1457.

8 S. A. Krachkovskiy, A. D. Pauric, I. C. Halalay and G. R. Goward, *J. Phys. Chem. Lett.*, 2013, **4**, 3940–3944.

9 L. Castanar, P. Nolis, A. Virgili and T. Parella, *Chem. – Eur. J.*, 2013, **19**, 15472–15475.

10 Y. N. Mitrev, *Bulg. Chem. Commun.*, 2017, **49**, 4.

11 M. Vega-Vazquez, J. C. Cobas and M. Martin-Pastor, *Magn. Reson. Chem.*, 2010, **48**, 749–752.

12 R. Freeman, *Prog. Nucl. Magn. Reson. Spectrosc.*, 1998, **32**, 47.

13 J. N. Dumez, *Prog. Nucl. Magn. Reson. Spectrosc.*, 2018, **109**, 101–134.

14 P. Trigo-Mourino, C. Merle, M. R. M. Koos, B. Luy and R. R. Gil, *Chem. – Eur. J.*, 2013, **19**, 7013–7019.

15 (*a*) Y. Yuan, Y. Song, W. Jing, Y. Wang, X. Yang and D. Liu, *Anal. Methods*, 2014, **6**, 907–914; (*b*) N. H. M. Rubel Mozumder, Y.-R. Lee, K. H. Hwang, M.-S. Lee, E.-H. Kim and Y.-S. Hong, *Appl. Biol. Chem.*, 2020, 63.

16 E. Munz, P. M. Jakob and L. Borisjuk, *Biochimie*, 2016, **130**, 97–108.

This journal is © the Owner Societies 2022